

1994

An Adaptive Partial Response Data Channel for Hard Disk Magnetic Recording

DARRAGH, NEIL

<http://hdl.handle.net/10026.1/2594>

<http://dx.doi.org/10.24382/3904>

University of Plymouth

All content in PEARL is protected by copyright law. Author manuscripts are made available in accordance with publisher policies. Please cite only the published version using the details provided on the item record or document. In the absence of an open licence (e.g. Creative Commons), permissions for further reuse of content should be sought from the publisher or author.

**An Adaptive Partial Response
Data Channel for Hard Disk
Magnetic Recording**

by

NEIL DARRAGH

A thesis submitted to the University of Plymouth
in partial fulfilment for the degree of
DOCTOR OF PHILOSOPHY

School of Electronic, Communication and Electrical Engineering
Faculty of Technology

July, 1994

This copy of the thesis has been supplied on condition that anyone who consults it is understood to recognise that its copyright rests with its author and that no quotation from the thesis and no information derived from it may be published without the author's prior written consent.

07/1/94

Copyright © 1994 by Neil Darragh

AN ADAPTIVE PARTIAL RESPONSE DATA CHANNEL FOR HARD DISK MAGNETIC RECORDING

by Neil Darragh

Abstract

An adaptive data channel is proposed which is better able to deal with the variations in performance typically found in the recording components of a hard disk drive. Three such categories of variation were investigated in order to gain an understanding of their relative and absolute significance; variations over radius, along the track length, and between different head / media pairs. The variations were characterised in terms of their effects on the step-response pulse width and signal-to-noise ratio. It was found that in each of the categories investigated, significant variations could be found in both longitudinal and perpendicular recording systems which, with the exception of radial variations, were non-deterministic over different head / media pairs but were deterministic for any particular head / media pair characterised.

Conventional data channel design assumes such variations are non-deterministic and is therefore designed to provide the minimum error rate performance for the worst case expected recording performance within the range of accepted manufacturing tolerance. The proposed adaptive channel works on the principle that once a particular set of recording components are assembled into the disk drive, such variations become deterministic if they are able to be characterised. Such ability is facilitated by the recent introduction of partial response signalling to hard disk magnetic recording which brings with it the discrete-time sampler and the ability of the microprocessor to analyse signals digitally much more easily than analogue domain alternatives.

Simple methods of measuring the step-response pulse width and signal to noise ratio with the partial response channel's electronic components are presented. The expected error rate as a function of recording density and signal to noise ratio is derived experimentally for the PR4 and EPR4 classes of partial response. On the basis of this information and the recording performance it has measured, the adaptive channel is able to implement either PR4 or EPR4 signalling and at any data rate. The capacity advantage over the non-adaptive approach is investigated for the variables previously identified. It is concluded on the basis of this investigation that the proposed adaptive channel could provide significant manufacturing yield and capacity advantages over the non-adaptive approach for a modest increase in electronic complexity.

Contents

Abstract	ii
Contents	iii
List of Figures	vi
Nomenclature	viii
Acknowledgement	ix
Declaration	x
Dedication	xi
1. Background to the Investigation	
1.1 Hard Disk Drive Technology Development	1
1.2 Partial Response Signalling for Magnetic Recording.....	13
1.2.1 Nyquist Signalling	13
1.2.2 Correlative Encoding.....	15
1.3 Partial Response Equalisation	26
1.4 Detection Issues.....	29
1.5 Summary	31
1.6 Thesis.....	33

2. Experimental Details

2.1 The Hard Disk Experimental Test Station	35
2.1.1 Mechanical Design	35
2.1.2 Automated Test System Hardware	40
2.1.3 Automated Test System Software.....	51
2.2 Software Modelling of the Data Channel.....	54
2.3 Head / Media Parameters	57

3. Results & Discussion 1 : Channel Response Variation Characterisation

3.1 Introduction.....	58
3.2 Channel Variation over Disk Radius.....	60
3.2.1 Step-response Pulse Width.....	60
3.2.2 Step-response Pulse Amplitude.....	67
3.2.3 Noise	70
3.2.3.1 Electronic Noise.....	70
3.2.3.2 Media Noise.....	71
3.3 Channel Variation along the Recorded Track	76
3.3.1 Underlayer Domain Noise in Perpendicular Recording Disks	76
3.3.2 Amplitude Modulation.....	83
3.4 Channel Variation over Head and Media Population.....	86
3.5 Summary	90

4. Results & Discussion 2 : The Adaptive Partial Response Data Channel

4.1 The Pulse Response and the Partial Response	92
4.1.1 Correction for non-linear Transition Shift	98
4.1.2 Signal and Noise Loss Through the Equaliser	101
4.1.3 Bit Error Rate	109
4.2 Determination of the Recording Performance.....	113
4.2.1 Measurement of Pulse Width (PW50).....	113
4.2.2 Measurement of Signal to Noise Ratio.....	117
4.3 Performance Comparisons of the Adaptive Channel	119
4.3.1 Performance Variation with Radius	120
4.3.2 Performance Variation along the Track Length.....	126
4.3.3 Channel Variations over Head / Media Population.....	130
4.3.4 The User-specified Self-optimising Disk Drive.....	135
4.4 Implementation Issues.....	137

5. Conclusions & Future Work

5.1 Conclusions 144
5.2 Future Work 148

Bibliography 149

Appendices:-

A. Published Paper 158

B. Circuit Diagrams 162

**C. Unpublished Paper : Method for Accurately Determining the Track
Radius Using In-situ Recording Measurements** 165

D. Software Models 175

E. Background Theory 199

List of Figures

1.1	Schematic diagram of the hard disk drive's primary components	2
1.2	The principle of the peak detection channel.....	9
1.3	Effects of intersymbol interference (ISI)	11
1.4	Nyquist signalling.....	14
1.5	A simple correlative encoding scheme.....	17
1.6	Spectral properties of example correlative encoding scheme.....	19
1.7	Spectral characteristics of the partial response schemes.....	22
1.8	Similarity between the frequency response of the magnetic recording channel and that of the Partial Response channel obtained by setting $n=2$ (EPR4).....	22
1.9	The magnetic recording channel step response.....	24
1.10	The step response for partial response system $(1-D)(1+D)$	24
1.11	The step response for partial response system $(1-D)(1+D)^2$	25
2.1	Schematic diagram of the experimental test station mechanics.....	36
2.2	Schematic diagram of adjustable head mounting unit.....	39
2.3	Schematic diagram of the experimental test system	41
2.4	The write channel	44
2.5	Timing synchronisation during write mode	44
2.6	Modular software functions.....	45
2.7	Schematic diagram of the read channel	48
2.8	Laser index method.....	48
2.9	DISKLAB software user interface	53
2.10	The software data channel.....	56
2.11	Model waveform generators	56
3.1	MR head replay pulses at track radii of 21mm, 33mm, 45mm.....	62
3.2	Dependence of pulse width (time) on track radius	62
3.3	Theoretical MR replay pulse length and transition length vs flying height.....	64
3.4	Flying height characteristic over radius.....	64
3.5	Signal amplitude as a function of radius.....	69
3.6	Normalised signal amplitude as a function of write current	69
3.7	Reverse erase noise characteristic.....	74
3.8	Perpendicular recording layer media noise	78
3.9	Perpendicular low-frequency noise	78
3.10	Principle of underlayer domain noise imaging.....	81
3.11	Picture of low frequency perpendicular noise over section of disk surface.....	82
3.12	A picture of noise from the same section of disk as figure 3.11 after it has been subjected to a magnetic field.....	82
3.13	Amplitude modulation of recorded data signal.....	85
3.14	Pulse width at 50% amplitude for a single head and 6 recording surfaces.....	88
3.15	Pulse width at 50% amplitude over radius for a single disk and 4 heads	88
3.16	Signal amplitude over radius for a single head and 6 recording surfaces.....	89
3.17	Signal amplitude over radius for a single disk and 4 heads	89

4.1	The pulse response and the partial response	94
4.2	Measured recording channel pulse response	96
4.3	Target PR4 responses with signalling rates corresponding to figure 4.2.....	96
4.4	Required equaliser transfer functions.....	97
4.5	Pulse response measurement technique	97
4.6	Impulse response of recording channel derived using PRBS sequence	100
4.7	Non-linear transition shift (% of bit period).....	100
4.8	Channel model for response analysis.....	104
4.9	SNR loss through PR4 and EPR4 equaliser	104
4.10	Recording channel, target response and required equaliser transfer function at normalised recording density of 1.64	105
4.11	Recording channel, target response and required equaliser transfer function at normalised recording density of 2.6.....	105
4.12	The MR step response and Lorentzian model	108
4.13	Cross-correlation between Lorentzian model and MR head step response.....	108
4.14	Error rate vs signal to noise ratio at input to Viterbi detector	111
4.15	Lines of constant error rate for actual signal to noise ratio vs normalised density.....	111
4.16	PW50 measurement circuit.....	115
4.17	Principle of PW50 measurement	116
4.18	Samples from the PW50 measurement circuit.....	116
4.19	SNR measurement technique principle.....	118
4.20	SNR measurement technique applied over 2mm length of track	118
4.21	Assumed nominal pulse width variation characteristic over radius	121
4.22	Operation of the adaptive channel to maximise capacity in the presence of radial changes in pulse width	124
4.23	Model of signal to noise variation along the track length.....	129
4.24	Capacity that adaptive channel recovers over a fixed-design approach.....	129
4.25	Illustration of the distribution of recording component performance.....	131
4.26	The adaptive partial response data channel.....	138
4.27	Output from sampler showing PLL lock field and the non-equalised data samples.....	139
4.28	Schematic diagram of adaptive equaliser.....	139
4.29	Operation of the adaptive equaliser	140

Nomenclature

A.C.	Alternating Current
ADC	Analogue to Digital Convertor
AGC	Automatic Gain Control
BER	Bit Error Rate
CRIST	The Centre for Research in Information Storage Technology
D.C.	Direct Current
DFT	Discrete Fourier Transform
EPR4	Extended Partial Response Class IV
EQ	Equalisation
FFT	Fast Fourier Transform
GPIO	General Purpose Input / Output
HEX	Hexadecimal
IBM	International Business Machines (corporation)
IEEE	Institute of Electrical and Electronics Engineers
ISI	Intersymbol Interference
LMS	Least Mean Squares
MIG	Metal-In-Gap
MLSD	Maximum Likelihood Sequence Detection
MR	Magnetoresistive
NRZ	Non Return to Zero
NRZI	Non Return to Zero Interleaved
PC	Personal Computer
PLL	Phase Locked Loop
PR4	Partial Response Class IV
PR	Partial Response
PRBS	Pseudo Random Binary Sequence
PRML	Partial Response Maximum Likelihood
PRS	Partial Response Signalling
PW50	Pulse With @ 50% zero to peak amplitude
RAM	Random Access Memory
RMS	Root Mean Square
SNR	Signal to Noise Ratio
ZBR	Zoned Bit Recording

Acknowledgement

I would like to express my gratitude to all those people and organisations who have been associated with this project, in particular,

My supervisors Professor D.J. Mapps (Director of Studies), Dr. J.G. Wade, Dr. T.Donnely of the School of Electronic, Communication and Electrical Engineering, for their constant support, encouragement and guidance throughout the project.

All the technical staff within the C.R.I.S.T. facility and in particular Mr Philip Brown without whose ingenious mechanical expertise and enthusiasm many of the experiments in this work would not have been possible.

The Science and Engineering Research Council and Pilkington Group Research, Pilkington PLC, for their financial support.

The Data Channel Engineering group at Rodime Europe PLC for the three-month training period at the beginning of this project.

Mr Martin Jevons and Mr Dave Lockwood of Myrica U.K. Ltd. for their many useful discussions and insights into the practical and commercial aspects of hard disk drive design.

Mr Paul Davey of the C.R.I.S.T. research group, who, through the many useful (and sometimes heated) debates has aided my understanding immeasurably.

Ms. Sue Locke and Ms.Emine Ibrahim for their constant friendship and support.

Declaration

At no time during the registration for the degree of Doctor of Philosophy has the author been registered for any other University award.

This study was financed with the aid of a research fund from the Science and Engineering Research Council and carried out in collaboration with Rodime Europe PLC.

A programme of advanced study was undertaken, which included the extensive reading of literature relevant to the research project, a three-month industry training in Rodime Europe PLC and attendance of international conferences and seminars on magnetics and magnetic recording.

A paper from a part of the work in this thesis has been presented at The 1993 IEEE International Magnetics Conference (Intermag '93), Stockholm, Sweden. In addition the author attended The 1990 IEEE International Magnetics Conference (Intermag '90) in Brighton, U.K.

Neil Darragh



Date 12/7/94

This thesis is dedicated to the memory of my mother,

Mavis Barbara Ann

(1932 - 1986)

Chapter 1

Background to the Investigation

1.1 Hard Disk Drive Technology Development

The first hard disk product, the 'RAMAC 350', was introduced by International Business Machines (IBM) in 1956. It stored 5 MBytes of data on fifty, 24" diameter disks. A recent product from the same company, the IBM 0664, stores 2 GBytes of data on eight, 3.5" diameter disks [Kerwin et. al., 1993]. The enormous improvements in storage capacity, product size, data rate and file access time achieved over these four decades are attributable to a number key developments in each of the drives constituent components (figure 1.1).

Namely,

- The record / replay head;
- The recording media;
- The head tracking (servo) system;
- The signal processing system (The Data Channel).

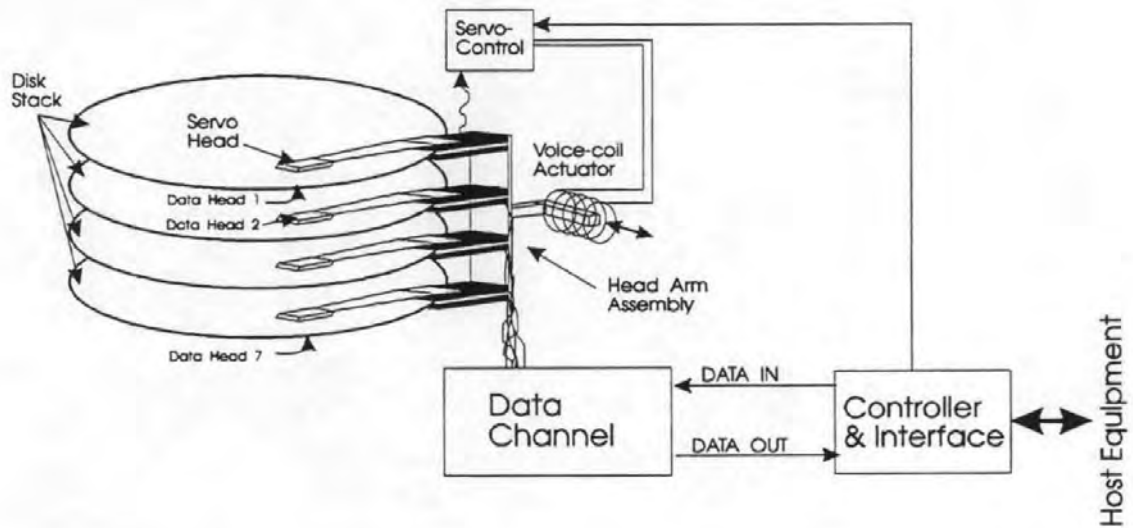


Figure 1.1 - Schematic diagram of the hard disk drive's primary components.

Record / Replay Heads

Record / replay heads for hard disk drives have seen a number of major developments since the original RAMAC design. In 1973 the Winchester head design was introduced in the IBM 3340 disk drive [Warner, 1974]. This design removed the need for the bulky hydraulic systems previously required to address the head against the spinning disk and then keep it accurately suspended over the surface. Rather, the Winchester head employs a slider body that takes-off and flies over the surface of the disk whilst it is spinning. This enables smaller head-medium separation to be achieved (typically a few micro-inches) and a corresponding increase in linear storage density. The Winchester head is constructed using ferrites which have a high resistivity (limiting Eddy current losses) and good machining and wearing properties.

The requirement for higher linear storage capacities brings with it the need for higher coercivity media which supports narrower transitions [Koster & Arnoldussen, 1989]. Consequently, to be able to saturate such media, higher head fields are required. This causes the ferrite material at the trailing edge of the gap (where the flux density is maximum) to saturate, thus destroying its flux guiding abilities. Correspondingly, this leads to a reduced field gradient (broader transitions) and limits the maximum attainable magnetisation. A method to overcome this problem has been developed known as Metal-In-Gap (MIG) recording [Nishiyama et. al, 1987]. Here, a film of Ni-Si-Al (Sendust) with a much higher saturation magnetisation than ferrite, is deposited on the trailing pole of the head. Therefore, much higher fields can be generated in the head without the risk of saturating the pole tip. The use of MIG technology has extended the use of ferrite heads for rigid-disk applications.

Heads fabricated using thin-film techniques have been in development since the late 1970's [Jones, 1978; Miura et. al., 1978; Berghof & Gatzel, 1980; Kakehi et. al., 1982]. This type of head fabrication provides several advantages over the existing milled ferrite core type. Thin-film heads may be manufactured with smaller features and tighter tolerances. This allows the track widths and the gap / pole lengths to be smaller, leading to an increase in storage capacity. Also, the reduced volume of core material leads to reduced inductance and therefore a wider frequency response. On the negative side, thin-film heads are more complex to manufacture and give rise to non-symmetrical undershoots in the read back signal caused by the relatively short length of the poles and their unequal width.

The principle of magnetoresistivity, where the resistance of a material is altered according to the magnitude of an external magnetic field, has provided alternative possibilities for read head design [Hunt, 1971; Gorter et. al., 1974; Shelledy & Brock, 1975; Druyvesteyn et. al., 1981]. The signal from a magnetoresistive (MR) head, unlike its inductive counterpart, is not proportional to the rate of change of flux. Therefore, MR heads are particularly suitable in applications where the relative velocity between the head / medium is low and / or changing. Such is the case in small form-factor hard disk drives, where the linear velocity at the inside track may be less than half that on the outside. An MR head can provide greater output than a film head, and, the single-sense element of the MR head is small compared to the multi-turn thin-film type. Hence, the heads can be used to read significantly narrower tracks with little loss in signal amplitude [Jones, 1986]. However, MR heads are a read-only device and so for recording applications, the head must be mounted along with an inductive type write element. This imposes further complications and restrictions (expense) on the fabrication process and has therefore limited their use in rigid-disk applications so far, where MIG and thin-film inductive head technologies still adequately serve. On the other hand, the separate write and read elements allows each of them to be individually

optimised. This is an advantage over the inductive head, where, the design is always a compromise to give adequate writing performance (wide gap) and high resolution reading performance (narrow gap). Furthermore, the MR read element can be made narrower than the write element allowing for a reduction in servoing tolerance and closer track spacing.

Because of its high sensitivity and low resistivity, the MR head generates less thermal noise but is more susceptible to media noise than its thin-film inductive counterpart. Media noise is already an important noise element in today's inductive head applications. It is expected to become *the* dominant noise component in the future. High storage capacities employing a write-wide inductive head coupled with a narrower MR read head have been demonstrated for rigid-disk applications [Mowry et. al., 1986; Yogi et. al., 1990]. In the latter demonstration, very low noise media was specified, which even then, contributed 90% of the total noise power.

Recording Media

Thin-film recording media has progressively replaced the original particulate type during the 1980's. Particulate media is comprised of elongated particles of gamma ferric iron. The particles are mixed with a binder material and then deposited onto the disk surface. The elongated particles are oriented circumferentially during manufacture by means of a magnetic field, which for longitudinal recording aligns their easy axis of magnetisation with the head writing fields. The ratio of volume of particles per volume of surface film is known as the packing fraction. Typical packing fractions for rigid-disk particulate media are 40-50%.

Thin-film media is composed of a homogeneous film of Cobalt alloy (for example, Co-P or Co-Ni-P for longitudinal recording, and, Co-Cr for perpendicular recording) which is often sputtered onto the disk surface (other deposition methods are electroplating, chemical plating or evaporation). The homogeneous nature of thin-films means that their packing fraction is very close to 100%. This enables higher magnetisation to be achieved with thinner layers than particulate media which results in narrower transitions, and therefore, higher linear recording densities. Also, thin-films may be made smoother than particulate media allowing for lower flying heights and therefore also increased linear density. The fabrication of thin-film media is more involved than that of particulate media since additional non-magnetic material layers have to be deposited to achieve satisfactory tribological and film-growth properties.

The perpendicular mode of recording first suggested by Iwasaki and his co-workers in the late 1970's has offered the potential of inherently higher storage densities than longitudinal recording [Iwasaki, 1977]. In perpendicular recording, where the plane of magnetisation is normal to the surface of the film, the adjacent recorded bits do not suffer from the demagnetisation effects ultimately limiting the inter-bit transition length in longitudinal recording [Kryder, 1990]. Thus, the way to increase the linear density in longitudinal recording media is to produce thinner films with higher coercivities. In perpendicular recording these constraints do not apply, and in fact, the demagnetising fields actually improve at high recording densities [Mapps & Pan, 1993]. The world record linear recording density for magnetic disk recording has been demonstrated on a perpendicular film [Yamamoto et. al., 1987]. This study highlighted the fact that although the media could support extremely high linear densities, 680,000 flux changes per inch (26,771 flux changes per mm), it is the head technology that limits the practically achievable density limit. In both longitudinal and perpendicular technologies, the recording density improves

with reducing flying height. However, the advance of the improvement in the perpendicular mode is greater than that of longitudinal. Therefore, as we move towards flying heights below 150nm, the advantages of perpendicular recording over longitudinal will become very significant [Mapps et. al., 1988].

Servo System

In servoing technology, closed loop feedback control and voice-coil actuators have replaced the open-loop stepper motor actuators, allowing for an order of magnitude increase in track following resolution [Mitsuya et. al, 1982]. Current servo systems are capable of following a 5 μm track to within $\pm 0.5\mu\text{m}$. Systems may rely on one disk surface of the drive being reserved for the positioning information, with a consequential loss in overall capacity. The possibility of embedding all the servo information in the data surfaces either by means of a servo underlayer [Hansen, 1981], or, by optical tracking over pre-grooved tracks [Koshino & Ogawa, 1980] would free up the servo surface for information storage and also lead to finer track following capability and therefore higher track densities.

Data Channel

Whereas there have been significant technology developments in the heads, media and servo system, the analogue Peak Detection (PD) method of data recovery (figure 1.2) has consistently dominated the magnetic recording data channel technology for over 30 years. In Peak Detection, information is recorded as reversals of magnetisation in the media where a reversal represents the binary digit '1' (so-called NRZI recording). When the replay head passes over the recorded track, the reversals of magnetisation (so-called *transitions*) cause pulses of electric current to be generated through it. A phased-locked loop is synchronised to the replay signal waveform and the pulses are detected with respect to the clock phase by differentiating and thresholding the replay signal. A detected pulse within a clock window is decoded as a binary '1' and no detected pulse within a clock window is decoded as a binary '0'. Information in the Peak Detection channel is decoded on a bit-by-bit basis.

The error events in the peak detection channel are classified as being missing bit or peak-shift errors. Missing bit errors are caused by pulses falling below the threshold (or equivalently noise exceeding the threshold). Peak shift errors are caused by pulses being detected outside their correct window. Noise and interference effects conspire to cause these effects in a number of ways. Band-limited white Gaussian noise arising from the resistive elements of the head and amplifier input stages, adjacent track interference, intersymbol interference (ISI) and old information signal reduce signal to noise ratio and can cause missing bit errors. Linear and non-linear intersymbol interference cause peak shift errors when transitions are recorded very close. This is particularly so for thin-film longitudinal media where at close transition spacing a non-linear transition shift effect becomes significant and the principle of linear superposition no longer applies [Arnoldussen & Tong, 1986; Tang, 1986; Melas & Arnett., 1988].

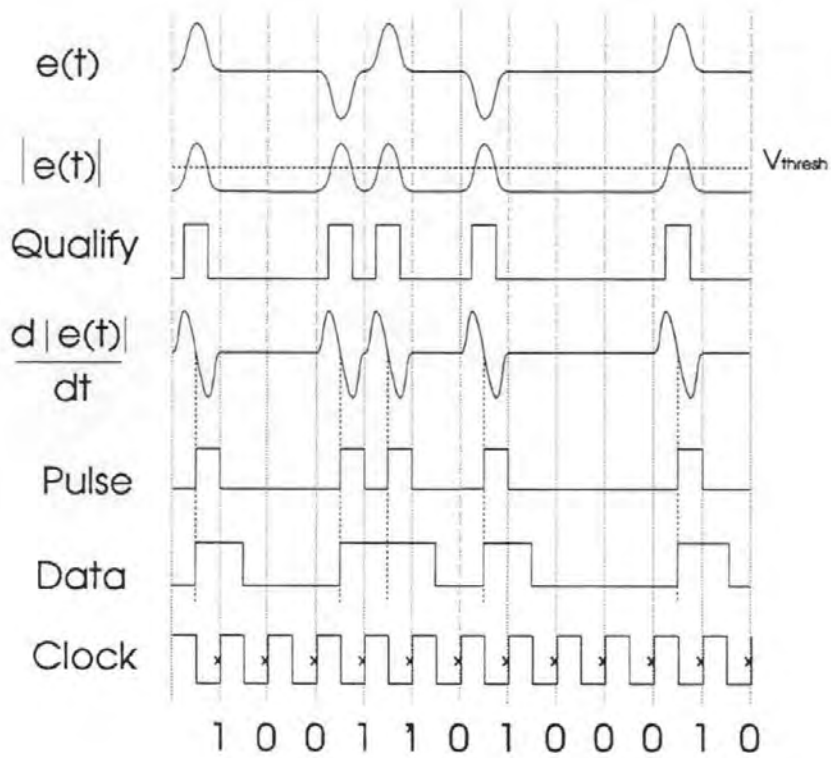
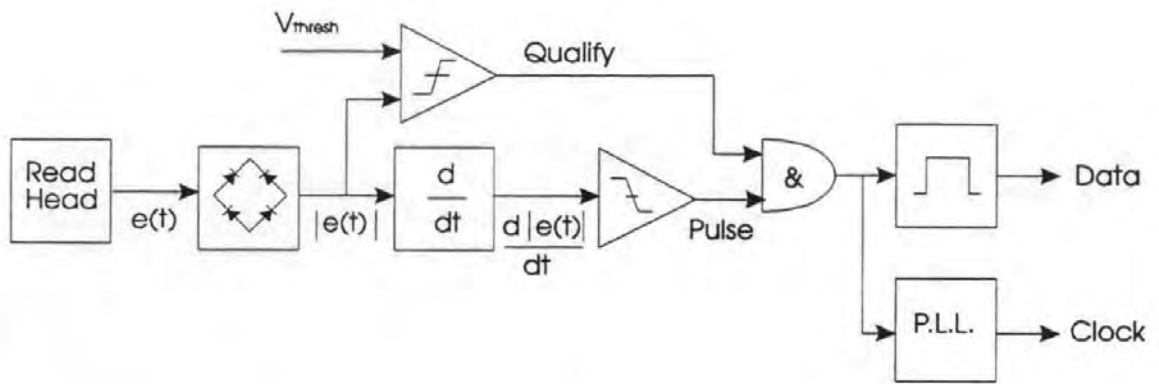


Figure 1.2 - The principle of the Peak Detection channel

In the peak detection channel the linear storage density is determined by the minimum allowable spacing between two adjacent pulses before they suffer excessive intersymbol interference, increasing Bit Error Rates (BER) to unacceptable levels (figure 1.3). To this end it is important for the pulses to be as separated / narrow as possible, the recording process to be linear and for the frequency content of the information to match as closely as possible that of the recording channel. Hence, prior to recording, the data stream is channel encoded [Franaszek, 1970; Cohn et. al., 1982; Wolf & Siegel, 1991] to maximise information rate in the presence of ISI and equalised (write-precompensated) to counter peak-shift [Thornley, 1981; Schneider, 1985]. During reading, equalisation is applied to slim the pulses, once again to maximise information rate in the presence of ISI [Schneider, 1975; Barbosa, 1981; Arai et. al., 1984].

Whilst the analogue peak detection method has been acceptable in the past in terms of simplicity, low cost and speed, it has become increasingly apparent that to make more efficient use of the information bandwidth available, a revolutionary rather than evolutionary approach to information representation and recovery is required.

One such approach lies in the application of digital signal processing techniques within the rigid-disk data channel. Digital techniques process discrete time digitised samples of the head replay signal. Once digitised, complex signal processing techniques can be implemented much more easily and precisely than they can using the analogue domain alternatives [Proakis, 1989]. Historically, the introduction of this technology to rigid-disk drives has been held up by speed, large scale integration and cost issues. Hence, it has only recently been made feasible following the introduction of the low cost, high speed compact mixed signal digital and analogue signal processor [Coker et. al., 1991a; Schmerbeck et. al., 1991].

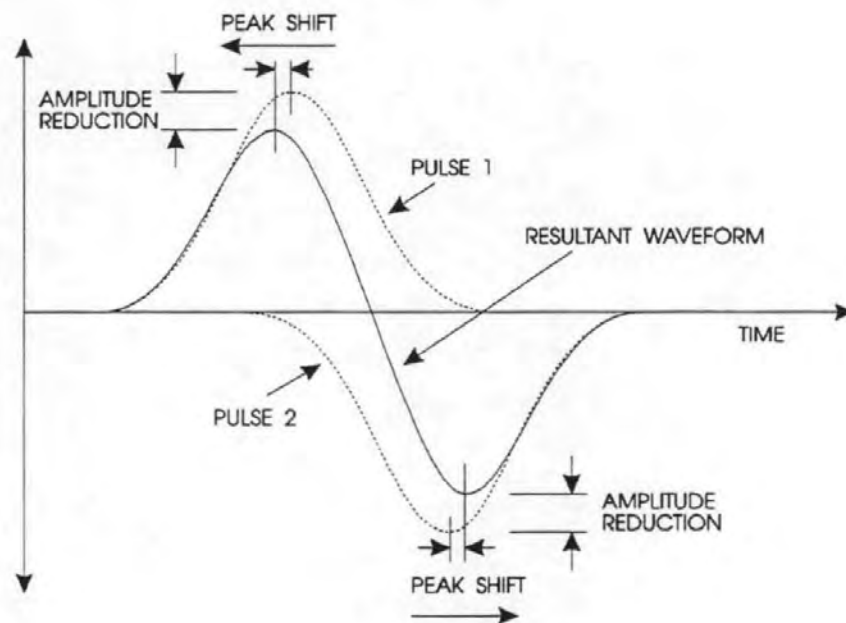


Figure 1.3 - Effects of Intersymbol Interference (ISI). The peak positions are shifted away from each other and signal amplitude is reduced. If excessive, both effects can cause errors in the peak detect channel.

Of particular interest has been the application of Partial Response (PR) signalling which has been used successfully in digital communications systems for many years [Kobayashi & Tang, 1970; Kabal & Pasupathy, 1975, Thapar & Patel., 1987]. Coupled with Maximum Likelihood Sequence Detection (MLSD), so called PRML, significant density increases can be realised over peak detection with the same physical recording components [Kobayashi, 1971; Forney, 1973]. The application of PRML to magnetic recording disk drives has so far led to two state-of-the-art product releases; the industry's first PRML drive, the 1 GByte IBM 0681, 5.25" disk drive [Coker et. al., 1990; Coker et. al., 1991a] and, the industry's first 2 GByte 3.5" disk drive, the IBM 0664 [Kerwin et. al., 1993].

1.2 Partial Response Signalling for Magnetic Recording

The transmission rate (capacity) in the Peak Detection data channel is determined by the maximum rate at which adjacent pulses may be transmitted without them overlapping excessively (intersymbol interference) and degrading the error rate to unacceptable levels.

1.2.1 Nyquist Signalling

The problems of ISI constraining the information capacity of a digital communications transmission channel were investigated by Nyquist in the 1920's of this century [Nyquist, 1928]. Nyquist demonstrated that the theoretical minimum bandwidth required to transmit R symbols/sec without intersymbol interference was $R/2$ Hz (the so-called *Nyquist Bandwidth*). In other words, he showed that for any communication channel with a bandwidth of B Hz, the maximum theoretical signalling rate is $2B$ symbols/sec (the so-called *Nyquist Rate*). He showed that this could be achieved by a channel with a rectangular frequency response cutting off at $R/2$ Hz. The time domain response, $h(t)$, of such a channel is a cosine function decaying at the rate $1/t$ (figure 1.4). Despite there being considerable pulse overlap, the tails of the overlapping pulses always pass through zero at the detection points. Hence, at the detection instants, the ISI is always zero and the pulse stream, in the absence of noise and timing offsets, may be decoded without error.

However, in practice such a scheme requires an exceedingly complex detector to implement. The rectangular frequency response corresponds to the pulse tails extending to infinity thus making the system intolerant of timing errors. Also, such a pulse is non-causal and therefore requires an infinite delay to generate. Nyquist therefore explored

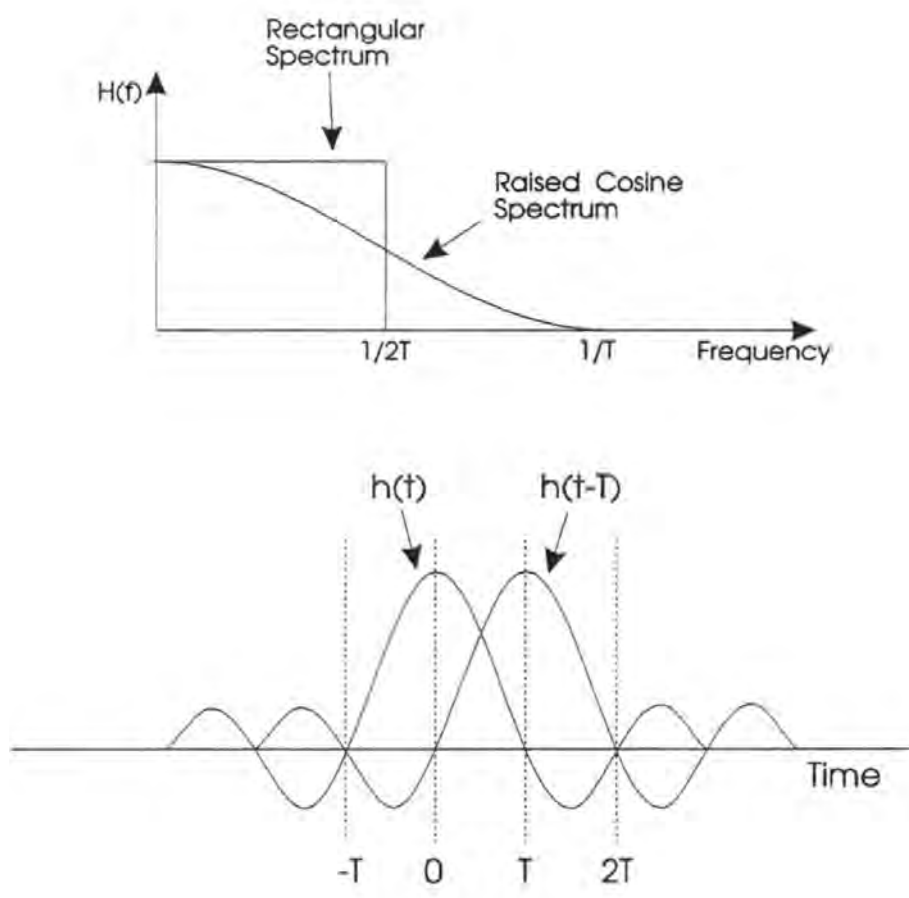


Figure 1.4 - Nyquist Signalling. Note the tails of the adjacent pulses always pass through zero at the sampling instances, defined by the clock rate, T .

more practical spectral shapes that would also yield zero ISI at the detection instants. One such function, the raised cosine spectrum, has a frequency response which decays more gradually thus limiting the extent to which the tails of the pulses interfere with neighbouring pulses in the data stream. However, the penalty is that it requires more bandwidth than the minimal Nyquist bandwidth.

1.2.2. Correlative Encoding

Nyquist's work made the assumption that successive symbols in the information stream could take on any of the arbitrary values defined for the n -ary signal set, i.e. that successive symbol values were completely uncorrelated. Lender observed that if correlation between symbols in the transmitted sequence could be introduced, transmission schemes could be devised that would practicably be able to transmit at the Nyquist rate [Lender, 1964]. He termed such schemes 'correlative coding'.

In correlative level coding, correlation between transmitted symbols is introduced by algebraically combining sequences of source symbols into one transmission symbol in a manner illustrated in figure 1.5. In this simple scheme, the transmitted symbol, b_k , is determined from the source symbols, a_k & a_{k-1} by the relation,

$$b_k = a_k + a_{k-1} \quad (1.1)$$

Hence, each transmitted symbol is correlated with the previous one.

At the receiver, the original source symbol values are obtained by performing the reverse algebraic operation on the received correlated symbols,

$$a_k = b_k - a_{k-1} \quad (1.2)$$

Such a scheme differs from the Nyquist transmission channel in that it requires a memory of previously received symbols in order to decode the present one, i.e. the Nyquist channel is memoryless and the correlative channel is not. Also, the introduction of correlation between symbols is equivalent to introducing intersymbol interference between them since a correlative coded symbol value is the result of an algebraic sum of its original value and some other symbols in the immediate proximity.

The introduction of correlation between transmitted symbols imparts an overall structure to the sequence of symbols, or equivalently, shapes its frequency spectrum. Through careful selection of the correlative encoding scheme, the frequency response of the symbol sequence¹ can be shaped to yield certain desirable attributes such as nulls at d.c., and/or, nulls at the Nyquist frequency (to allow Nyquist rate signalling). This is shown for the scheme described by (1.1) in figure 1.6(a). Note that the frequency response is periodic as $1/2T$ and extends to infinity.

To enable transmission of the symbols at the Nyquist rate over a practical bandlimited channel, the frequency response must be limited to only the first period. Hence, the practical correlative coding channel also requires a filter cutting off at $1/2T$. For this task a raised cosine filter may be employed. The filter will, of course, convert the correlative coded digital symbols (perhaps represented as impulses) into dispersive (Nyquist) pulses. However, at the sampling instances, determined by the symbol rate, the interference from adjacent pulses will be zero. The resulting signal will resemble a Nyquist transmission

¹Note that the symbol sequence may be arbitrarily represented as either impulses, NRZ or NRZI waveforms; the spectral shaping function of the correlative coder will be the same.

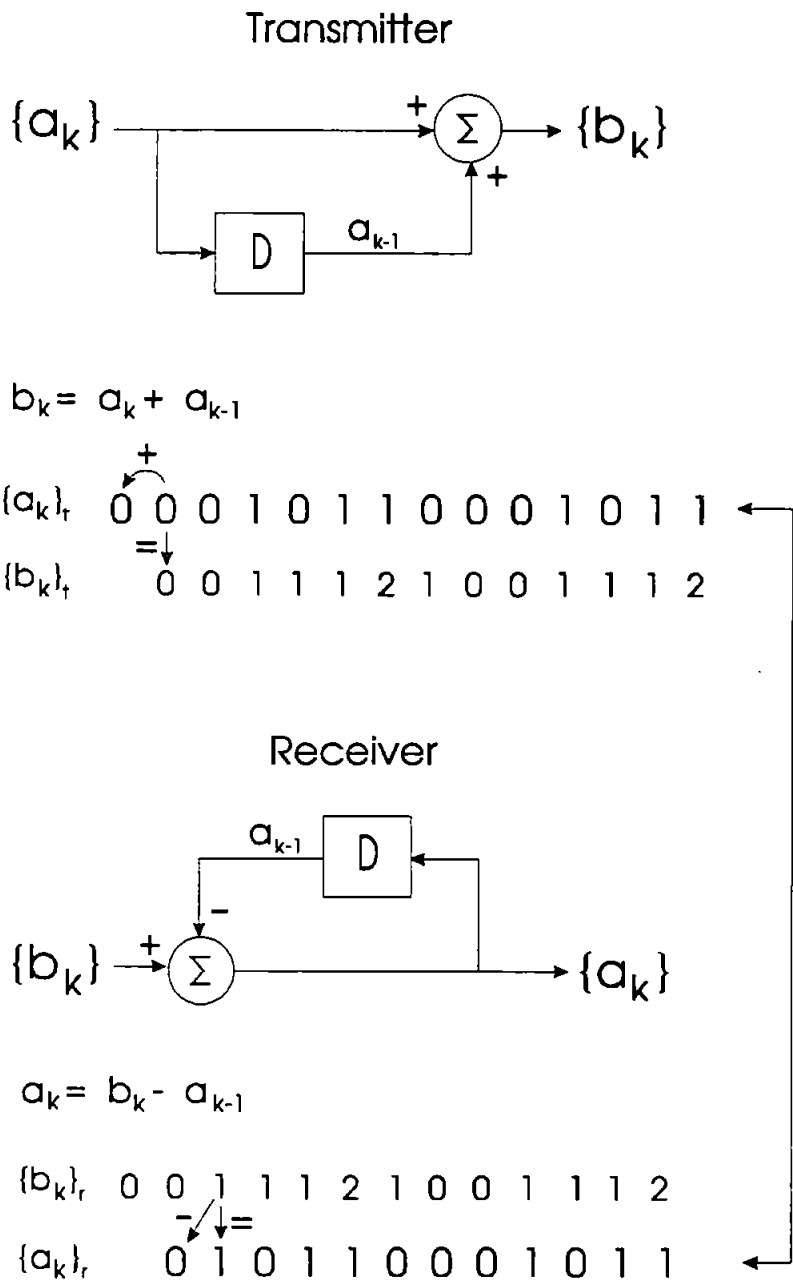


Figure 1.5 - A simple correlative encoding scheme. The source symbol sequence is coded into a correlated transmission sequence comprising 3-levels. At the receiver, the reverse operation is performed to recover the original source symbols.

channel, but, where correlation between successive symbols has been introduced by the correlative level coder. Hence, the overall response is shaped to some different function from that of the pure Nyquist channel.

An alternative method of correlative encoding the source symbol sequence would be to replace both the algebraic encoder and Nyquist filter with a single transmission filter whose (impulse, step or pulse) response was such that, at the sampling instances, it was directly equivalent to the correlative coding function. This is shown in figure 1.6(b) for the encoding scheme described by (1.1). Here, the symbol rate is adjusted such that the samples of a transmission pulse span two or more source symbols (in fact, precisely the number of source symbols defined by the correlation function). We can see that as symbols are transmitted at the symbol rate, the resulting transmission pulses will interfere with each other. At the sampling instances, the intersymbol interference will correspond exactly to the required values of the correlative encoding scheme. Hence, the process of correlative encoding is exactly equivalent to introducing intersymbol interference between successive source symbols and that the introduction of correlation can be done in two ways; algebraically using a digital source encoder followed by bandlimiting filter or dispersively using a suitable transmission filter and appropriate symbol rate.

Conventionally, correlative coding techniques have been viewed as a transmission coding & signal generation technique, where the response of the signal is derived at the transmitter. In magnetic recording, the step response to a transition and the pulse response to a (so-called) dibit bear close resemblance to a class of simple correlative encoding schemes, i.e. these schemes are therefore inherently well suited to an application that demands maximal symbol transmission rate (storage capacity) in a limited bandwidth.

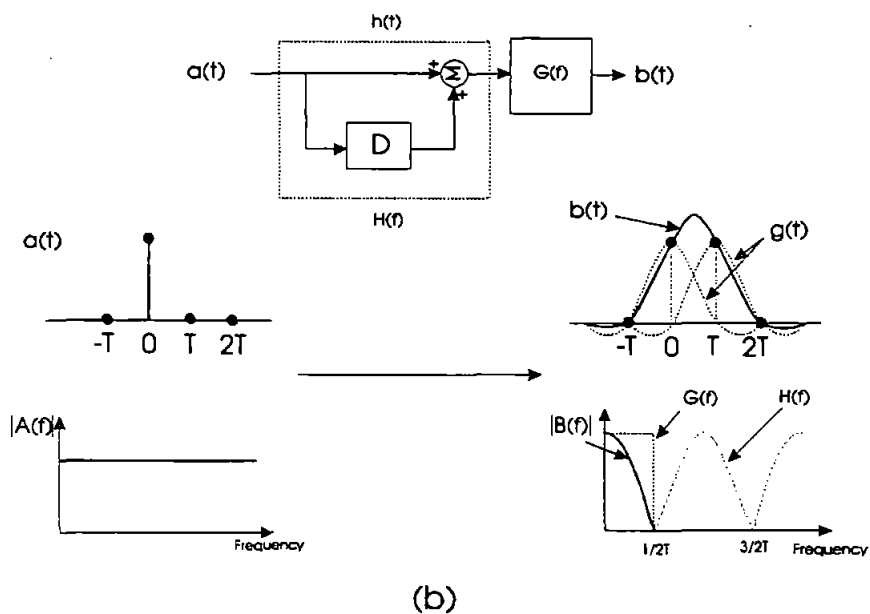
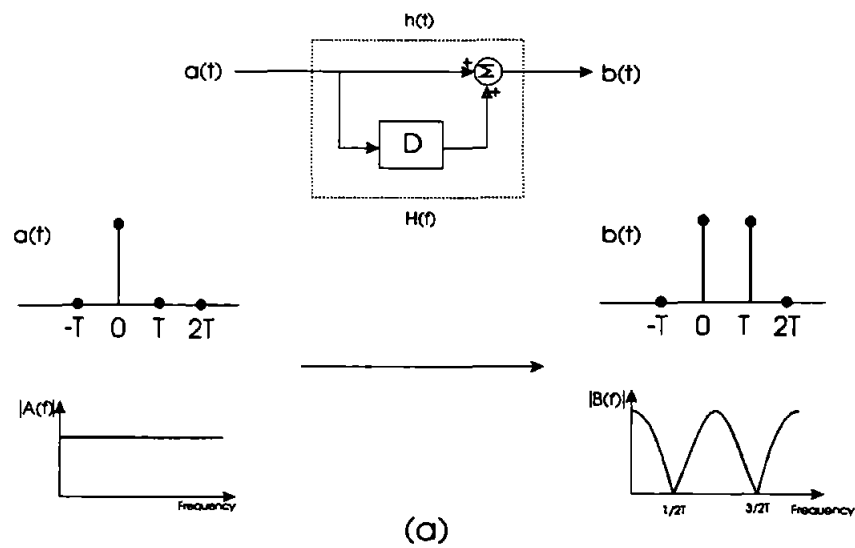


Figure 1.6 - Spectral properties of example correlative encoding scheme. (a) The frequency response of the correlative encoder is periodic as $1/2T$ and extends to infinity. (b) The practical bandlimited channel limits the frequency response to only the first period with a filter, $G(f)$, cutting off at $1/2T$. The resultant channel is capable of transmitting at the Nyquist rate but with realisable filters.

Subsequent to Lenders work, correlative signalling techniques have become commonly known as Partial Response Signalling (PRS). The term partial response arises from the idea of conveying information in a channel subject to controlled amounts of Intersymbol Interference. In a full response channel, the information is conveyed with, assumed, zero ISI. The Peak Detection channel, described previously, is a full-response channel. Also, a simpler notation has developed, by means of the D-transform, which allows a bandlimited correlative encoding scheme to be described more compactly than an expression describing an algebraic sum of raised cosine (or sine) time domain waveforms. A number of schemes suitable for (general) digital communications systems have been classified and reported on [Kretzmer, 1966; Kabal & Pasupathy, 1975]

Partial response schemes are characterised by system polynomials of the form,

$$F(D) = \sum_{n=0}^{N-1} f_n D^n, \quad (1.3)$$

where f_n are the sample values of the desired (impulse) response, and, D is the delay operator equal to one symbol delay. The desired samples of the impulse response define the structure (correlation) between symbols in the information sequence.

The transmitted sequence, B(D) is related to the source sequence A(D) by,

$$B(D) = A(D)F(D), \quad (1.4)$$

where,

$$A(D) \equiv \sum_{k=0}^{\infty} a_k D^k \quad \text{and} \quad B(D) \equiv \sum_{k=0}^{\infty} b_k D^k$$

Hence, for the scheme described by (1.1),

$$F(D) = 1 + D$$

$$B(D) = \sum_{k=0}^{\infty} A(D)(1+D)^k \quad (1.5)$$

$$b_k = a_k + a_{k-1} \quad k = 0, 1, 2, \dots \quad (a_0 = 0)$$

Thapar & Patel have noted that a family of partial response schemes characterised by the polynomial,

$$P_n(D) = (1-D)(1+D)^n \quad n = \{0, 1, 2, \dots\} \quad (1.6)$$

are particularly suited to the magnetic recording channel [Thapar & Patel, 1987]. The frequency response of this polynomial is given by substituting the transform, $D = e^{-j\omega T}$, which yields,

$$S_n(\omega) = jT(2)^n \cos^{n-1}(\omega T / 2) \sin(\omega T) \quad (1.7)$$

The spectrum for various values of n is shown in figure 1.7. As n increases, the increasing number of $(1+D)$ factors cause the roll off at the Nyquist frequency, $1/2T$, to become less severe. The $(1-D)$ factor causes the response to roll-off at D.C. By way of comparison, figure 1.8 shows the general form of the magnetic recording channel frequency response. That the family of partial response schemes in (1.6) are suited to the magnetic recording channel is clear by noting the similarity between the spectral distributions in figures 1.7 and 1.8.

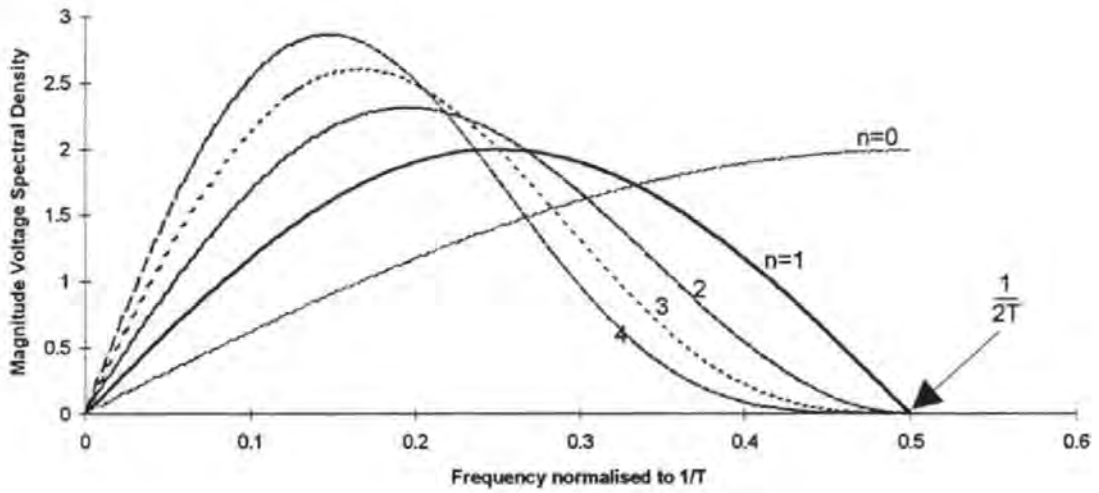


Figure 1.7 - Spectral characteristics of the Partial Response schemes defined by (1.6) for constant signalling rate and various values of n [Thapar & Patel, 1987]

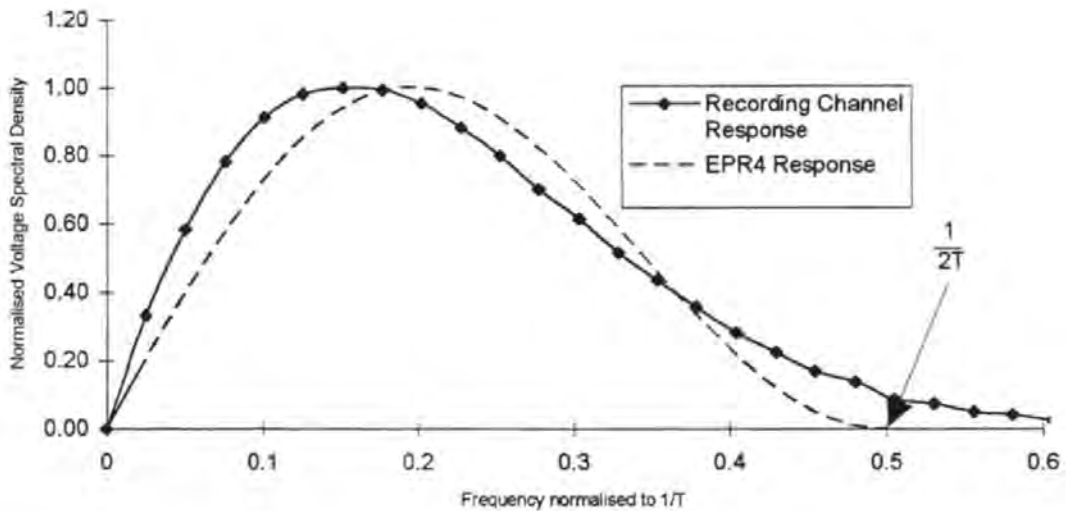


Figure 1.8 - Similarity between the frequency response of the magnetic recording channel and that of the Partial Response channel obtained by setting $n=2$ (EPR4).

In the time domain the similarity is explained by reference to figures 1.9, 1.10 and 1.11. The magnetic recording channel step response (the output from the replay head as it passes over a transition in the media) is shown in figure 1.9. The step responses for the partial response systems obtained by setting $n=1$ and $n=2$ are shown in figures 1.10 and 1.11. (These two systems have become known as class IV and extended class IV partial response respectively).

The $(1+D)^n$ factor in (1.6) is equivalent to the step response in the magnetic recording channel and the effect of the $(1-D)$ factor is to convert this step response into a pulse response. Therefore, the magnetic recording channel is equivalent to a dispersive transmission filter which approximately shapes the transmitted symbols into a partial response waveform. Increasing the value of n and adjusting the signalling period accordingly, squeezes more bits (and more signalling levels) into the natural width of the step response. Alternatively, increasing n for the same signalling period requires a broader step response, with the spectral energy being distributed to the lower frequencies.

Therefore, increasing n allows for a higher signalling rate in the same bandwidth. On the other hand, the number of signalling levels increases with n and so the signal to noise ratio falls. Some or all of this SNR loss can be recovered by the use of a maximum likelihood detector, but, when n is equal to 3 or above, the theoretical recovery gain in the detector is less than the loss in SNR for when $n=2$ [Thapar & Patel, 1987]. Furthermore, the complexity of the maximum likelihood detector rises exponentially with n since the number of required states is equal to 2^n . Therefore, only the two schemes characterised by the polynomials generated by letting $n=1$ (PR4) and 2 (EPR4) have received significant attention in recent years.

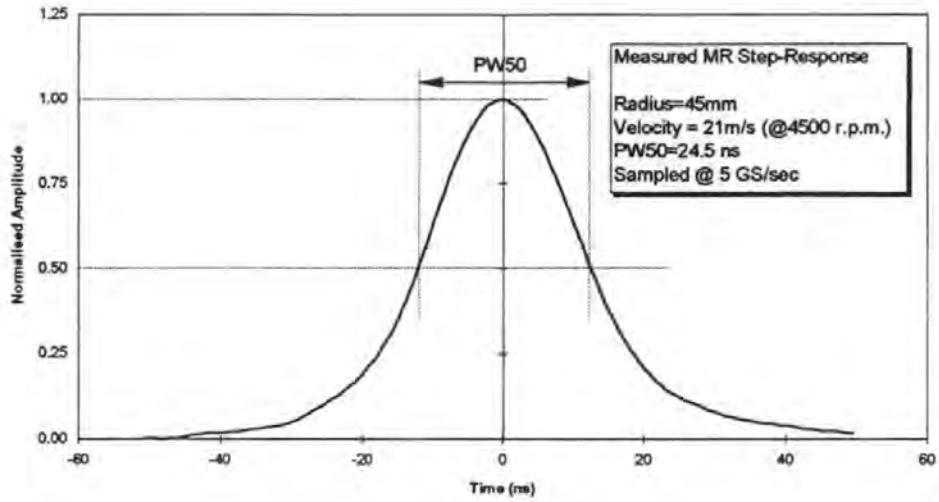


Figure 1.9 - The magnetic recording channel step response (for an MR head).

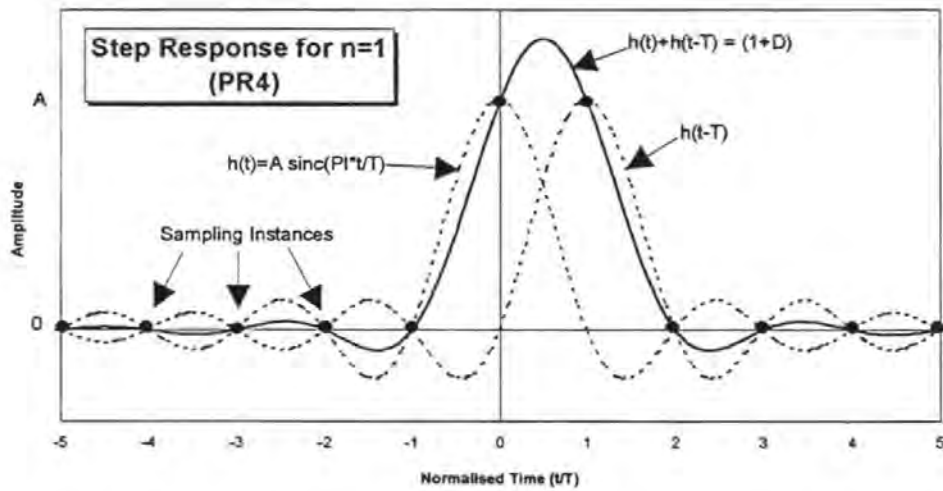


Figure 1.10 - Step response for partial response system $(1-D)(1+D)$ - Partial Response Class IV (PR4)

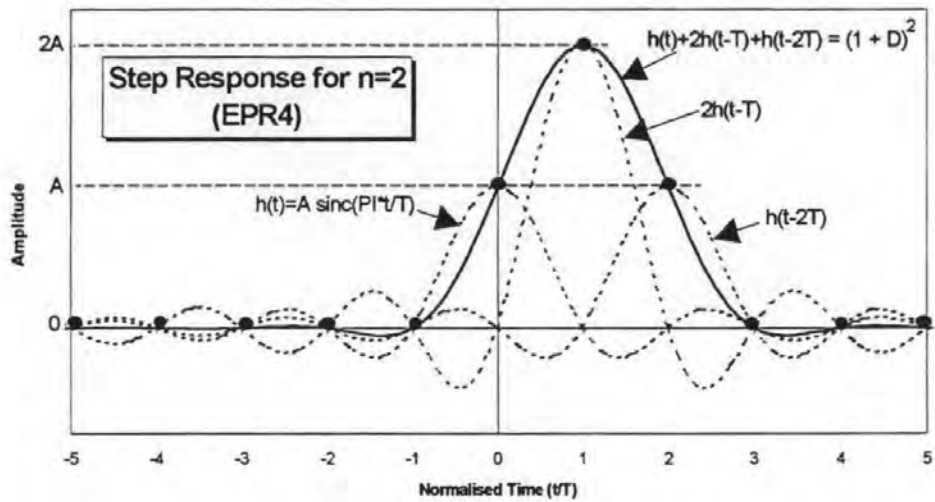


Figure 1.11 - Step response for partial response system $(1-D)(1+D)^2$ - Extended Partial Response Class IV (EPR4)

1.3 Partial Response Equalisation

The magnetic recording step response does not exactly match the PR4 or EPR4 step response. Therefore, equalisation is required before the detector in order to shape the replay waveform to the correct response.

When the spectrum of noise has a dissimilar distribution to a signal being equalised, the signal to noise ratio at the output of the equaliser differs from that at its input and there is a corresponding SNR loss through the equaliser. The SNR loss is dependent on the 'amount' of equalisation required to shape the actual channel response to the target response. For example, comparing figures 1.7 and 1.8 it can be seen, qualitatively, that EPR4 ($n=2$) bears a closer resemblance than PR4 ($n=1$) to the magnetic recording channel and therefore requires less equalisation.

Thapar and Patel have shown that for a modelled Lorentzian² channel, the loss through the required equaliser is greater for PR4 than EPR4 at normalised densities ($PW50/T$) of greater than 1.6³ [Thapar & Patel, 1987]. At a normalised density of 3, the loss through the EPR4 equaliser is approximately 3dB less than that through the equivalent PR4 equaliser - this is due to the closer match of the spectrum and therefore the lower noise enhancement of EPR4. On the other hand, at a normalised density of 1, PR4 outperforms EPR4 with the SNR loss through the equaliser being 1.5 dB greater for EPR4. This is due

²A Lorentzian pulse is often used to approximate the step response in magnetic recording systems. This is discussed in chapter 4.

³PW50 is a commonly used measure of resolution in magnetic recording. Its significance is discussed in detail in chapter 3.

to more signal power than noise being attenuated for EPR4 equalisation compared to that for PR4⁴.

Using Lorentzian simulation, Moon & Carley have compared the performance of a number of partial response schemes, confining the equaliser to a raised cosine type [Moon & Carley, 1988]. At normalised densities of 1 they have found that PR4 has a 2.5 to 4 dB advantage over EPR4 assuming perfect timing. At higher densities ($PW50/T=3$) EPR4 outperforms PR4 by 3.5dB. However, in the presence of timing errors and amplitude modulation of the replay signal due to medium inhomogeneities, they have shown that the EPR4 system degrades rapidly due to its increased number of controlled ISI terms.

Using a Lorentzian simulation, Moon has studied the effect of channel mismatch on signal to noise ratio for PR4 and EPR4 signalling [Moon, 1991]. Such is the case when equalisers have been tuned to one value of $PW50$ and are required to equalise a range of values - for example, when equalisation has been fixed for a range of tracks⁵. This study reports that when the $PW50$ is 10% smaller or larger than the assumed value, PR4 and EPR4 show considerable degradation from the nominal performance and can actually fall below that of a peak detect channel under certain conditions.

Coker et. al. have described the equalisation issues in the industry's first implementation of Partial Response signalling in a disk drive product [Coker et. al., 1991a]. They use a fixed passive equaliser to provide the bulk of the equalisation to PR4. In addition a 3-tap adaptive equaliser is employed to cope with channel variations over the disk surface, and, between different heads and disk. A single signalling rate is chosen such that at a particular

⁴This is discussed in detail in chapter 4.

⁵The magnetic recording channel response varies with linear velocity which itself varies as a function of radius. This is discussed in detail in chapter 3.

radius, the unequalised channel response is "roughly matched" to the required response. In a later paper, Coker et. al. explain the modifications made to this existing design in the second generation Partial Response disk drive product [Coker et.al., 1993]. The combined passive and 3-tap adaptive equaliser is replaced with a single 10-tap to better deal with the changes in channel response over disk radius and between different head / disk pairs.

Using a Lorentzian simulation, Moon evaluates the sensitivity of partial response equalisers to timing errors [Moon, 1993]. Evaluating the performance for 3, 5 and 9-tap equalisers this study reports that PR4 equalisation is highly sensitive to timing errors for a 3-tap equaliser but reduces dramatically for a 5-tap implementation. A 9-tap equaliser provides little improvement over the 5-tap. EPR4 shows much less sensitivity to timing errors for all equaliser lengths, but, as with PR4, performance improves markedly with a 5-tap instead of a 3-tap equaliser. This is also the case at higher densities ($PW50/T=3$) but the absolute sensitivity to timing errors is reduced over the lower density case because of the band limiting. The conclusion is that 9-taps offer the same performance as infinitely long equalisers but 5-taps are adequate and may be preferable in terms of complexity.

1.4 Detection Issues

It has been widely recognised that maximum likelihood sequence detection (MLSD) techniques are best able to exploit the inherent correlation in partial response signalling and provide some degree of detection gain over simple bit-by-bit threshold (full-response) detectors [Forney, 1972; Forney, 1973; Cioffi & Melas 1986; Clark, 1989].

For a given received sequence, the maximum likelihood detector selects an output (decoded) sequence that most closely matches the received sequence out of all the possible output sequences. In its simplest form, the detector finds this by computing the square error between the received sequence and all the possible output sequences and chooses the output sequence corresponding to the minimum squared error. A practical algorithm for implementing this, called the Viterbi Algorithm, was first proposed as a means for decoding convolutional codes [Viterbi, 1967]. However, its use has been extended to decoding signals with intersymbol interference, and in particular partial response signals [Forney, 1972]. A particularly elegant tutorial on the Viterbi algorithm is given by Forney [Forney, 1973].

A number of published works have analysed the performance of the Viterbi detector for magnetic recording applications. Kobayashi describes the application of the Viterbi detector to NRZ and NRZI recording schemes [Kobayashi, 1971]. Cioffi & Melas have analysed the performance of maximum likelihood detection for magnetic recording and have concluded that it offers a theoretical four-fold improvement over that achieved with peak detection (at that time) [Cioffi & Melas, 1986].

Wood & Petersen have described how the Viterbi detector for PR4 signalling can be split into two interleaved (1-D) detectors, each operating at only half the data rate [Wood & Petersen, 1986]. Zeng & Moon have suggested a modified Viterbi algorithm that provides superior performance in a jitter dominant PR4 system [Zeng & Moon, 1992]. Shafiee & Moon have investigated methods to reduce the complexity of the Viterbi detector for EPR4 since it cannot be decomposed into interleaved sequences [Shafiee & Moon, 1992]. Wood has also suggested a method by which EPR4 detection may be implemented more economically than by a full-state Viterbi detector [Wood, 1993]. Sugawara et. al. have proposed an integrated Viterbi detector which will operate as PR4 at low densities (below 1.8) but as an EPR4 detector at high densities [Sugawara et. al., 1993].

Using simulations Newby discusses the sensitivity of PR4 detection in the presence of variations in the nominal parameters of a hypothetical recording channel [Newby, 1989]. Newby notes that the PR4 system is sensitive to variations in variable channel parameters such as head-medium spacing and head gap length and suggests that *"the utilisation of receivers which provide the ability to compensate for variations in channel parameters are likely to become as important in magnetic recording as they are presently in other communications channels"*.

Coker et. al. have proposed how, using the sampler and microprocessor present in a partial response disk drive, a number of value-added features could be added to the drives operation [Coker et. al., 1991b]. Specifically, these are media surface analysis to detect defect sites for subsequent de-allocation, flying height change analysis to detect imminent failure modes and error detection performance estimation to check equalisation performance. The methods rely on the ability of the microprocessor to take control of the channel electronics, write test patterns and analyse the digitised replay samples.

1.5 Summary

A summary of the preceding discussions reveals the following observations. Recent advancements in digital signal processing technology have allowed the data channel designer to step up to the challenge of increasing storage capacity through signal processing means, in addition to those improvements being made elsewhere in the underlying recording component technologies. To this end, partial response signalling has been identified as a suitable way to proceed. This is due to the recognition of the fact that a family of such schemes are particularly suited to the magnetic recording channel.

The signal-to-noise ratio advantage of some of these schemes over peak detection methods has been shown both theoretically and experimentally. Practical issues regarding the reliable detection of multi-level signals dictate that only the schemes known as PR4 and EPR4 are of immediate interest. At moderate densities, PR4 signalling has been shown to give a 2-3dB advantage over peak detection channels which corresponds to a 30% to 50% increase in capacity. The performance of EPR4 over PR4 has been demonstrated to be between 10% and 20% due to its closer match to the recording channel and correspondingly less-severe equalisation. However, whilst the PR4 detector can be split into two interleaved sequences each running at half the data rate, the detector for EPR4 cannot. Therefore, whilst EPR4 provides higher density for the same SNR and error rate, it cannot run at the same potential speed as PR4 if they are both governed by the same signal processing speed constraint.

Both response classes show significant sensitivity to equalisation mismatch if the actual response of the channel is different from that to which the equaliser has been tuned. For this reason it is concluded that adaptive equalisation is essential in the disk drive where not only does the response change with track radius, it can also change significantly between

head and disk pairs. It has been found that 5-taps provides adequate performance in simulation and 9-taps provides the same performance as an infinitely long equaliser. In an actual disk product it was found that 10-taps provided sufficient equalisation and increasing the number of taps beyond this provided no extra benefit.

Even for perfect equalisation, the signal to noise loss through the equaliser required to match the recording channel response to either the PR4 or EPR4 target has been shown to vary as a function of normalised density. At low densities the SNR loss is greater for EPR4 than PR4 because signal power is attenuated more so than the noise power for EPR4 than PR4. At high densities the situation is reversed because more severe equalisation (and therefore noise enhancement) is required for PR4 than EPR4. A dual mode detection system has therefore been suggested which operates with PR4 at low densities and EPR4 at high densities.

It has been suggested that variations in recording channel response may lead to the need for the data channel to pre-determine the recording conditions in order to maximise storage capacity. It has also been shown that the sampler inherent in the partial response signalling method can also be used to provide information about the recording conditions such as flying height changes, the magnetic non-linearities, and, the effectiveness of the equalisation.

1.6 Thesis

The conventional approach to data channel design has been to select an operating point such that in the presence of (apparently) random variations in recording component performance, a minimum required error rate will always be achieved. In practice this means that the data channel is de-tuned from the nominal performance achievable to a performance that yields the minimum error rate for the worst case recording conditions. This is done to ensure that when the hard disk drive is manufactured, a large proportion of the products will actually work. It is noted that whenever recording conditions are better than this worst case, the error rate is better than that required and information capacity is wasted.

It is shown in chapter 3 that some of these seemingly non-deterministic variations in recording channel performance become deterministic once a particular set of recording components are assembled together into a disk drive. However, they are only deterministic from the data channels point of view if it is able to measure them first of all. Therefore, it is noted that the introduction of partial response signalling which has brought with it the sampler and the microprocessor, has also enabled the channel to characterise these deterministic variations for any particular set of recording components to which it is married.

It is shown in chapter 4 that because the recording channel pulse response varies as a function of data rate and the signal to noise loss through a partial response equaliser varies as a function of the recording channel pulse response, the data rate may be used as a variable to tune the performance of detection. Furthermore, if the option is also available to select different classes of partial response, it is shown that considerable flexibility is

provided in achieving maximum storage performance for a given set of recording conditions.

Therefore, it is proposed that a new kind of approach can now be taken towards the design of the data channel. That is, to allow the data channel to become much more adaptive and allow it, on the basis of performance measurements it has made, to select recording strategies that maximise storage capacity whilst maintaining the minimum error rate requirements. i.e., allow the data channel to recover the lost capacity over a fixed-design approach. This new channel is termed *The Adaptive Partial Response Data Channel*.

This thesis investigates and reports on this new concept. Chapter 2 describes the experimental details of this investigation. In chapter 3 a number of recording channel performance variations are investigated. In chapter 4 the proposed adaptive partial response data channel is described and its performance is evaluated with respect to these variations over the fixed design approach. In chapter 5, conclusions are drawn about the investigation and suggestions for future work are made.

Chapter 2

Experimental Details

2.1 The Hard Disk Experimental Test Station

All recording experiments and signal analysis were carried out using the custom designed disk test station shown in plate 2.1.

2.1.1. Mechanical Design

The read/write heads used in this investigation typically 'fly' at heights of 100 nm or less and at relative velocities up to 35 m/s. The integrity and reliability of the head / disk mechanical interface under these conditions is highly susceptible to contaminants and vibration during operation. Sub-micron sized particles or vibration can cause failure of the interface resulting in catastrophic damage to the head surfaces & magnetic components and also the disk surface. These issues necessarily place high demands on the design and quality of the test station.

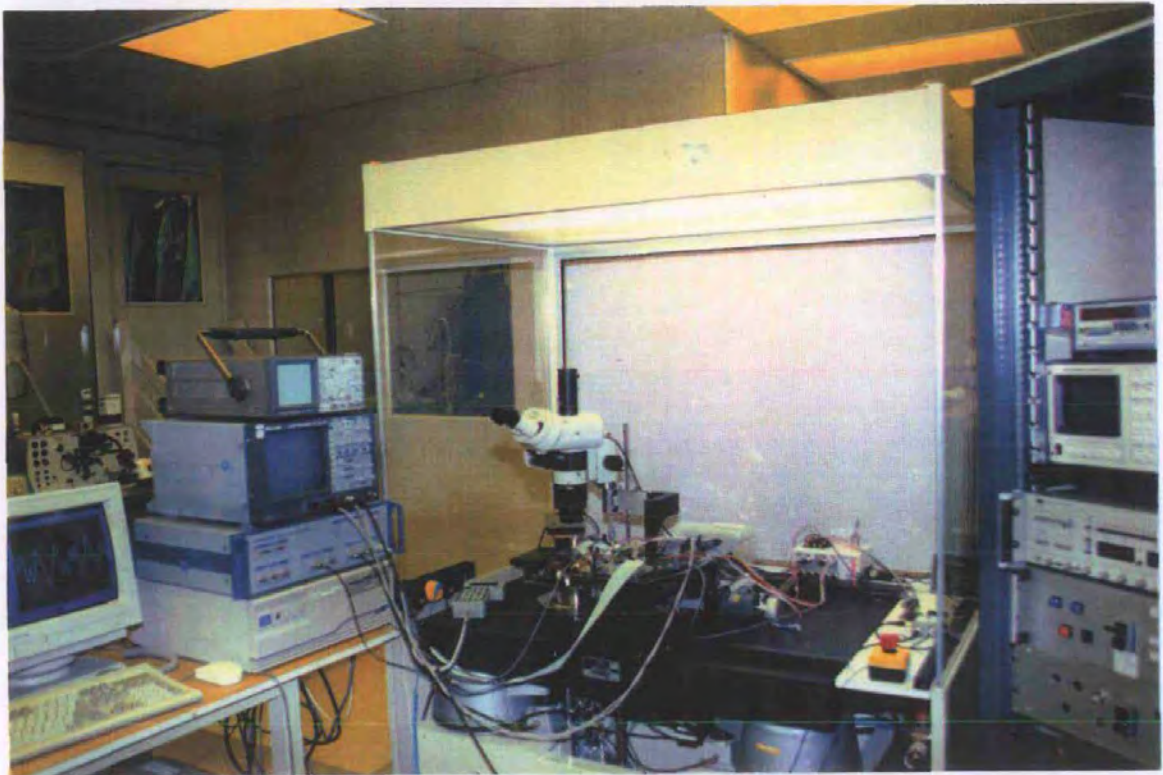


Plate 2.1 - The hard disk experimental test station

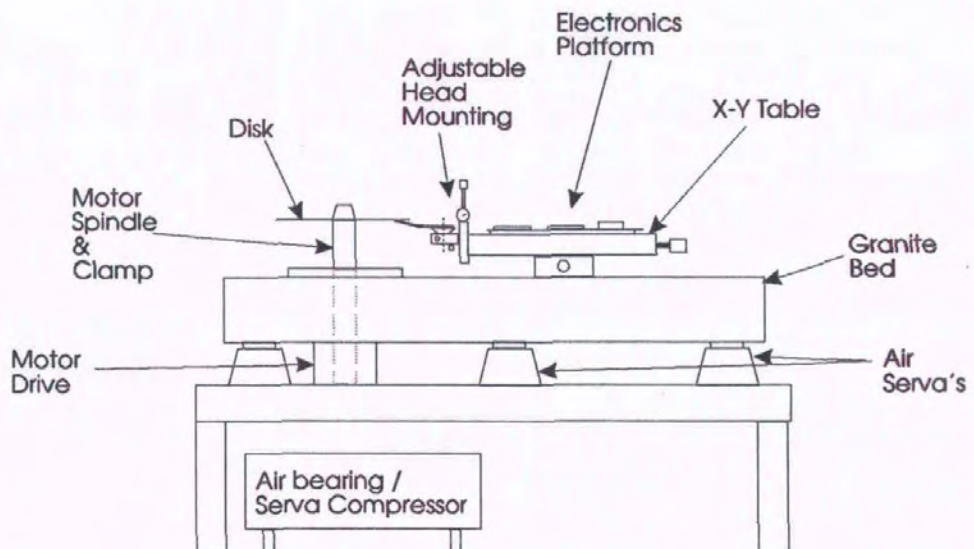


Figure 2.1 - Schematic diagram of the experimental test station mechanics

The mechanical assembly of the test station is shown schematically in figure 2.1. The spindle, clamp, head mounting and head positioning components are mounted on a granite bed supported by air 'servas'. The large mass of the granite bed conjoined with the air serva support suppresses any external vibration being transmitted to the head / disk interface. To minimise the threat from particle contamination, the granite bed and mechanical assembly are housed within a class 100 air booth which itself is located within a class 1000 clean room facility.

Air Bearing Motor and Clamp Mechanism

The disk under test is mounted on a spindle which is supported on air in an arrangement known as an 'air bearing'. The air bearing provides the spindle with almost zero rotational friction and less than 0.1 μm (measured) non-repeatable radial runout. The spindle and clamp mechanism are of considerable mass and are mechanically balanced to ensure stability when they are rotating. The spindle is driven by a 3 phase brushless motor and digitally controlled electronic drive and can operate at speeds between 1000 and 5400 rpm..

It was found that the motor drive gave rise to a large noise component which was picked up by the read head during testing. This could be significantly reduced by shielding all the electronic apparatus in metal boxes and providing each shielded unit with a large braided earth strap to a central earthing point. The best results were obtained when the motor and clamp metal work were also earth strapped but to a separate earthing point.

The disk is clamped firmly in place by a sprung rod which pulls the clamp face against the disk surface and down onto the spindle. The clamp is operated by an air hydraulic pump.

Head Micro-positioner

The majority of the work in this investigation requires that the head may be positioned to sub-micron accuracy. Primarily, this requires accurate positioning of the head in the x-y plane normal to the spindle. This is achieved by employing two stepper motor beds mounted orthogonally, one on the other. Relative accuracy is achieved by employing a closed loop feedback path with optical diffraction sensing.

The stepper motors both have a rotational resolution of 40000 steps per revolution and are attached to a 0.25 revolution per mm lead screw. This yields a lateral movement of 10000 steps per mm, or, $0.1\mu\text{m}$ per step. The tables are able to position to an absolute accuracy of $\pm 0.5\mu\text{m}$ when racked fully out and in again from a known position. Calibration marks on the diffraction grating allow the table position to be calibrated before recording tests begin. Incremental position accuracy is of the order of plus or minus 0.1 micron.

Adjustable Head Mounting Unit

In addition to the two degrees of freedom provided by the head micro-positioner, the necessities of this investigation require further degrees of freedom which are provided for by a specially designed head mounting unit shown in plate 2.2 and schematically in

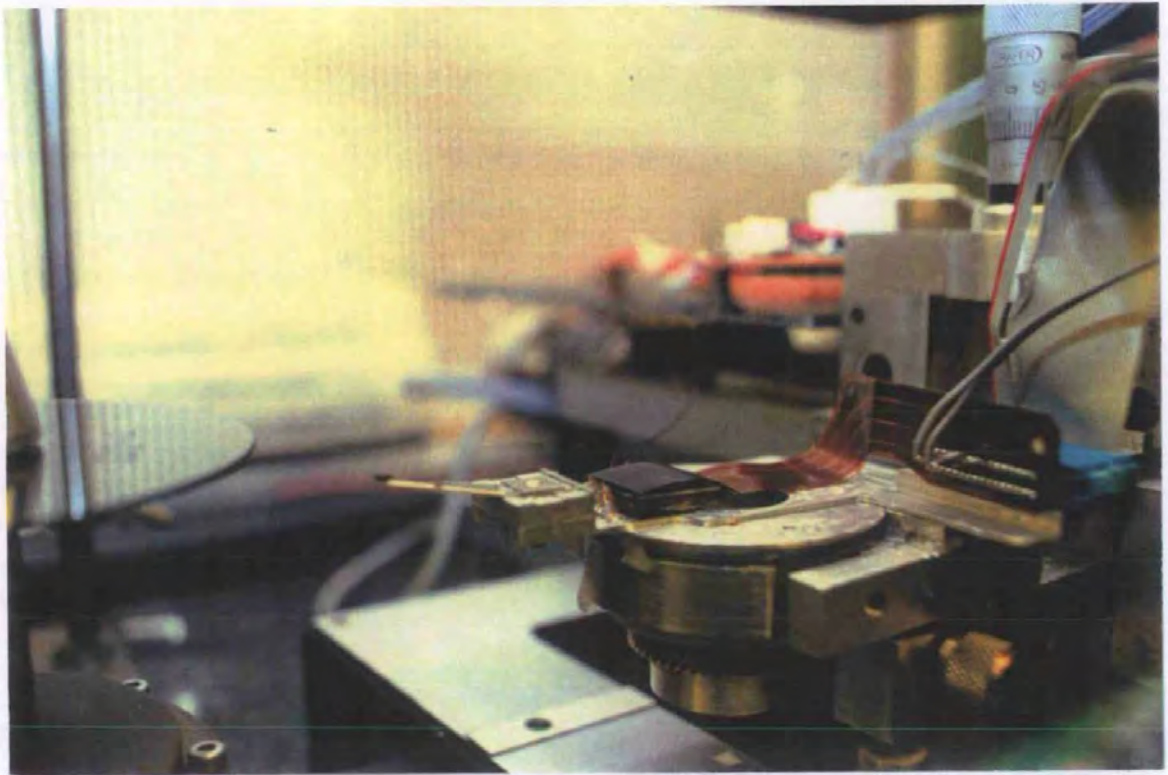


Plate 2.2 - Adjustable head mounting unit

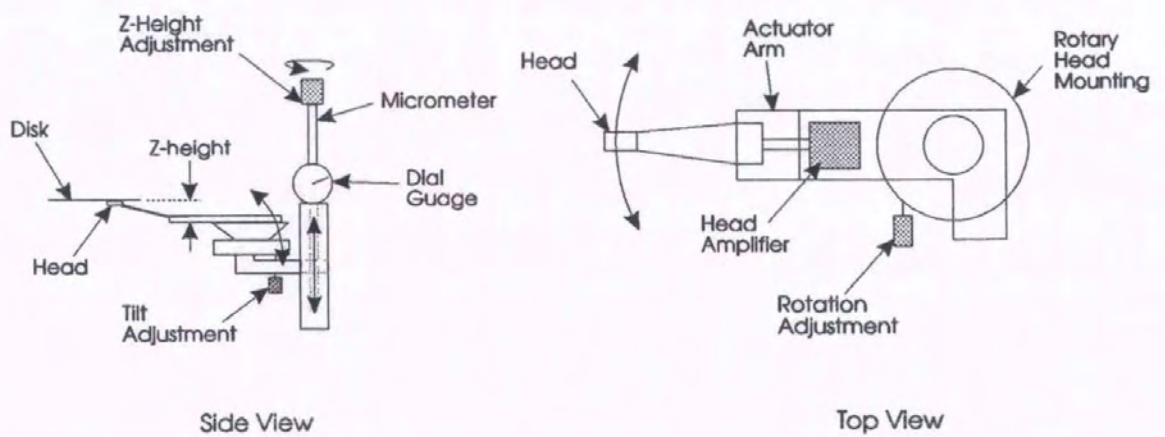


Figure 2.2 - Schematic diagram of adjustable head mounting unit.

figure 2.2. The mounting unit attaches to the head micro-positioner and has numerous mounting holes and attachments onto which the recorded head(s) may be mounted.

The head mounting unit provides z-height adjustment in the plane parallel to the spindle and allows the loading force and therefore flying height of the head to be adjusted. The dial gauge allows z-height adjustment to an accuracy of $\pm 50\mu\text{m}$. The bed onto which the head attaches can be rotated through 360° . This facility is used for adjusting the skew of the head pole / gap with respect to a recorded track and for emulating actual disk drive actuator geometries. Finally, the bed also tilts which allows the attitude of the head to be adjusted with respect to the disk surface.

2.1.2 Automated Test System Hardware

Figure 2.3 shows schematically the hardware components of the automated experimental test system. Circuit diagrams are given appendix B. The write channel comprises a data generator, write current programmer and head write-driver and is synchronised by the write controller. The head amplifier, pre-amplifier, low-pass filter and digital storage oscilloscope form the read channel. The write and read channel, as well as the x-y tables and motor, are controlled via RS232, IEEE488 and GPIO interfaces from the PC running custom designed software developed by this author, called 'DISKLAB'. This software allows virtually any testing procedure to be automated by allowing the user to write test programs in a high level control language and run them in DISKLAB. This facility was particularly important in the gathering of the media noise results and response measurements detailed later in this investigation.

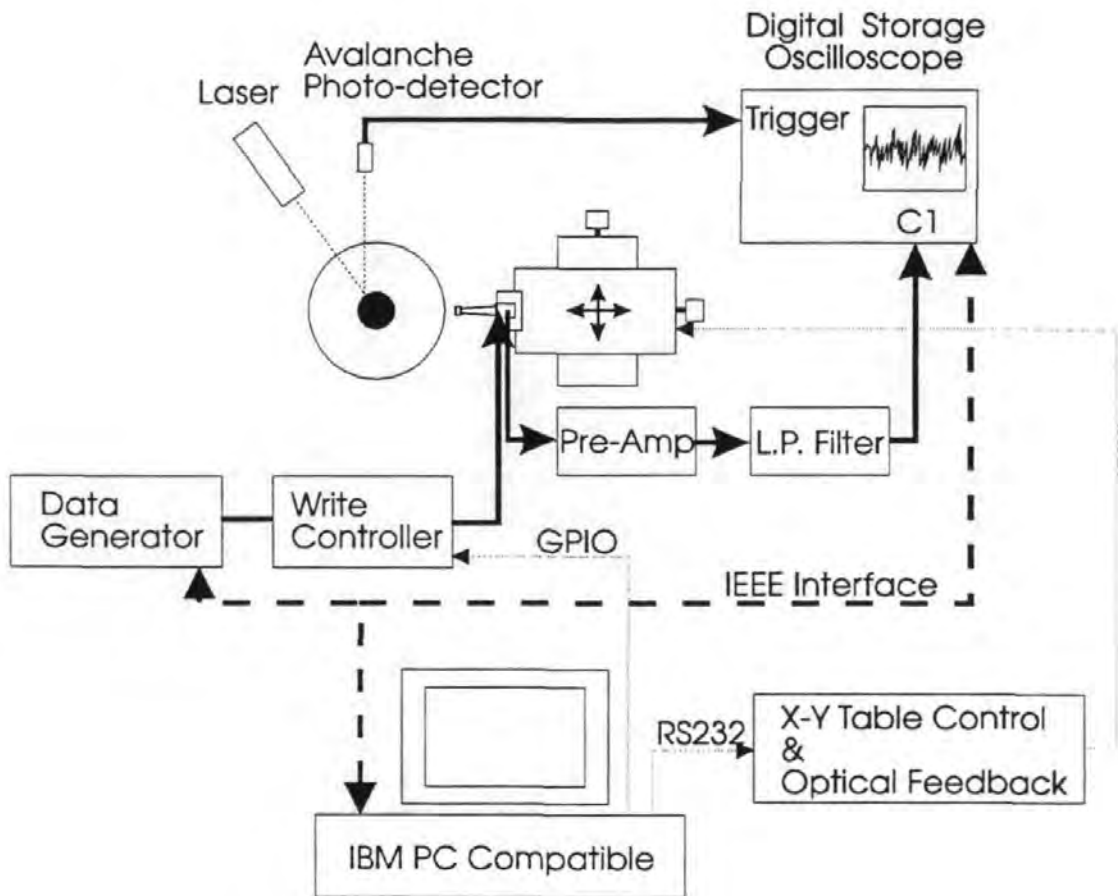


Figure 2.3 - Schematic diagram of the experimental test system

The Write Channel

Figure 2.4 shows schematically the operation of the write channel. Data is generated in the PC either automatically or by the user in an ASCII text file format. It may then be encoded and precoded if desired using software algorithms and sent to the data generator as a file of 8-bit words through the IEEE interface. A Lecroy 9109 data generator was employed for this task. This instrument can store up to 512k bytes of data in separate files with each file containing up to 65 kbytes. Data streams of unlimited length can be generated by linking different files together and repeating them indefinitely. Data rates of up to 200 Mbits/sec can be generated. The data appears differentially at the output of the Lecroy 9109 terminals and is connected to the write driver either via coaxial connectors or ribbon cable (depending on the write device being used). The versatility of the Lecroy 9109 generator allowed permanent sector patterns such as equaliser training field and Phase-lock field to be stored in the memory and inserted into the data stream as and when necessary.

The write device is a fast differential current driver which alternately reverses the current direction through the writing head according to the data pattern sent from the Lecroy 9109. For the dual mode inductive write / MR read head, a VTC 7800 device was used with a switching time of 7 ns. For the perpendicular pole head an SSI 521R device was employed with a switching time of 32 ns. The magnitude of write current is set externally using the programmable constant current source. The current source is programmed via the interface connected to the computer controller. Inside the write driver a current mirror drives the selected value of current through the recording head.

The write driver and data generator are triggered by the 'write controller' which provides all the necessary control signals to the various components of the system (figure 2.5). The write controller monitors the angular position of the disk via the 'index pulse' which it receives from either the opto-detector on the spindle or the laser index (to be described later). At some arbitrary time the write controller receives an asynchronous write trigger from the PC. At the start of the next index pulse the write enable line is brought low and the write driver goes into write mode. At the end of the index pulse the write data enable line is brought low which triggers the data generator to start sending data. At the start of the next index pulse both write data and write data enable lines are reset until the next write trigger request. The action of bringing write enable low before write data enable ensures that the write driver has settled down before it starts writing data. Also, it always erases the section of track before the recorded test pattern. This enables the oscilloscope to easily locate and trigger on the start of the recorded pattern during read mode.

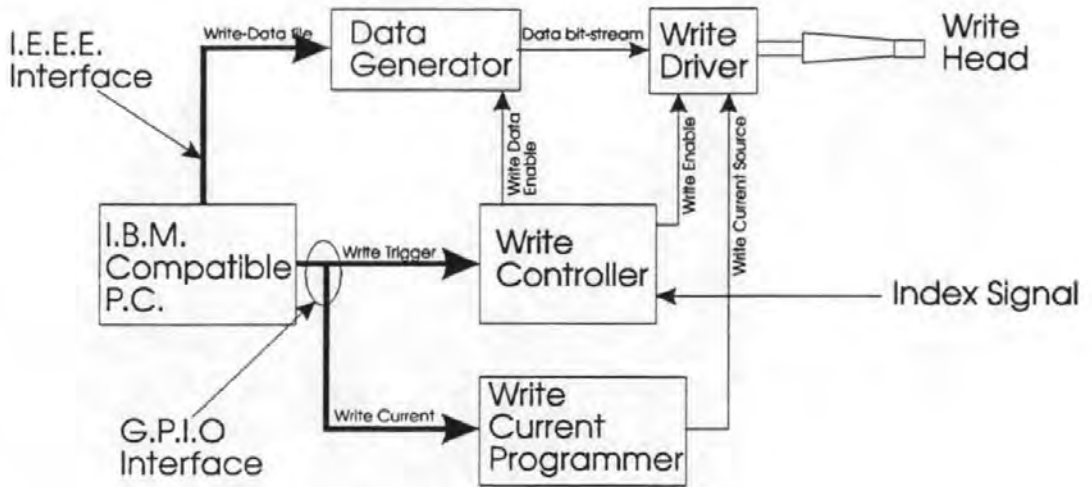


Figure 2.4 - The Write channel

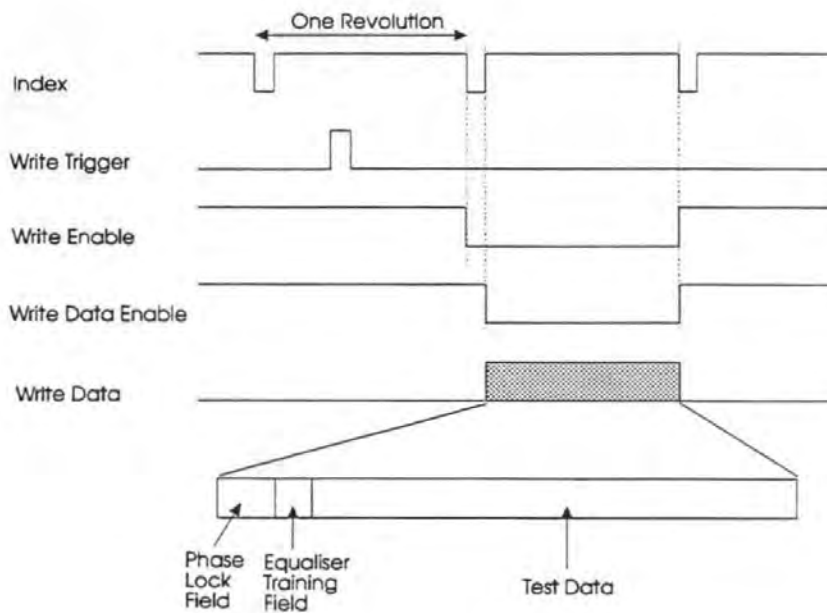


Figure 2.5 - Timing synchronisation during write-mode

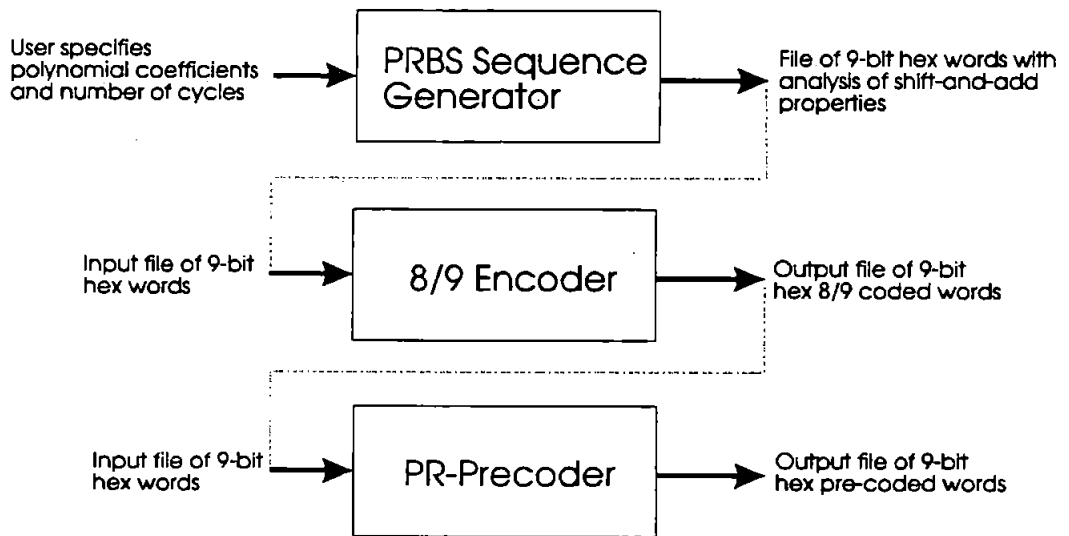


Figure 2.6 - Modular software functions (optionally) generate test data sequences.

The Read Channel

Figure 2.7 shows schematically the operation of the read channel. The head is connected to a dedicated head preamplifier which acts as a low noise differential amplifier with a typical gain of 100 V/V. It is important for this preamplifier to operate at as low a noise level as possible as it is always the first amplification stage in any cascaded amplification system that dominates the overall noise performance. Therefore, typical hard disk read amplifiers have an input noise figure of only 0.5 - 1 nV / $\sqrt{\text{Hz}}$. Similarly, it is important that the head amplifier is located as closely as possible to the read head to reduce external pickup and transmission line effects in the interconnection. For this reason, the head read / write device is usually located within the head arm & disk enclosure as close to the end of the head arm as practically feasible. In this investigation, the read amplifiers were mounted on the rotating head mounting assembly, some 10mm away from the head base. It was found that severe noise pickup from the motor drive and/or oscillation occurred if the preamplifier was mounted on the main circuit platform.

Following the read amplifier an optional second amplification stage is employed which provides wideband gain up to 50 MHz of approximately 10V/V. This amplifier is based around an NE592 video amplifier and was typically only needed for the investigations into the perpendicular media noise characterisation.

Following the amplification stage(s) an optional low-pass filter is employed to cut out unwanted noise and interference signals. Two equiripple differential filters were constructed providing cut-off frequency at 40 or 50MHz. The oscilloscope also had optional filtering with a cut-off at 30MHz. With these three options all filtering

requirements were met. The NE592 amplifier and low-pass filters were constructed using common input / output connectors for versatility.

This investigation is primarily concerned with signal processing in the digital domain. To this end a digital storage oscilloscope connects directly to the output of the read amplification / filtering system. The oscilloscope digitises the read signal into discrete time samples. The samples are then transferred to an IBM compatible Personal Computer (PC) for further analysis and processing. The use of the digital storage oscilloscope and PC are in direct replacement, and equivalent to, the Analogue to Digital Converter (ADC) available in a hard disk partial response detection channel. This implementation allows for ease of flexibility in the choice of processing techniques without compromising the validity of the experimental data.

The oscilloscope is capable of sampling at up to 1 GSamples/sec and storing up to 50000 consecutive samples. Additionally using repeated sampling of repetitive waveforms it is able to effectively sample at up to 10 GSamples / sec by interleaving the acquired records. On-board waveform processing enables common signal analysis techniques to be performed in the oscilloscope including Fast Fourier Transform (FFT), signal averaging and waveform arithmetic.

The Laser Index

The work on media noise in this investigation requires accurate angular location of the head with respect to the disk to allow readings to be taken from exactly the same place each time the disk rotates. A number of schemes have been reported [Tang, 1985;

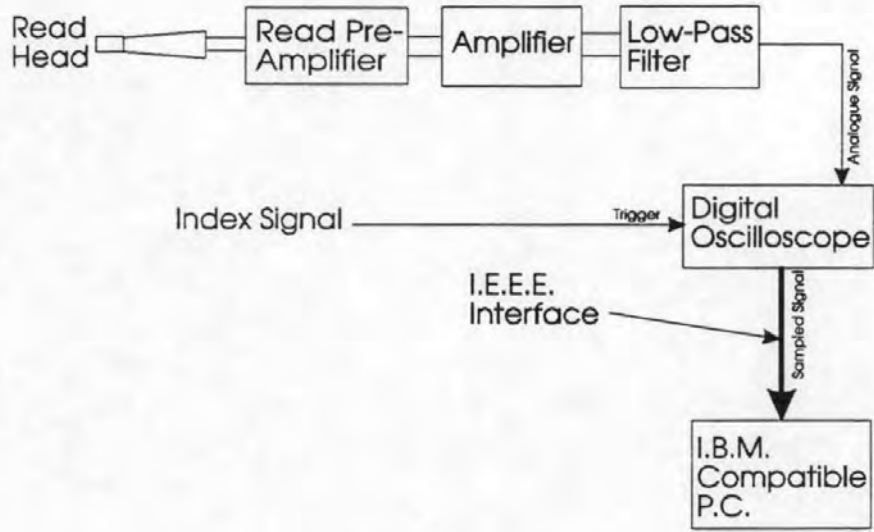


Figure 2.7 - Schematic diagram of the read channel

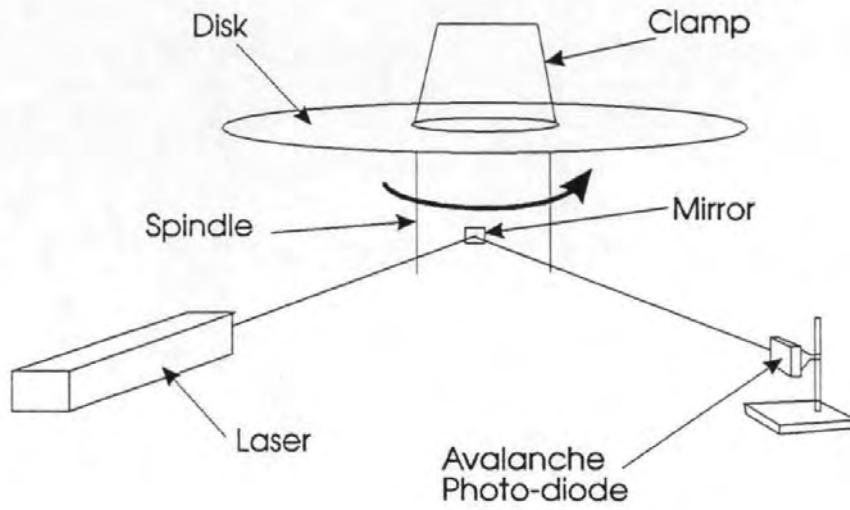


Figure 2.8 - Laser Index method to provide stable angular reference independently of head position

Yarmchuk, 1986; Hoinville, 1991] but here a different approach is taken based on the use of a laser and an avalanche photo-diode.

The technique is illustrated in figure 2.8. A small front silvered mirror is attached to the spindle and the laser and photodiode are arranged such that each time the spindle rotates the laser spot is scanned over the photodiode's sensitive area. Each time the laser scans the diode it rapidly breaks down giving rise to a large amplitude current pulse. This is amplified and brought out on a connector. Providing the mirror, laser and photodiode are stable, the pulse generated by the diode will correspond to an exact angular position on the disk. This position is then used to provide an index by which to take measurements. The advantage of this system is that the indexing is highly stable (jitter is measured to be $\pm 5\text{ns}$) and is unrelated to head position which means that no matter where the head is on the disk, it is possible to determine an absolute angular reference. The use of the laser index has also led to a method of accurately determining the head radius and absolute co-ordinates with respect to the disk centre. This is detailed in appendix C.

There were occasions when even the laser index could not provide a stable enough trigger for the measurements being undertaken. Namely, when the sampling rate of the oscilloscope exceeded 50 Msamples/sec to capture signals with frequency components greater than 25 MHz. In this case, the state triggering modes of the oscilloscope were employed. Here, a low frequency trigger pattern is written to the disk some distance before the test data. In read mode, the oscilloscope trigger system is set up to trigger off the replay signal only when it has firstly detected an index pulse. In this manner, a trigger accurate to the jitter in a replay pulse is generated. The low frequency nature of

the trigger signal compared to the test data ensures a high signal to noise ratio and low jitter.

Many of the experiments undertaken in this investigation relied on the ability of the oscilloscope to average the replay signal over many disk revolutions to reduce the random electronic noise and interference and leave only the deterministic signal. This was particularly the case for the investigations on media noise where the amplifier being used to amplify the head signal yielded a higher noise voltage than that which was attempting to be measured.

By averaging a deterministic signal, all the non-deterministic noise is reduced as the square root of the number of averages taken. Therefore, if the signal to non-deterministic noise ratio is 30dB and it is required that a signal to non-deterministic noise ratio of 40dB is needed to measure a particular effect, the non-deterministic noise must be reduced by 10 times. Therefore, 100 averages are required. Typically, the number of averages required varied from 100 to 1000 depending on the phenomena being investigated.

2.1.3 Automated Test System Software

Initially, the test-stand control and data measurement functions of the test system were separate software routines but as the complexity of the system grew and the need for tight linking between the control and measurement aspect became apparent, these two functions were merged into one. Consequently, a disk test station operating system has been developed which allows the user to program complex control and measurement sequences quickly and easily using a high level control language and programming interface.

Figure 2.9 shows a captured screen image of the automated software system (which has been called 'DISKLAB') which illustrates its operation. The upper window shows details of waveforms which have been captured by the oscilloscope and transferred to the PC. The lower window is the command editor which allows the user to enter commands via the keyboard. The command line editor part of the software interprets the pseudo-english command and calls the relevant software routine to perform the task. Such tasks include setting the write current, moving the head to a desired position, writing data, transferring waveforms from the oscilloscope to the PC, sending data patterns to the Data Generator etc. The lower bar of the screen display informs the user of the current working disk directory, the position of the head co-ordinates and the number of waveforms currently active in the computer memory.

The software allows the user to save and load waveforms to the computers' hard or floppy disks. This enables waveforms to be stored indefinitely for future processing and makes them available to other analysis packages. Typically this post processing involved many calculations and so it was performed 'off-line' on another, faster computer.

In addition to the command line features, the software also allows complex test procedures to be implemented by means of so-called 'script' files. Script files are text files that contain the same commands that can be typed in at the keyboard. The user is allowed to 'run' a script file which passes the commands one-by-one to the command line interpreter. Therefore, script files may be written to perform tests that require many repeated operations and that would otherwise take a lot of time to perform manually. Another advantage of this approach is that once script files have been debugged and are known to work, operator errors in the method and measurement of the experiments are eliminated from the results. From this authors experience this was a major advantage since some of the results presented in this thesis required more than 100 individual experimental measurements. An example script file which measures signal output as a function of write current (the saturation curve) is shown below figure 2.9.

```

DISKLAB - Magnetic Recording Analysis Application - (c) N.Darragh C.R.I.S.I.
----- Waveform Memory -----
No. 1  502 pnts  22-03-19  00:13:33  EQTRAIN.WFM
No. 2  502 pnts  11-05-19  13:13:38  oscilloscope

----- Command Editor -----
send 9109 ch2_filter off
send 9109 ch2_invert.off
> load eqtrain.wfm
Loaded waveform No.1
> current 30
Write current is now : 30
> 9109load square.wav 1
> write
> transfer c1
Grabbed waveform No.2
> save 2 fred.wfm
Waveform 2 saved to file : FRED.WFM
>

C:\NC600\SOURCE\DISKLAB1      X=UNDEF  Y=UNDEF      W'fns : 2

```

Figure 2.9 - 'DISKLAB' software user interface

Example Script file to perform Saturation Curve measurement : -

```

current 0                ; resets write current to 0
clock 10mhz              ; sets clock rate to 10 MHz
dgen load square.wav    ; loads a square wave pattern

loop 10{                 ; perform the following 10 times :-
  write                  ; write the pattern
  scope clear_sweeps    ; clear the oscilloscope & acquire signal
  wait 10                ; wait 10 seconds for acquisition
  scope cursor c1 amplitude ; get amplitude of waveform
  current +2ma rel      ; increment current by 2mA
}                        ; repeat until finished

```

2.2 Software Modelling of the Data Channel

It was noted in section 2.1 that the oscilloscope was equivalent, and in direct replacement to, the sampler found in a partial response detection channel. This is the case if the sample rate and phase of the oscilloscope analogue to digital convertor is the same as that as the real sampler. In practice, this is not the case since it is not possible to clock the oscilloscope with an externally derived clock. Therefore, to overcome this problem, the replay signal is 'over-sampled' by many times to form a pseudo-analogue waveform. The waveform is then passed through a software timing recovery algorithm to yield the samples that would be generated in a real sampler. Linear interpolation is used to derive the amplitude of the waveform between two oscilloscope samples. Provided the signal is sampled fast enough, the linear interpolation is accurate. Typically the signal was oversampled by 10 times. That is, if the highest frequency component in the signal was 50MHz, the minimum sampling rate (according to Nyquist) would be 100 MS/s and the signal was actually sampled at 1GSamples/sec (to yield 10 times oversampling).

The functional elements of the adaptive channel have been implemented using software models which mimic the operation of the corresponding hardware solutions. These include, Automatic Gain Control (AGC), adaptive equalisation, decision directed timing recovery, and Viterbi Maximum Likelihood detection (figure 2.10) Furthermore, waveform generators which produce waveform samples in exactly the same format as those transferred from the oscilloscope have been implemented to produce perfect Partial Response and Lorentzian waveforms. A White Gaussian noise generator may be used to add noise to the real or model waveforms and test the abilities of the detection system. The use of this modularised approach, where the performance of the data channel can be

analysed using real or simulated disk data, has greatly enhanced the understanding process (figure 2.11). The software algorithms for these functions are listed in appendix D.

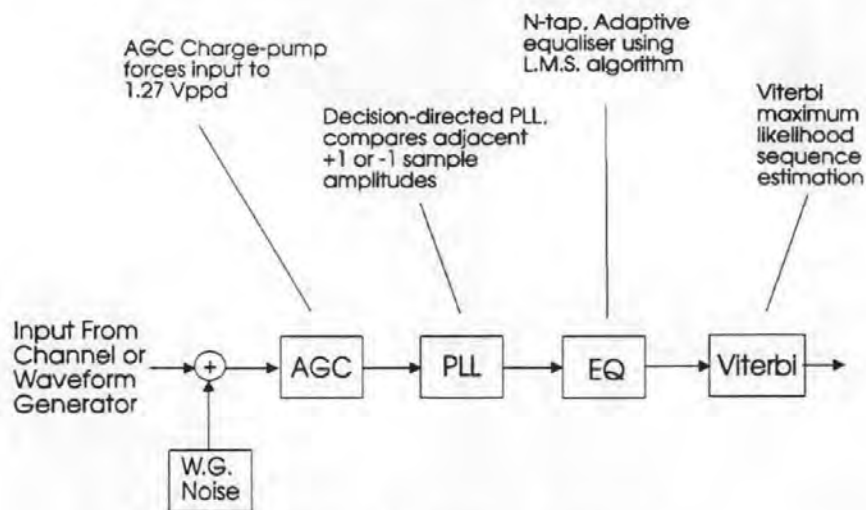


Figure 2.10 - The software data-channel

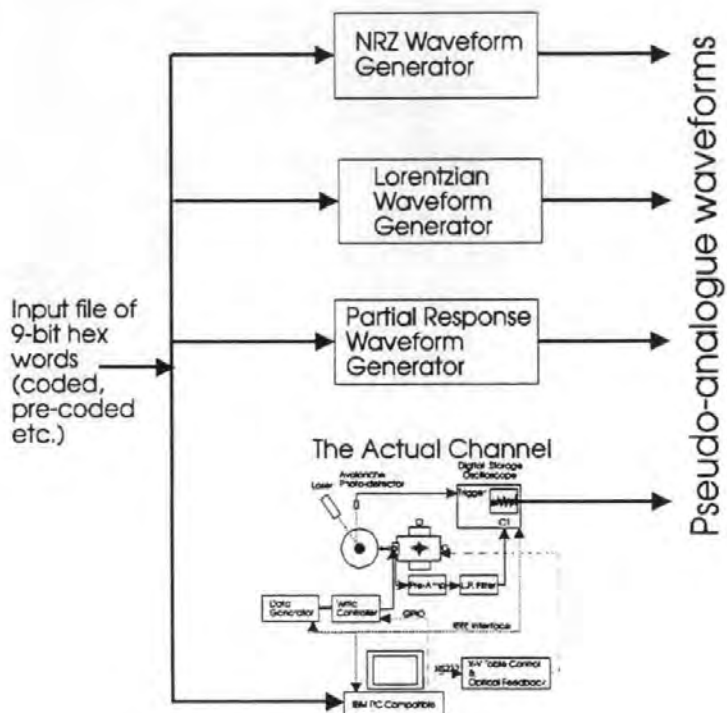


Figure 2.11 - Model waveform generators have the same format as real sampled data. Therefore they can be interchanged and compared easily in the software detector.

2.3 Head / Media Parameters

The parameters for the perpendicular recording components used in this investigation are as follows.

Head : Single-pole, thin-film
 25-turn, 50 Ω , 2-wire common inductive write / read
 12 μm track width
 0.3 μm pole length

Disk : Dual layer perpendicular anisotropy
 Underlayer :-
 10 μm , 80:20 NiFe (wt%)
 Relative Permeability 500
 Recording Layer :-
 160 nm, 79:21 Co:Cr (at%)
 Coercivity 800 Oe
 Saturation Magnetisation 225 emu/cm^3 .

For reasons of confidentiality, it is not possible to list all the above parameters for the longitudinal head and disk used in this investigation, only that the head is a dual-mode inductive write (4 μm width), MR read (3 μm width), thin-film design. The reader is asked to note that this investigation is not concerned with the absolute recording performance of these longitudinal components, only the variations in recording performance between them and over the disk surface - they are used as typical examples of state-of-the-art longitudinal recording components.

Chapter 3

Results & Discussion 1 :

Channel Variation Characterisation

3.1 Introduction

In this chapter the magnetic recording channel is characterised in respect to the variations in signal and noise phenomena that the data channel is required to cope with in a typical hard disk system. In such a system, the information is stored linearly along concentric tracks over the disk surface. The signal and noise characteristics of the system are shown to vary over two key parameters; head position over the disk surface (both radially and linearly along the recorded track) and between head-media pairs (for a system which contains multiple recording surfaces). The changes in channel response are measured as a function of these variables and the measured response characteristics are quantitatively related to the underlying recording process. Predictions concerning the current and future significance of these variables are made in the light of the observations and the expected trends in hard disk recording technology. Finally, since it is the purpose of the adaptive channel to overcome some or all of these variables, the information that the channel will need in order to make its adaptive decisions must be identified.

The signal is characterised by the channel step response, that is, the response of the replay head to a step change in magnetisation from one direction to the other (an isolated

transition in the media). In many linear systems, the response of the system to a step input is an output step which exhibits oscillation with an exponentially reducing amplitude over time. In that case it is often convenient to characterise the system by its step-response rise-time. In the magnetic recording channel, the response to a step input is normally a pulse. Therefore, in this case it is convenient to characterise the step response in terms of its zero-peak amplitude and output pulse width. This is defined as the pulse width in time at 50% zero-to-peak amplitude, and is termed PW50. Because the information is stored on a medium moving at a velocity, v m/s, there is a relationship between the time domain (in which most of the measurements are taken) and the spatial domain (which relates to how the information is physically represented in the medium). Therefore, PW50 may be expressed in terms of time or distance and the relationship between the two is given by,

$$PW50_{\text{distance}} = PW50_{\text{time}} \times \text{velocity} \quad (3.1)$$

Whereas the PW50 yields important information about the resolution of the channel, the step-response pulse amplitude yields important information about the error rate performance of the channel. The bit error rate is determined by the statistical variance of noise with respect to signal amplitude at the input to the data detector. The step response pulse forms the basic unit of information in the magnetic recording channel. Therefore, characterisation of step response pulse amplitude will yield information regarding the signal to noise power and therefore error rate. The noise characteristics in the recording channel may be correlated or uncorrelated with the signal, and may vary independently to signal amplitude. It is therefore necessary to study noise in its own right and later combine both signal variance and noise variance to determine signal to noise ratio over the variables under consideration.

3.2 Channel Variation over Disk Radius

3.2.1 Step-Response Pulse Width

Figure 3.1 shows the step response of the recording channel at track radii of 21mm, 33mm and 45mm for the MR head used in this investigation. The pulses were obtained by averaging the read signal from a written track comprising equally spaced transitions recorded at a low enough frequency such that the replay pulses are distinctly separated. The amplitudes have been normalised and only the positive going pulses are shown here, corresponding to a step change in magnetisation from the reverse direction to the forward direction (arbitrarily chosen - it is noted that for step magnetisation reversals in the opposite sense, the replay pulses are negative going).

One can see from figure 3.1 how the pulses broaden in time as the head is moved from the outer towards the inner radius. Figure 3.2 shows the relationship between track radius and $PW_{50\text{time}}$ normalised to the pulse width at the inside radius. At the outside radius the pulses are almost half the width of those at the inside and the characteristic is somewhat curved between the two. There are two primary effects that produce this characteristic; linear velocity variation and flying height variation.

The linear velocity between the disk surface and the head varies over the radius of the disk according to the simple relationship, $v=\omega r$, where v is the linear velocity, r is the track radius and ω is the angular velocity of the disk. The signal produced by the read head is a geometric convolution of the transition perpendicular field distribution and the head sensitivity function [Middleton, 1989]. Therefore, assuming a constant physical transition length, the widths of the replay pulses in time vary inversely proportionally to the speed at

which the transitions pass under the head. The inverse velocity relationship is also shown in figure 3.2 (normalised to the inside radius). The disagreement between the inverse velocity characteristic and the observed pulse-width characteristic is explained by consideration of the second major effect, flying height variation. This alters both the recorded transition length and the replay pulse width.

The flying height of the head varies over radius because the flying height is a function of the air velocity between the head and disk. For an MR head, the replay pulse width in the spatial domain ($PW50_{\text{distance}}$) has been shown to approximately relate to the head geometry, head-media separation and transition length via the relationships [Middleton, 1989],

$$PW50 = \sqrt{(l+t)^2 + 4(d+a)(d+a+\delta)} \quad nm \quad (3.2)$$

where, d is the head - media separation, t is the thickness of the MR stripe, l is the distance from the shield to the MR stripe, and δ is the media thickness. The transition length parameter, a , for a thin-film disk is given by,

$$a = \left(\frac{2}{\sqrt{3}} \frac{M_r \delta d}{\pi H_c} \right)^{\frac{1}{2}} \quad (3.3)$$

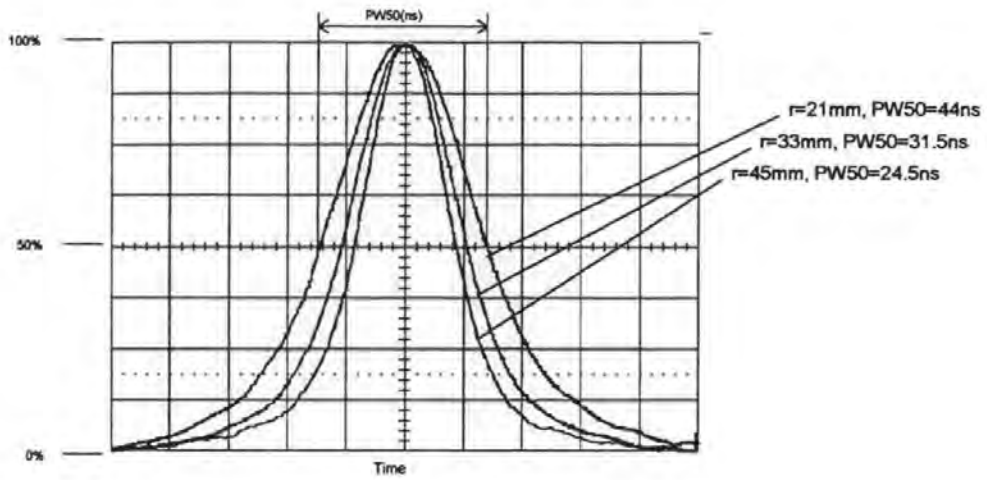


Figure 3.1- MR head replay pulses at track radii of 21mm, 33mm and 45mm. The amplitudes have been normalised

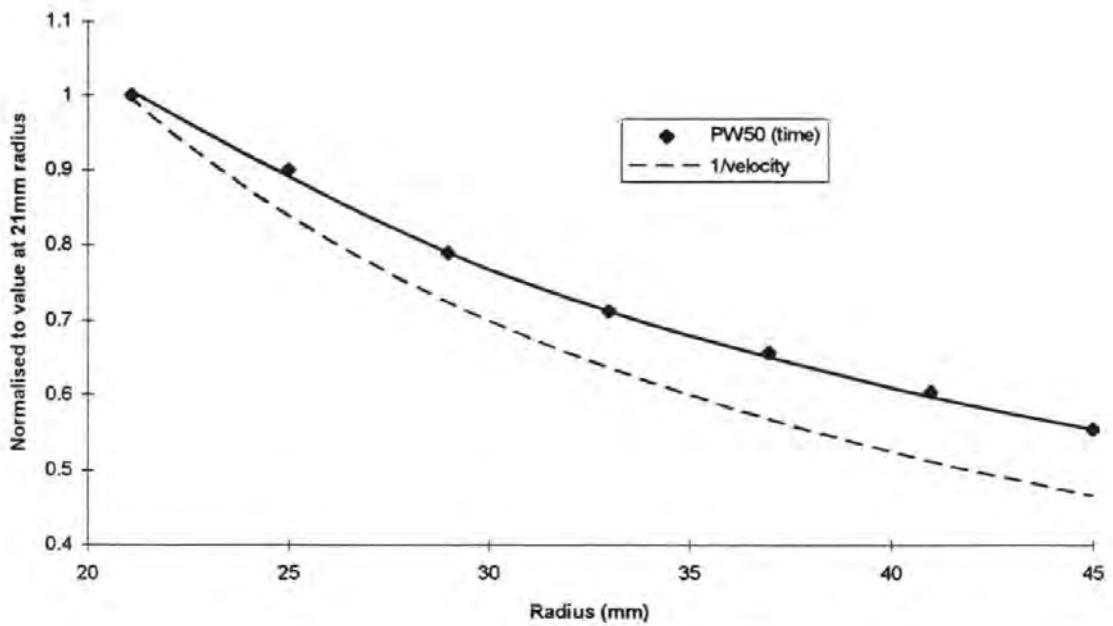


Figure 3.2 - Dependence of pulse width (time) on track radius

where M_r and H_c are the remanence and coercivity of the disk respectively. The head-media separation is linearly related to the flying height but with an additional factor to account for media overcoat thickness and pole-tip recession from the head flying surface. Consequently, even with a zero flying height, there will always be some small additional gap between the head poles and the medium magnetic layer.

These empirical relationships, have become commonplace tools which provide good agreement with experimental data and which are useful for comparative measures. Using (3.2) and (3.3), $PW50_{\text{distance}}$ and the transition length parameter are shown plotted in figure 3.3 for the fabrication data and range of flying heights applicable to this head and media.

One can see from this figure that $PW50_{\text{distance}}$ and flying height are approximately linearly related over this range. Hence, a simplified expression relating head-media separation to $PW50_{\text{distance}}$ may be determined,

$$d = \frac{PW50_{\text{distance}} - 277}{3.3} \quad (3.4)$$

Using the experimentally measured data in figure 3.2, the $PW50(\text{nm})$ may be calculated from (3.1) and therefore the flying height profile for this head over the radius of the disk may be obtained. This is shown plotted in figure 3.4. One can see that the radial variation in flying height is somewhat linear with the exception of the deviation at the inside radius. Overall there is about a 40% change in flying height from the inside to the outside radius. The measured range of flying heights from 60-90 nm are in good agreement with the manufacturers data.

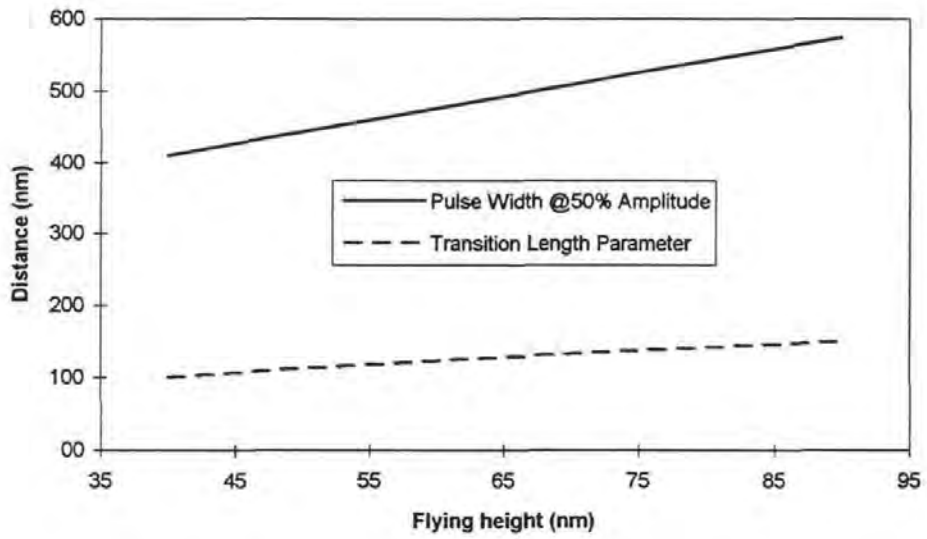


Figure 3.3 - Theoretical MR replay pulse length and transition length vs flying height

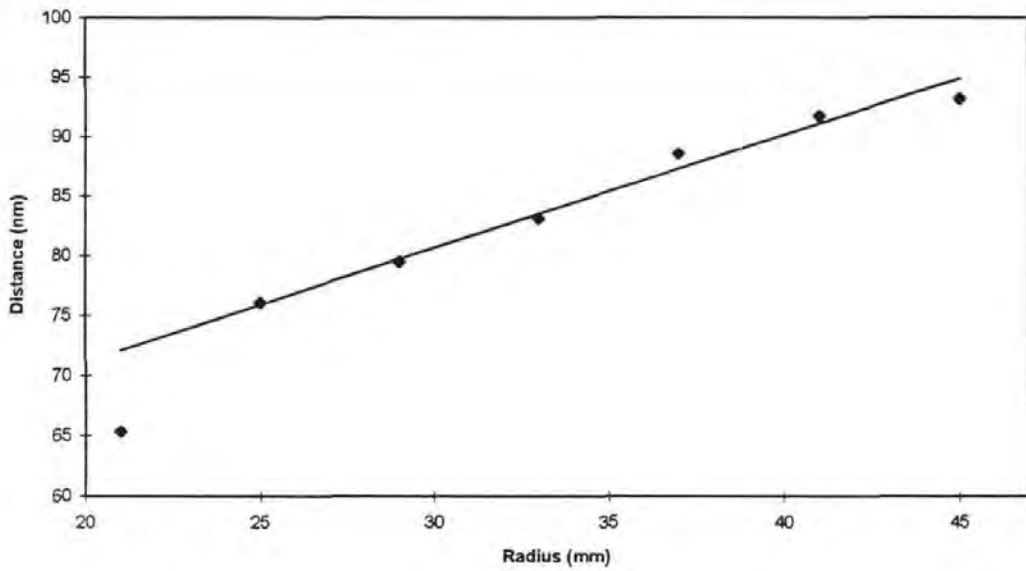


Figure 3.4 - Flying height characteristic over radius.

The transition length parameter plotted in Figure 3.3 indicates that the recorded transition length also varies as a function of flying height. This may be explained by the fact that at greater head-media separations the media is influenced by relatively weaker head field gradients. Consequently, the writing field is not so well defined and the transition region tends to broaden. However, it is also noted that the transition length is approximately one quarter of the measured pulse width. Therefore, it is the head sensitivity function (determined by the shield gap length) that primarily determines the width of the replay pulses and not the recorded transition length [Schneider, 1985].

The range of velocities encountered by the head (and therefore, flying height variance) depends on the ratio of the outer to the inner recording radius; a factor which tends to increase with the continuing trend towards smaller disk sizes [Grochowski & Hoyt, 1993]. This is because as the diameter of hard disks reduces, the total mass reduces as a near cubic function of radius (the thickness also tends to reduce in addition to the surface area). A lower disk mass requires lower torque. Therefore, smaller motors may be employed with a corresponding greater than proportional reduction in disk clamp area and inner recording radius.

Summary

The $PW_{50\text{distance}}$ provides a measure of the spatial resolution of the channel - the narrower the pulses, the closer they can be placed to each other and the higher the recording density. Therefore, as $PW_{50\text{distance}}$ increases, the spatial resolution of the channel decreases and so too does the achievable recording density for a constant error rate. It has been shown in this section that the spatial resolution of the channel reduces as a function of flying height, which itself is a function of track radius. Therefore, achievable

storage density (bits/mm) along the recorded track for a constant error rate must reduce as a function of radius. In the future, the ratio of the outer recording radius to the inner recording radius is expected to increase and therefore yield an even greater difference in achievable storage density between the two extremes. On the other hand, if in-contact recording is achieved (or equivalently, constant flying height) the spatial resolution of the channel will no longer change as a function of radius and the achievable storage density at the outside radius will be the same as that at the inside for the same error rate.

This result has important implications for the proposed adaptive channel. In a flying height varying channel it would not be correct to measure the pulse width at some arbitrary radius on the disk and then assume the same spatial resolution (bits/mm) would be achievable at any radius on the disk surface. Indeed, unless the flying height profile for that particular head were precisely known, the channel would have to measure pulse width over all radii in order to accurately determine the spatial resolution. On the other hand, if the flying height was known to be constant over radius then it would be possible to measure the pulse width at one location and assume that the same spatial resolution was available over the disk surface.

3.2.2. Step-Response Pulse Amplitude

Figure 3.5 shows the step response pulse amplitude plotted as a function of radius for the MR head. The signal amplitude measurements were made by recording a constant frequency pattern of isolated transitions and then measuring the average peak-peak amplitude of the read signal along the track. One can see from figure 3.5 that the signal amplitude decreases as a function of radius, with the amplitude at the outer radius being approximately 10% less than that at the inside. As was the case for the PW50(nm) characteristic, this may be explained by the increasing flying height as the head moves from the inside to the outside radius.

For the MR head the peak pulse amplitude is determined by the magnitude of the perpendicular flux coupled into the head sensing element when it is over the centre of the recorded transition. Amongst other parameters this is a function of head/media spacing and the magnitude of the remanent magnetisation of the media. In digital magnetic recording it is assumed that the media is always in either one of the two saturated states, or, in transition between them. However, in order for this to be the case, the writing current through the record head must be great enough to ensure media saturation. The required magnitude of writing current is determined by reference to the saturation curve, which is shown plotted for this media and head in figure 3.6. The curve shows the output signal amplitude as a function of recording current for a constant recorded frequency. One can see from this figure that at 10mA write current the output signal amplitude rises rapidly with increasing recording current and then peaks and remains constant for recording currents greater than about 20 mA. At recording currents greater than 20 mA, the media is assumed to be saturated and relaxation of the recording field (whatever it may be) always results in the same remanent magnetised state. This important result shows that the magnetic recording

channel is peak amplitude limited. At recording currents above the saturating value, signal amplitude does not increase. Therefore, for saturation recording, the recorder (transmitter) has no control over signal amplitude whilst the information is being stored (transmitted). Furthermore, it is the hysteretic nature of the recording medium that makes anything other than saturation recording impractical. In any state other than saturation, the recording channel is highly non-linear. This is because the application of a non-saturating field to the medium results in a new remnant magnetisation which depends not only on the magnitude of the applied field but also on the existing magnetisation of the medium. Hence, the combined applied and existing field cause the hysteresis curve to be traversed in a non-deterministic way and the meaning of the conveyed information is lost. Consequently, conventional multi-level signalling techniques for digital data recording have met with only limited success [Price et. al., 1978; Mackintosh & Jorgensen, 1981].

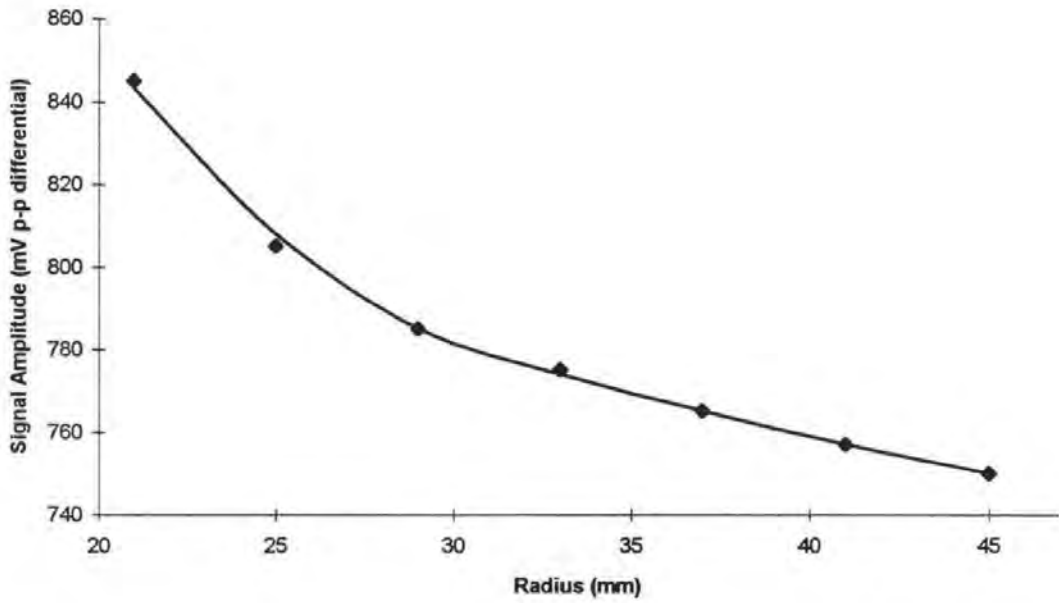


Figure 3.5 - Signal amplitude as a function of radius

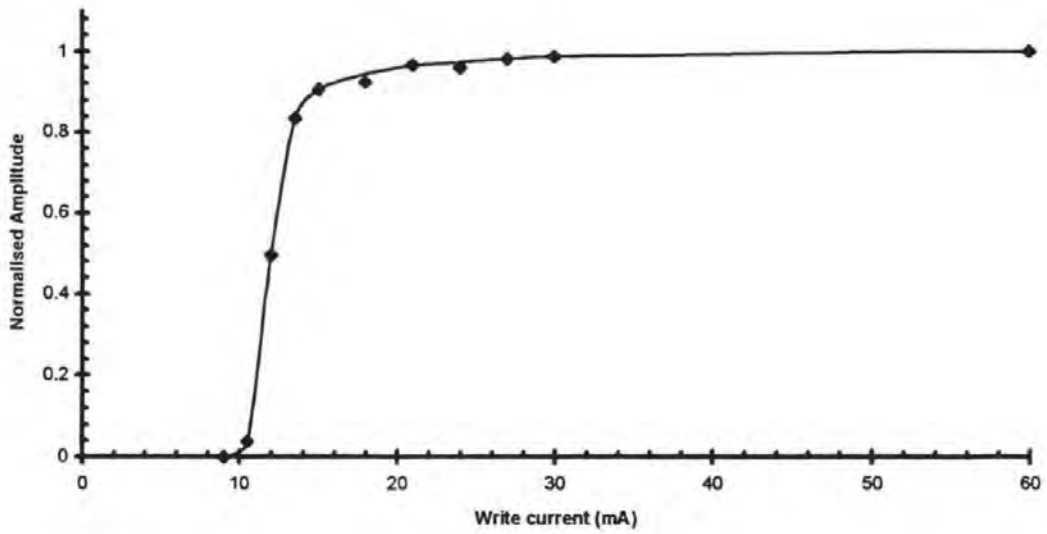


Figure 3.6 - Normalised signal amplitude as a function of write current

3.2.3 Noise

The noise in the replay signal for a hard disk system comprises two primary sources; thermal noise arising from the head resistance and amplifier input impedance (electronic noise), and, media noise arising from irregular discontinuities in the magnetic structure of the medium.

3.2.3.1 Electronic Noise

The electronic noise of the system is determined by calculating the r.m.s. amplitude of the noise signal voltage at the output of the amplifier terminals and averaging the result over 100 measurements. For this measurement the digital storage oscilloscope is used to capture segments of the noisy signal and calculate the r.m.s. amplitude. The noise is considered to be stationary and so the ensemble of segments have the same statistical properties as the noise signal itself. The sum of all thermal and noise contributions at the output of the amplifier and with the disk stationary was measured and found to be 8.3 mV r.m.s in a bandwidth of 30 MHz. The noise generated by the amplifier was not precisely known but was determined by subtracting orthogonally the contribution from the head resistance via,

$$V_{Nhead} = \sqrt{4KTBR} \quad V_{r.m.s.} \quad (3.5)$$

where K is Boltzmann's constant, 1.38×10^{-23} joules per degree, T is the temperature (degrees Kelvin), B is the bandwidth (Hz) and R is the resistance of the element (ohms). In a 30MHz bandwidth at room temperature the thermal noise generated by the 15Ω MR element appearing at the output terminals of the amplifier is calculated from (3.5) to be 2.6 mV r.m.s. Hence, the thermal and electronic noise generated by the amplifier is calculated to be

7.89 mV r.m.s and accounts for 90% of total electronics noise. From the data in figure 3.5, the signal to electronic noise ratio (defined as the ratio of zero-peak signal amplitude to r.m.s. noise) ranges from 33dB at the outside radius to 34dB at the inside radius.

3.2.3.2 Media Noise

Unlike electronic noise which is assumed to be stationary, white and Gaussian, media noise has been shown to be signal dependent. The primary source of media noise in longitudinal thin-film media arises from the irregularity of the transition between one saturated state and the other [Baugh et. al., 1983; Tong et. al., 1984; Belk et. al., 1985, Arnoldussen & Tong, 1986]. It has been noted that the common practice of analysing media noise using a spectrum analyser does not take into account its non-stationary aspects and can therefore yield incorrect conclusions [Tang, 1985; Yarmchuk, 1986]. In the spectral analysis method, the level of media noise is determined by integrating the spectrum of the head readback signal over the system bandwidth and subtracting the electronic noise power as calculated before. The problem with this method is that since the media noise is primarily associated with the transitions, the media noise amplitude is very much lower when the medium is in the d.c. erased state than if it has transitions recorded in it. Furthermore, for a medium with recorded transitions, the spectrum analyser averages the measurement over time and, importantly, does not give account of where the noise is actually located within the signal.

A more suitable measurement of medium noise is presented here and is based on the work by Bertram and Aoi [Bertram et. al., 1986; Aoi et. al., 1986]. It is argued that at the centre of the transition the medium is in a maximally disordered state - the domains being randomly organised in magnetisation direction. This state may be induced on a larger scale by DC-demagnetising the medium using the record head.

Here, a section of the track is forward erased to saturation. Next, the direction of write current is reversed and set equal to a fraction of its normal saturating value and the section of track is reverse erased. Then, using a stable trigger, repeated samples of the section of track are captured and averaged using a digital storage oscilloscope. After 1000 such averages the random (electronic) noise is reduced by some 30dB to leave a small, but measurable media noise signal. The r.m.s. amplitude of this sample is then calculated and noted. The experiment is repeated by forward erasing to saturation but with increasing magnitudes of reverse erase current. At some intermediate reverse current value, the media noise signal rises sharply in amplitude. At the point where this signal is a maximum, the write current through the head is that required to place the medium in a d.c. demagnetised state; a state where the medium domain structure is maximally disordered and random. As the reverse current increases beyond this value, the medium is more and more reverse saturated and the noise reduces again.

The reverse erase characteristic is shown in figure 3.7 at three radii. One can see from this figure that at the outside radius the maximum medium noise occurs at a higher reverse erase current than that at the inside radius. Also, the magnitude of the maximum media noise is lower at the outside radius than at the inside. Once again this phenomena may be attributable to variations in the flying height of the head [Bertram et. al., 1986]. At the outside radius the higher flying height requires that a higher write current is required to place the medium in the d.c.-demagnetised state. Similarly, at the inside radius, the lower flying height means more noise signal is coupled into the read element of the head. Relatively, the signal and media noise remain constant and the signal to media noise ratio is 27 dB at all measured radii. This is, of course, to be expected since the media noise and signal should change proportionally the same with flying height. It can be seen that with a

magnitude of 18 mV r.m.s, the media noise dominates all noise sources and accounts for approximately 90% of the total noise voltage (20 mV r.m.s.).

This is in contrast to the signal to noise characteristic produced by the more commonplace inductive thin-film head. The signal amplitude for an inductive head is proportional to the rate of change of the flux that is coupled into the head poles as it reverses between one bit cell and the next. Conversely, the MR head is sensitive to absolute flux magnitude, primarily perpendicular, which is maximum at the centre of the transition. The MR head output does not therefore decrease with decreasing linear velocity as it does with an inductive head (where the corresponding rate of change of flux is lower at the inside radius). Moreover, systems employing thin-film inductive heads give rise to a higher electronic noise component than MR heads since the resistance of the coil can be 3 or more times greater than that of the MR sensing element. Also, for an inductive head, the high-power (noisy) write-current transistors are permanently connected across the read coil (since the same coil is used for both write and read operations). Therefore, the associated thin-film amplifiers also tend to be much noisier.

Consequently, data channels employing inductive heads tend to be thermally noise limited with the media noise contributing a smaller proportion of the overall noise voltage. As in this investigation, with an MR element, the primary noise component tends to be media noise. Therefore, with an inductive head the signal to noise ratio (SNR) worsens at the inner radii since the noise is more or less constant over radius but where at the inner radius the signal is a minimum. For an MR head the SNR is more or less constant at all radii; the sensitivity to signal flux and noise flux remaining proportionally the same. Similar arguments have been noted by other authors [Comstock, 1989].

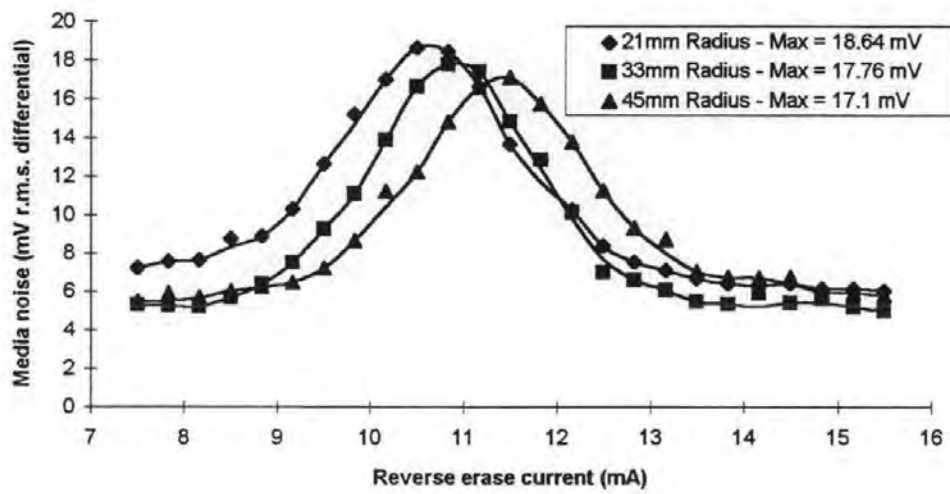


Figure 3.7 - Reverse erase noise characteristic.

The insensitivity of the MR head signal amplitude with respect to radius is one of the main factors driving their development for hard disk applications. The MR head is able to transduce flux into signal energy even at very low head-medium speeds. Therefore, as form-factors reduce and the velocity at the inner radius reduces, the signal to noise ratio remains acceptable for the MR head whereas that for the inductive head does not. Consequently, the trend towards smaller form factors inevitably means the widespread introduction of MR head technology.

Summary

The bit error rate of the channel for a given detection method and storage capacity is a function of the signal to noise ratio into the detector. It has been shown in this section that the SNR for an MR head is constant over radius; it is media noise limited and media noise scales with signal amplitude over radius. On the other hand, the SNR for an inductive head is not constant but varies according to radius due to the signal dependence on rate of change of flux, and, the dominance of electronics noise over media noise (which does not scale with signal). Therefore, depending on the underlying recording components, the proposed adaptive channel will need to determine what the distribution of noise is and whether it varies as a function of radius. If the latter is affirmed, the channel will be required to adopt a suitable strategy to recover the loss in signal to noise ratio at a given radius.

3.3 Channel Variation along the Recorded Track.

The variation in channel performance considered here is short to medium variations in recording performance over the surface of the media which, unlike the previous analysis, are generally not correlated with radial position. These range from short scale asperities or 'dropouts' which can corrupt the signal over the length of a few bits, or, medium-long scale variations which effect signal performance over relatively more bits but typically in a less dramatic way. The short scale asperities are typically caused by micron-scale particles, or holes, on or in the recording layer. The medium scale variations are typically attributed to variations in the magnetic quality of the recording layer due to non-uniform sputtering during the manufacturing process. The effect of both types of variation is to cause amplitude modulation of the replay signal as the head travels along the track.

The laser index and waveform averaging technique described in chapter 2 is used here to investigate a number of spatial phenomena in recording media. The results of the following investigation have led to a published paper [Darragh et. al., 1993].

3.3.1 Underlayer Domain Noise in Perpendicular Recording Disks

Whereas media noise in longitudinal disks as been shown to be associated with the recorded transition and therefore rises with recording density, it has been modelled [Zhu & Bertram, 1991] and shown experimentally [Okabe & Yamamoto, 1992] that the media noise in perpendicular recording reduces with increasing transition density. This is because it is believed to be associated with the recorded bit cell area between transitions rather than any irregularity in the transitions themselves. In this part of the investigation the technique described above is employed to demonstrate that there is an additional and significant noise

component in dual layer perpendicular recording media which arises from the inclusion of the magnetically soft underlayer.

Figure 3.8(a) shows a typical 12.5 mm sample of perpendicular media noise extracted from a d.c. erased track. The fine detail of the media noise is not visually resolved in this figure but ones attention is drawn to its dual frequency nature; a high frequency signal superimposed by low frequency perturbations. Figure 3.8(b) (upper trace) is an expanded 125 μ m section of the 12.5mm sample and shows the high frequency signal in closer detail and its spectrum (lower trace). The noise is characterised spectrally as being wide band with a peak at a spatial frequency of 0.5 cycles/micron which is of the order of a recorded transition length for this media. This noise is deterministic provided the medium is not re-written between measurements; repeating the experiment and calculating the cross correlation between the newly acquired sample and the first yields coefficients close to unity. When the medium is re-written by a field in the opposite direction and a new sample of media noise is extracted, it is found to be un-correlated with the first, with a cross correlation coefficient of zero. These observations and the spectral content of this noise source are in good agreement with results presented elsewhere [Indeck et. al., 1991]. Zhu has argued that this noise component arises from the random placement of reverse domains in the recording layer of the medium [Zhu & Bertram, 1991].

Of greater interest here is the low frequency noise signal which is observed as a result of the relatively long samples of noise that this experimental procedure is able to capture. In order to analyse this noise in greater detail the recording layer noise is filtered out by applying a 300 kHz low-pass filter to the captured signal in figure 3.8(a). The result is shown in figure 3.9(a). The perturbations range from widths of 100-500 microns. This is further concurred by the spectral analysis, figure 3.9(b), which shows a peak at a spatial

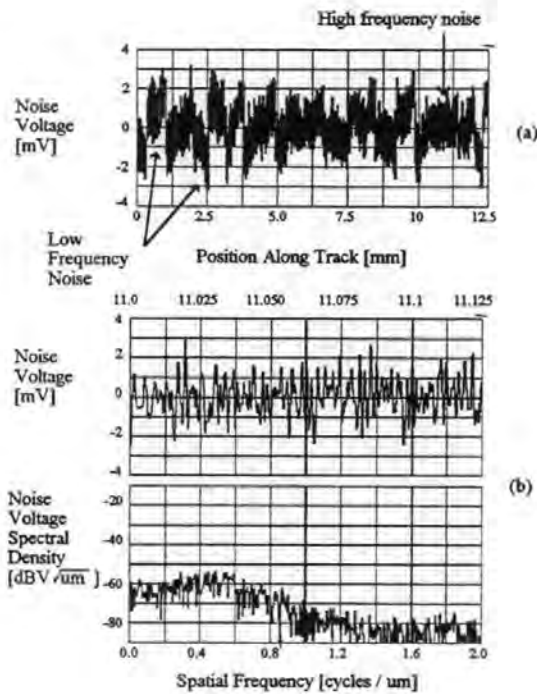


Figure 3.8 - Perpendicular dual-layer media noise samples.
 (a) 12.5 mm long sample of dual-layer perpendicular media noise
 (b) Section of sample in (a) showing the high frequency media noise. The lower trace is its spectral density.

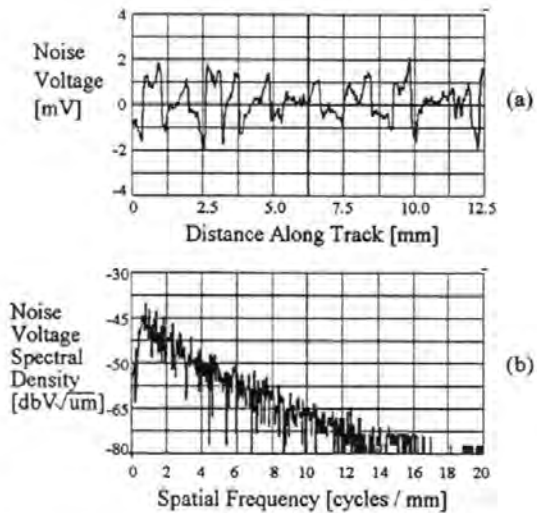


Figure 3.9 - Low frequency perpendicular media noise
 (a) Low frequency noise after the high frequency noise has been removed by a filter.
 (b) Spectral density of (a).

frequency of 1 cycle/mm and a sharp roll-off to around 12 cycles/micron. Unlike the recording layer noise which has a spatial frequencies of the order of the transition length (1 micron), this noise source is correlated over a distance corresponding to many hundreds of transitions (and therefore bits of data). The amplitude is of the same order as the recording layer noise and is therefore significant for a media noise limited system.

Correlation analysis of this noise source in a similar manner to that performed on the recording layer noise show contrary results. Firstly, repeating the experiment with no intervening write fields from the head yields a new sample which, like the recording layer noise, has a cross-correlation coefficient close to unity. However, when the medium is reverse erased and the experiment repeated, unlike the recording layer noise, this noise source does not change; the cross correlation remains as before, close to unity. The conclusion from this result is that the noise cannot arise from the recording layer of the medium, since if it did, the second sample would be the mirror image of the first yielding a cross correlation coefficient of minus unity.

If such a result had occurred, the low frequency noise could have been attributed to repeatable modulation of the flying height or large scale variations in the performance of the recording layer. However, the noise is deterministic and must arise from a magnetic source otherwise the head would not detect it. Therefore, it is concluded that the noise must arise from the underlayer of the recording disk.

In an attempt to show that the low frequency noise is arising from the underlayer an experiment is conducted to show whether there is any overall pattern to this noise source over the surface of the disk. This is done by extracting samples of the low frequency noise in steps from radii between 60mm and 30mm; each starting from the same angular reference

determined by the laser trigger. Using pixel brightness to represent the low frequency noise voltage amplitude each sample of each waveform is plotted in its correct radial and circumferential position to build up a grey-scale picture of the low frequency noise over that section of disk (figure 3.10). The result is shown in figure 3.11. From this figure one can see that the low frequency noise has a structure over the disk surface characterised by lines that span inwards radially from the outside diameter.

The previous correlation analysis showed that fields from the head have no effect on this noise structure. This is likely to be due to its relatively large geometric size compared to the geometric size of fields that can be generated by the head. The noise lines may, however, be re-set by placing the disk in a bulk A.C. eraser or by bringing a dimensionally large magnet near the sample space. The result of this is shown in figure 3.12 where the same sample space is shown after interaction by such a field. Comparing this to figure 3.11 one can see that although the lines show similar characteristics, they are in different locations. The appearance and behaviour of these lines are consistent with domain formation in the magnetically soft underlayer of the disk.

Similar noise properties in perpendicular recording disks have been reported on previously. Uesaka and co-workers reported on 3 kinds of noise arising from dual layer perpendicular medium [Uesaka et. al., 1985]. The spatial frequency of the component they call 'spike noise' is very similar to that of the underlayer domain noise reported here and they acknowledge that this may be caused by domain walls in the underlayer of the disk. Seagle and co-workers have also reported a noise source they attribute to domain walls in the underlayer of the disk [Seagle et. al., 1989]. They find that the noise can cause partial erasure of the data stored in the recording layer. They believe that this is due to flux being

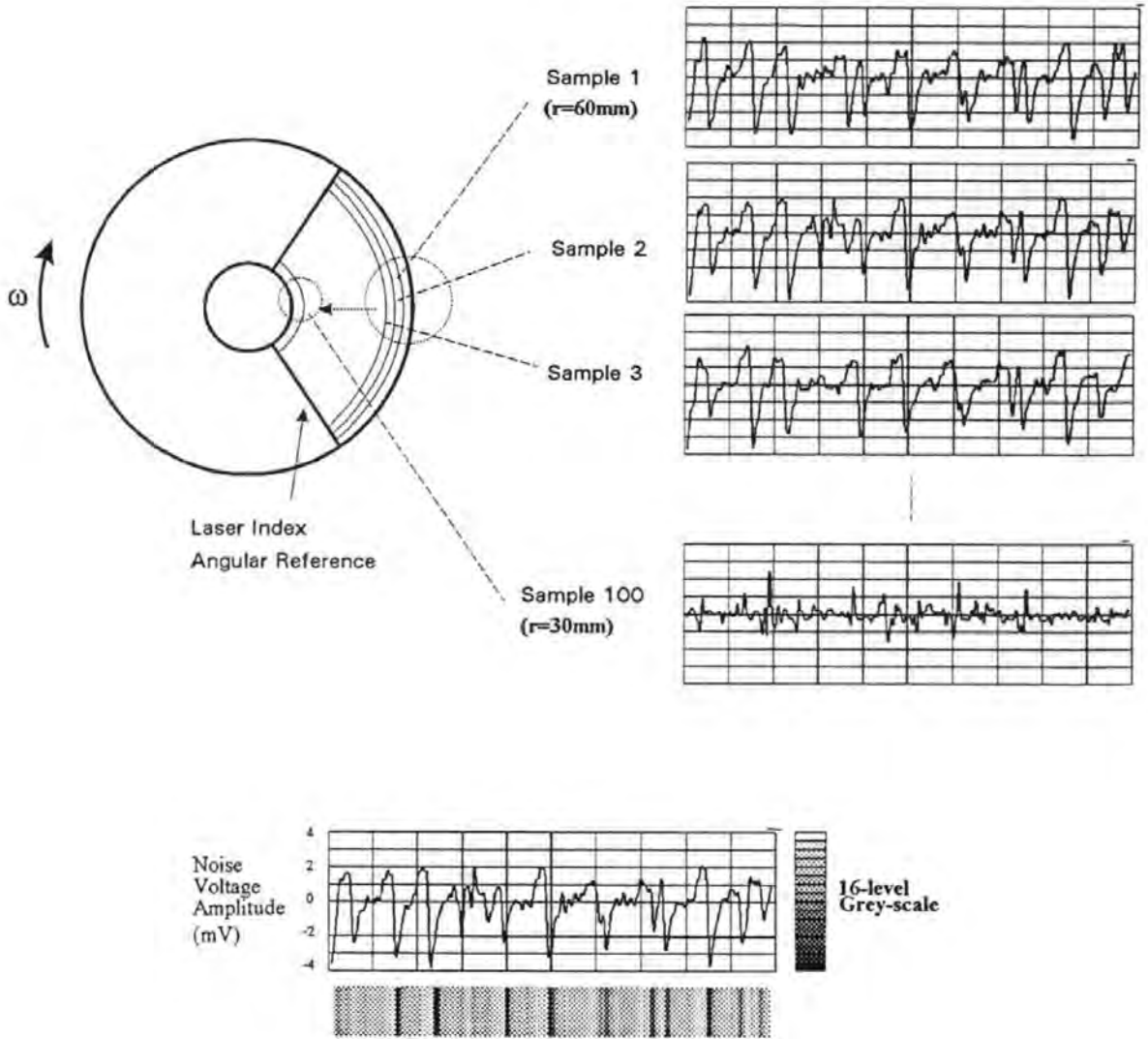


Figure 3.10 - Principle of underlayer domain noise imaging.

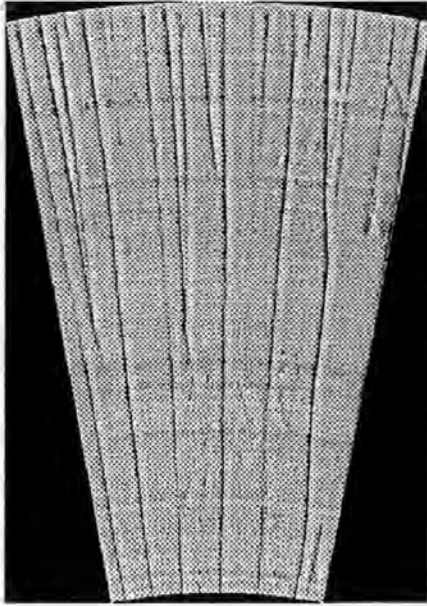


Figure 3.11 - Picture of low frequency perpendicular noise over a section of disk surface. Noise amplitude is represented by pixel brightness. The picture is to scale and 2.5 times actual size.

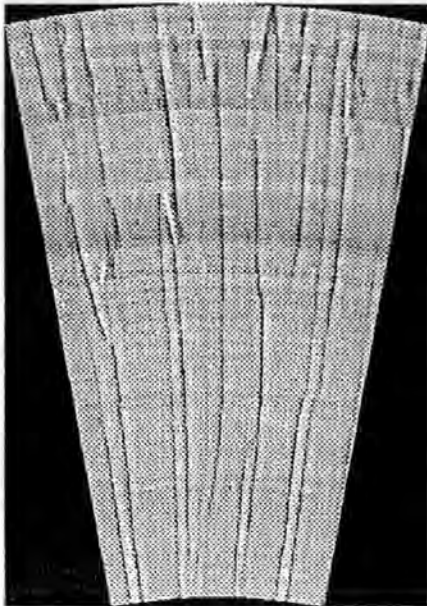


Figure 3.12 - A picture of the noise from the same section of disk as figure 3.11 after it has been subjected to a magnetic field. The noise lines have been re-set into new positions.

collected in the wide return pole and concentrated through the narrow pole. Sato and co-workers have shown that for high permeability underlayers, the spike noise arises from domain walls with widths of several tenths of a mm [Sato et. al., 1993]. In the work presented here, the structure of this noise has, for the first time, been observed over the surface of the disk and conjoined with the results of these other works is confirmed as being due to domain wall formation in the underlayer of the disk.

3.3.2 Amplitude Modulation

Amplitude modulation of the replay signal is an effect which is caused by variations in the quality of the medium over the disk surface [Koster & Arnoldussen, 1989]. It is usually recognised by the slowly undulating envelope of the signal from a track recorded with a square wave pattern. Because it is due to the magnetic performance of the medium, this effect repeats each time the disk rotates and is permanently superimposed onto the replay signal. It is primarily for this reason that, conventionally, hard disk data channels contain Automatic Gain Control (AGC) amplifiers at their inputs. If the modulation is slowly changing with respect to the signal, the AGC can reduce the variation effectively. If the channel is media noise limited there will be no change in signal to noise ratio since it is assumed that the media noise will also be attenuated in regions of poor media quality. However, if the channel is electronic noise limited then signal to noise ratio will degrade each time the signal drops below its nominal value and improve when it exceeds its nominal value. For this reason amplitude modulation is included in this investigation as one of the possible areas in which the adaptive channel could bring some improvement over the AGC approach.

Figure 3.13 shows the amplitude modulation effect over a 1.25mm section of track. The lower trace is an expanded section of the upper trace to show the detail of signal that has been recorded on the disk. In the upper trace this detail is not visible but the envelope of the signal can clearly be seen to be amplitude modulated. In this example the depth of modulation is about 20% - a typical figure for this phenomena. A 20% reduction in signal amplitude relative to the noise amplitude corresponds to a 2dB loss in signal to noise ratio; a clearly significant effect if the channel is electronic noise limited.

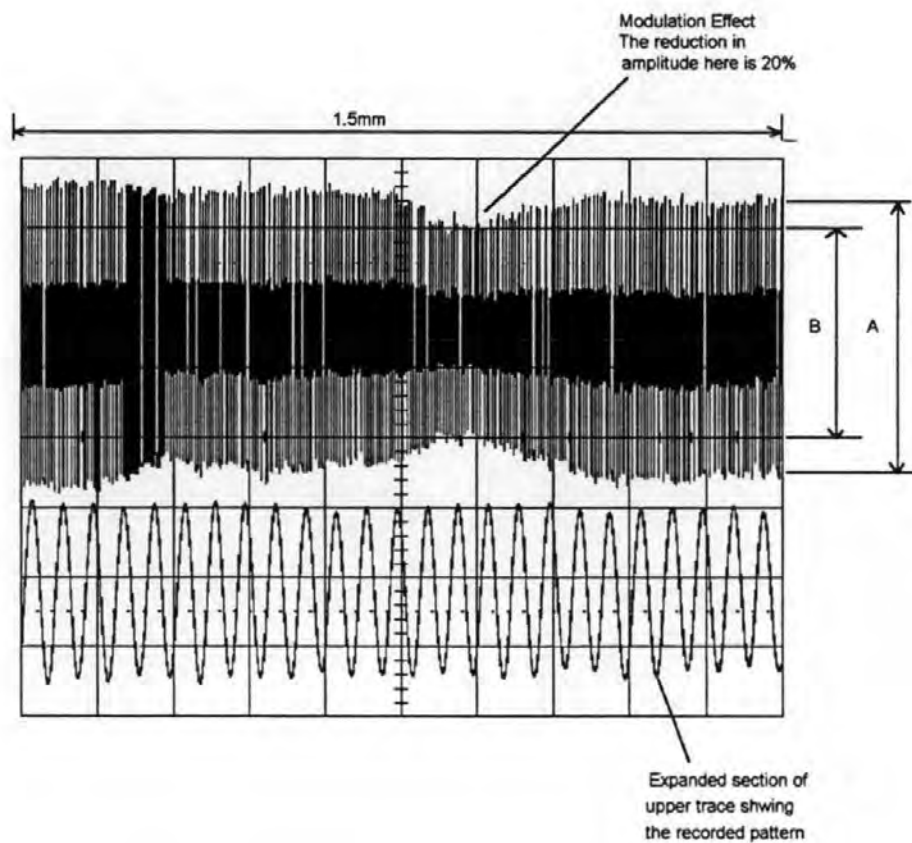


Figure 3.13 - Amplitude Modulation of Recorded Data Signal. Modulation depth is given by $(A-B)/A$.

3.4 Channel Variation over Head and Media Population

In a hard disk drive the number of recording surfaces will typically vary from two, for small form factor drives, to twenty for very large capacity drives. Therefore, it could be expected that due to manufacturing tolerances there would be a variation in recording component performance and therefore the channel response between selected head/media surfaces. In this section the spread of recording performance is investigated over a small, but typical, sample of recording components of the same type. Because the number of recording components of the same type was limited, no attempt is made to quantify the variation statistically. However, the results give a reasonable indication of the significance of the component spreads.

A single head is used to measure the step response of six 95mm longitudinal disks over head radius. For each disk the pulse width and amplitude was measured as a function of radius from 21mm to 45mm in 4mm steps. For each radius, the pulses were obtained by averaging the replay signal along the track length using a digital storage oscilloscope. The experiment is repeated for a single recording surface and 4 heads. Pulse width as a function of radius is shown plotted in figures 3.14 and 3.15 for the multiple disk and multiple head spreads respectively. One can see that the spread of heads has a greater effect on PW50 than does the spread of disks. For the samples here, the variation over recording surface is approximately 2ns compared with 4ns for the spread of heads. Therefore, if the best head were matched with the best disk the measured pulse widths could be 6ns better than if the worst head were matched to the worst disk. At the middle radius which has an average pulse width of 35ns this represents a 15% difference.

Figures 3.16 and 3.17 show the amplitude variation for multiple disk and head spreads respectively. Here, the difference in variation between the two is not so clear but unlike the pulse width variation for the spread of recording surfaces, the amplitude variation does show significant difference. Both graphs show amplitude variations of about 30 mV over the spread of recording components. Using the same assumptions as before, if the best disk were matched to the best head, the amplitude would be some 60mV better than the worst disk matched to the worst head. At the middle radius this represents a difference of approximately 10% in signal amplitude.

The PW50 relates to the resolution of the recording channel. Therefore, assuming a linear correlation between PW50 and achievable density (for a constant bit error rate), the density between a range of recording components would vary by at least 15%. If the channel is media noise limited then it is assumed that media noise amplitude varies proportionally with signal amplitude and there is no net variation. On the hand if the channel is electronic noise limited, the variation in signal amplitude between recording components of 10% results in signal to noise ratio variation of approximately 1 dB. It is concluded that the difference in PW50 between recording components is significant, whereas the difference in signal to noise ratio is not, particularly if the channel is media noise limited.

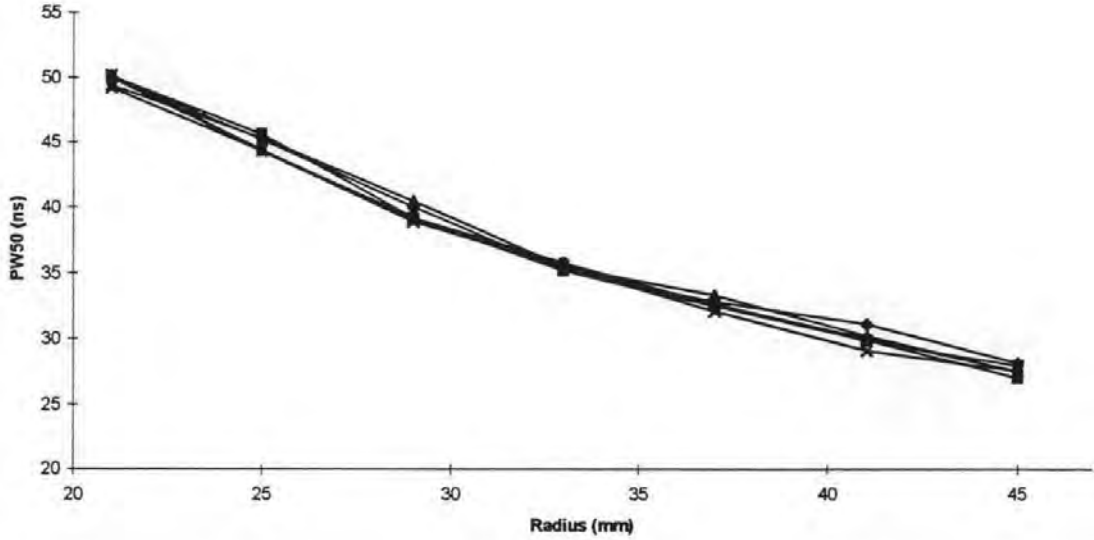


Figure 3.14 - Pulse width at 50% amplitude over radius for a single head and 6 recording surfaces.

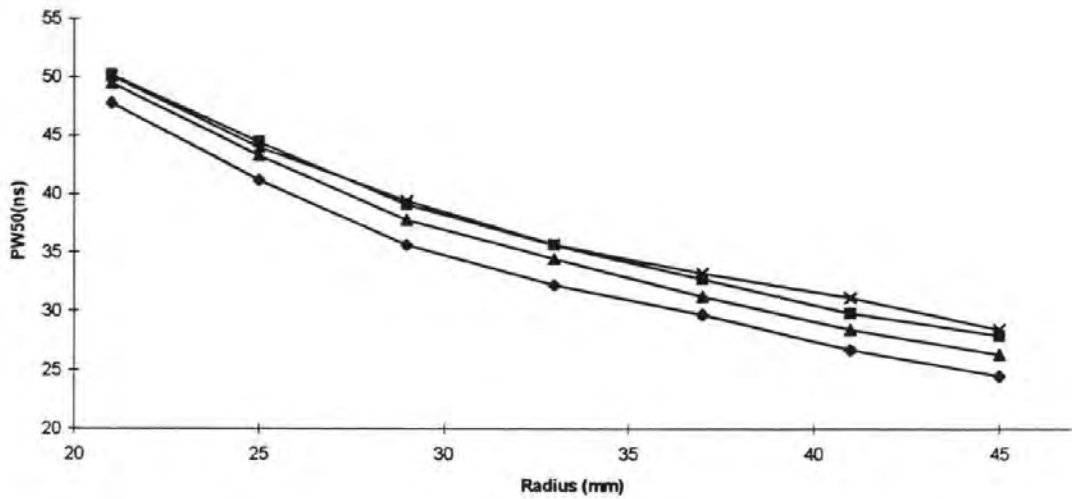


Figure 3.15 - Pulse width at 50% amplitude over radius for a single disk and 4 heads

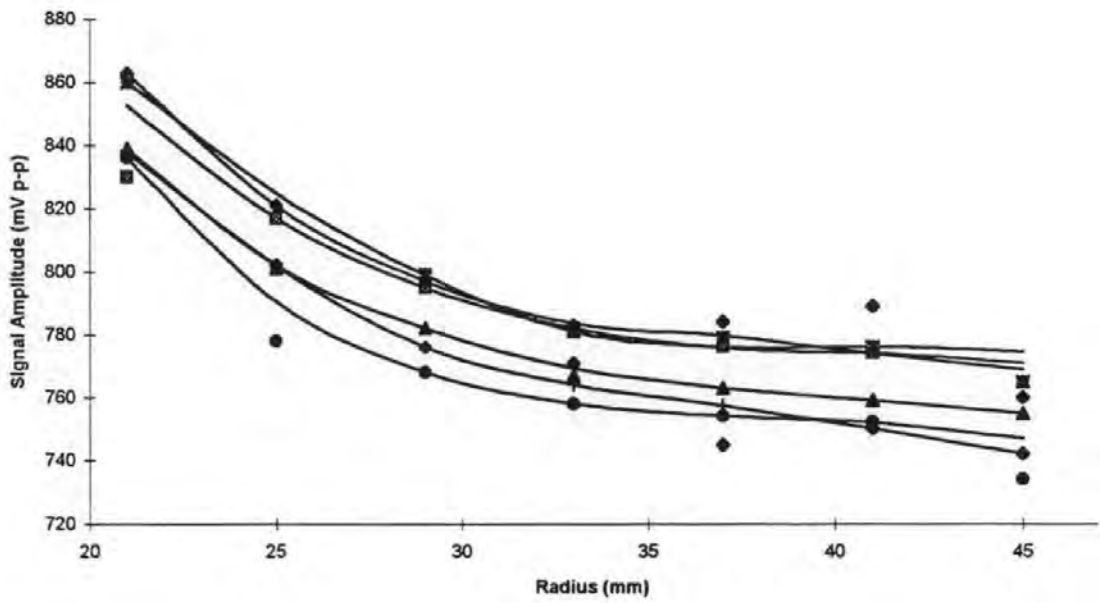


Figure 3.16 - Signal amplitude over radius for a single head and 6 recording surfaces

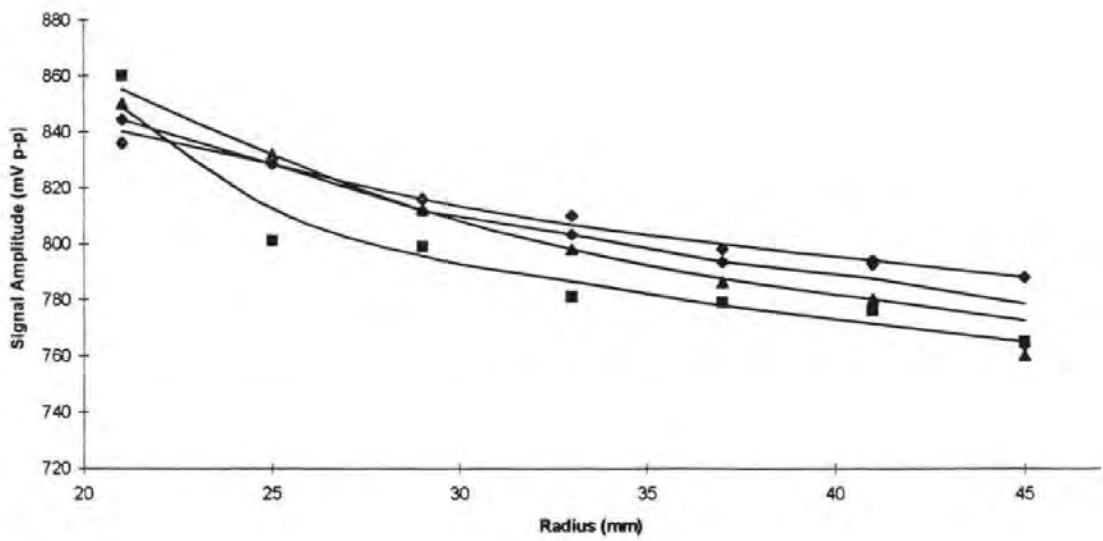


Figure 3.17 - Signal amplitude over radius for a single disk and 4 heads.

3.5 Summary

In section 3.1 the effects of track radius on signal and noise characteristics were investigated. The pulse width (in time) shows a strong dependence on track radius which is as a result of the proportional relationship between physical transition length and linear velocity. The variation is countered slightly by the increasing flying height towards the outer radius. However, in future this variation is expected to increase, due jointly to the reduction in flying height towards in-contact recording and the introduction of smaller form factors. In contrast, the variation in signal amplitude for the MR head is small (around 10%) and the variation in signal to noise ratio is therefore only 1dB for an electronic noise limited channel and zero for a media noise limited channel. As the technology progresses towards in-contact recording the variation in signal amplitude over radius is expected to reduce to zero and the variation in signal to noise ratio is expected to remain at zero for either the thermal, or media noise limited case.

In section 3.2 channel variations along the recorded track were investigated. Unlike the radial variation, changes in recording performance along the recorded track are randomly distributed and cannot be predicted for any particular sample space unless measurement is made first. The variations have typical correlation lengths (100 μ m-1mm) which are many times the transition length (100 nm) and are attributed to variables in the media manufacturing process. These variations primarily affect signal amplitude and they are significant (in the order of 2dB) if the channel is electronic noise limited but not so if the channel is media noise limited. This is because it is assumed that the effects are linked to the magnetic performance of the media which will affect the signal in a proportional manner.

In section 3.3 a limited study of channel performance over combinations of head media pairs was performed. It was found that the variance in pulse width between different heads using the same media was 15% whereas the difference in pulse width between different media using the same head was negligible. It was concluded that this was caused by variations in head-media spacing for the different heads, caused by finite tolerances in the head manufacturing process. The effect of component population on signal amplitude was found to be 10% between the worst and best head-media combination. In the electronic noise limited channel this accounts for a signal to noise variation of 1dB and zero signal to noise variation for the media noise limited case.

Therefore, it has been shown that the channel characteristics can vary somewhat deterministically with radius but non-deterministically along the recorded track and between head-media combinations. The total non-deterministic variation in signal amplitude (over head-media combinations and along the track length) of 2.5dB is significant compared to the deterministic change over radius of 1dB. The pulse width, which relates to the resolution of the channel, varies very significantly but deterministically with track radius but also varies non-deterministically over head and media population (by 15%).

The conventional approach to coping with these variations has been to design the channel to provide acceptable error rate performance for the worst case situation. In light of the variations that have been considered here it can be seen that in this approach considerable channel capacity is wasted between this and the other extreme of performance - the best case situation. It is the objective of the next chapter to introduce an adaptive data channel which, by adapting to changes in signal to noise ratio and resolution, will always attempt to maximise channel performance in the presence of these channel variables.

Chapter 4

Results & Discussion 2 :

The Adaptive Partial Response Data Channel

An adaptive partial response data channel is proposed that, in the presence of recording channel response variations, will determine an optimum recording strategy for a particular point in the disk drive based on the recording performance it has measured there. The key feature that the channel relies on to be able to do this, is prior knowledge of how the recording channel pulse response, partial response, data rate and equalisation loss are interrelated.

4.1 The Pulse Response and The Partial Response

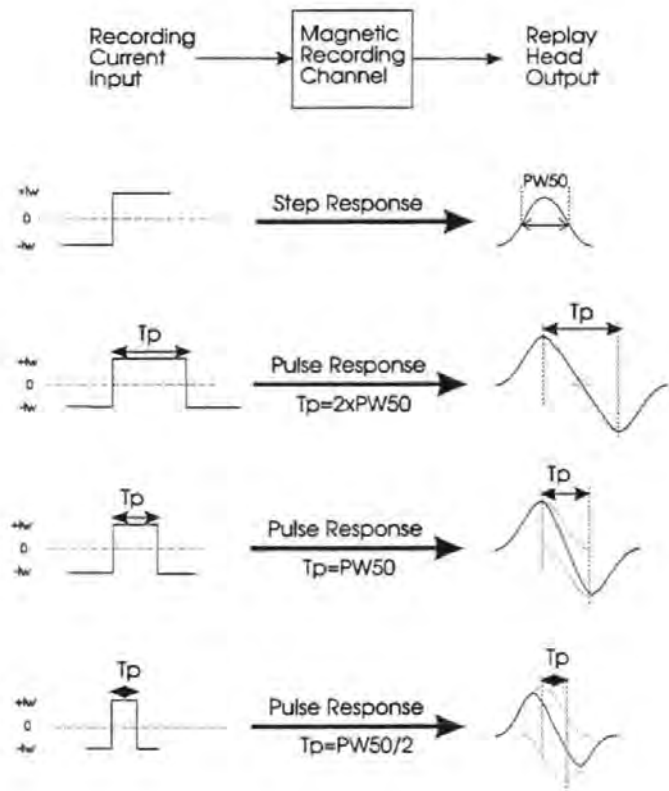
Figure 4.1(a) illustrates properties of the pulse response of the magnetic recording channel. The pulse response is formed by the linear superposition of two step response pulses, alternating in polarity and spaced T_p apart. The two step response pulses overlap causing

mutual intersymbol interference and an output dipulse which bears a resemblance to the impulse response of a class of partial response systems characterised by the polynomial,

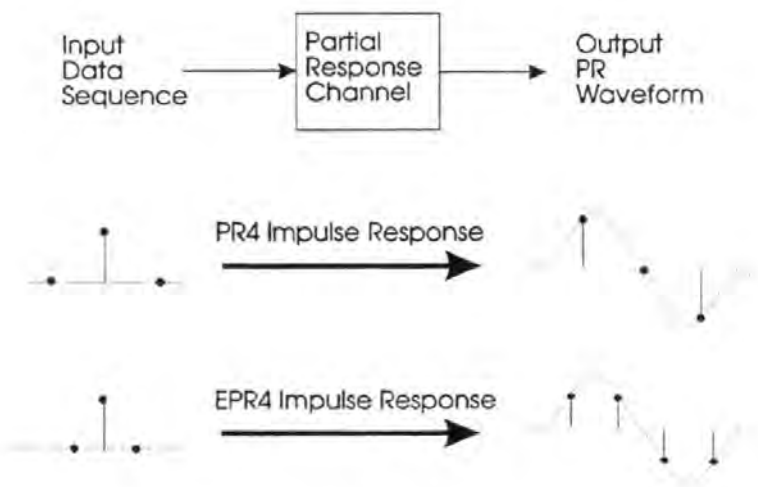
$$F(D) = (1 - D)(1 + D)^n \quad (4.1)$$

where D is the delay operator and $n = \{0, 1, 2, \dots\}$. Setting $n = 1$ or 2 yields the partial response schemes which have become known as PR4 and Extended PR4 (EPR4) (see chapter 1.2). The similarity between the magnetic recording channel pulse response and the Partial Response impulse response can be seen by comparing the output wave shapes in figure 4.1 (a) and (b).

The shape of the dipulse produced by the overlapping step response pulses will depend on the distance between them, T_p . Conversely, the *shape* of the Partial Response impulse response does not change but its width scales with signalling period. For any chosen T_p , the recording channel dipulse will require equalisation in order to shape it exactly to the required Partial Response characteristic. Therefore, the 'amount' of equalisation required will depend on T_p . In theory, any input signal can be equalised to the required response. However, equalisation of an input signal contaminated by noise which has a dissimilar spectral distribution to the signal causes the signal to noise ratio at the output of the equaliser to be modified from that at the input. Therefore, the signal to noise ratio at the output of an equaliser required to shape the recording channel pulse response to a particular class of partial response will vary as a function of T_p .



(a)



(b)

Figure 4.1 - The (a) recording channel pulse response and (b) the partial response

Figure 4.2 shows the spectrum of the recording channel pulse response over a range of normalised densities, $PW50/T_p$, for the MR head and thin-film media used in this investigation. T_p is the pulse period and $PW50$ is the pulse width at 50% zero-peak amplitude. Figure 4.3 shows the target PR4 spectra for the same range of normalised densities. For each normalised density, the target response is achieved by an equaliser, the transfer function of which, $H_e(f)$ is given by dividing the target PR4 response by the measured channel response,

$$H_e(f) = \frac{V_{PR4}(f)}{V_c(f)} \quad (4.2)$$

where $V_c(f)$ and $V_{PR4}(f)$ are the voltage spectral densities of the measured channel and target PR4 response respectively. The corresponding range of equaliser functions are shown in figure 4.4. From this figure one can see that the shape of the required equaliser function changes as a function of normalised density, requiring more and more high frequency boost as the density is increased.

The method used to measure the channel pulse response is illustrated in figure 4.5. A repeating pattern of dipulses, with input pulse width T_p and repeating period T_s , are recorded over a small length of track. The Discrete Fourier Transform of the replay signal is then computed. The spectrum is discretised, the distance between the spectral lines corresponding to the reciprocal of the period between the dipulses, T_s . The result is the sampled voltage spectrum of the dipulse signal. The sampled voltage spectral density of a single dipulse is then given by multiplying the amplitude of the discrete spectral lines by the fundamental period of the signal, T_s . By altering the input pulse width, T_p , and normalising to the measured $PW50$ over the sample space, the responses in figure 4.2 are obtained.

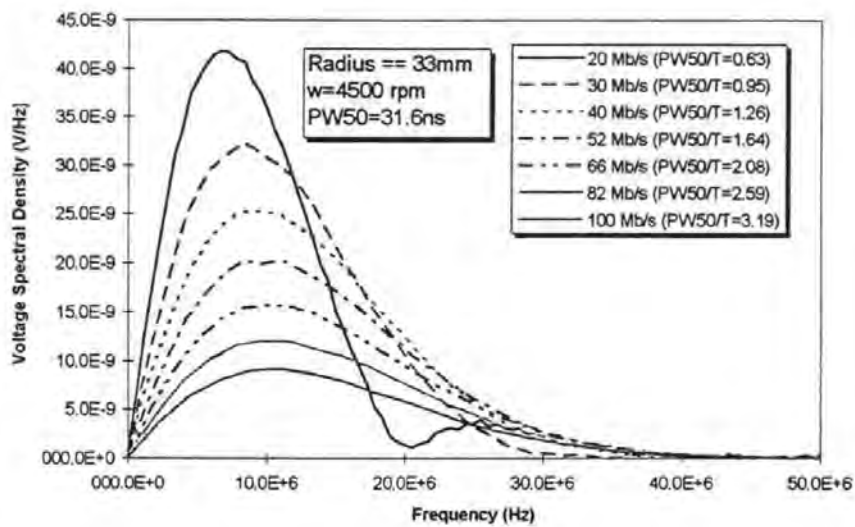


Figure 4.2 - Measured recording channel pulse response (for MR head) for a range of signalling rates (recording densities).

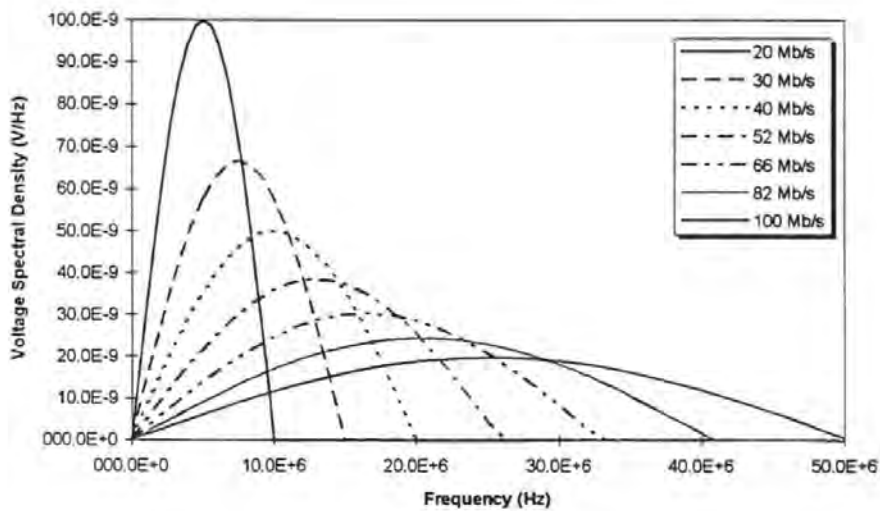


Figure 4.3 - Target PR4 responses with signalling rates corresponding to figure 4.2

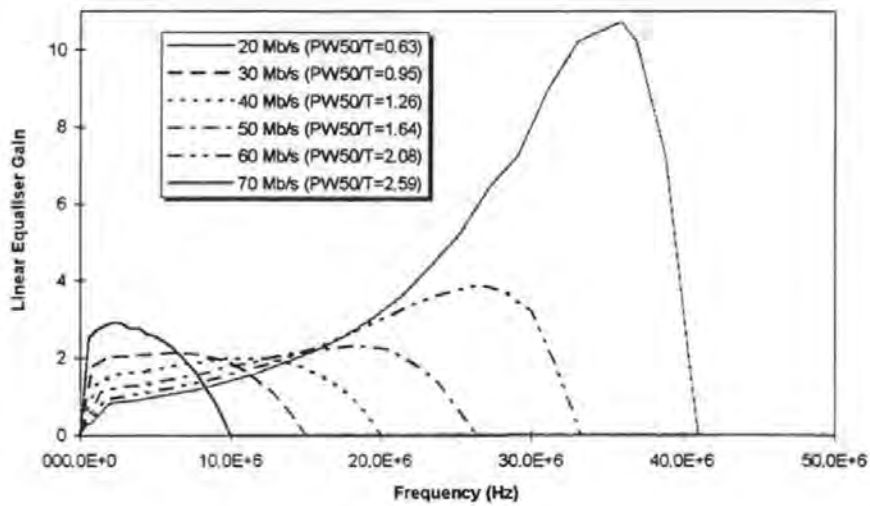


Figure 4.4 - Required equaliser transfer functions to match the recording channel responses to the PR4 responses shown in figures 4.2 and 4.3.

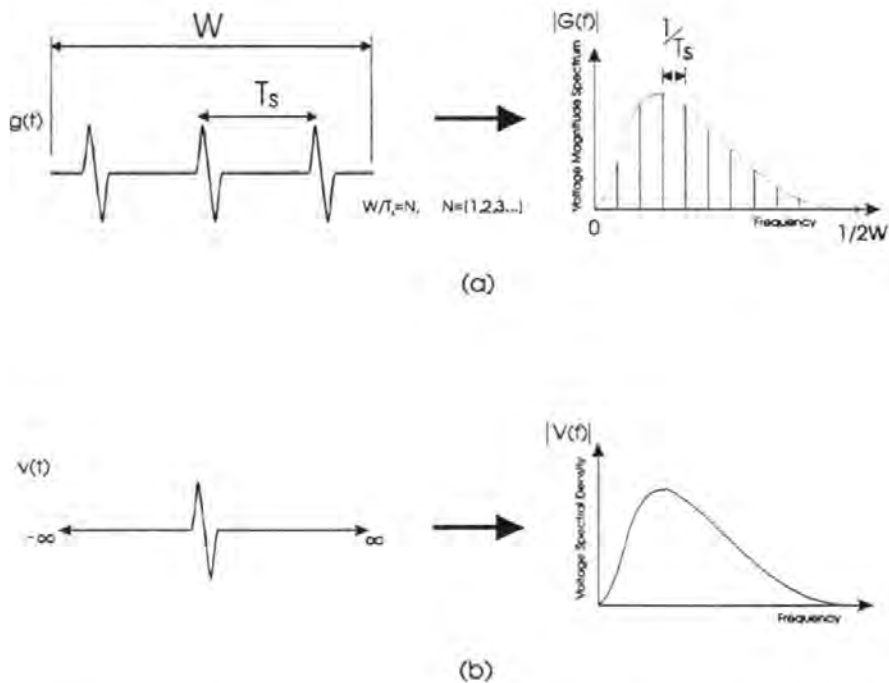


Figure 4.5 - Pulse response measurement technique. (a) FFT of periodic dibit signal yields discrete magnitude spectrum. (b) The voltage spectral density of a single dibit is obtained by noting that the spectrum in (a) is the sampled voltage spectral density scaled by the fundamental period of the signal.

4.1.1 Correction for Non-linear Transition Shift

It well known that for very small transition spacings, the demagnetising fields in the medium can cause the position of the transitions to shift towards each other whilst they are being written by the recording head; an effect known as non-linear transition shift [Tang, 1986; Arnoldussen & Tong, 1986; Madrid & Wood, 1986; Melas & Arnett., 1988] . Therefore, in order to measure the pulse response of the channel correctly, the non-linear transition shift needs to be measured as a function of transition spacing and a correction applied.

A particularly elegant method of measuring this and other channel non-linearities has been demonstrated using the unique shift and add properties of Pseudo Random Binary Sequences [Newby & Wood, 1986; Palmer & Ziperovich, 1987; Che et. al., 1993]. In this method a Pseudo-Random Binary Sequence is recorded on the track and the average replay signal for one complete cycle of the sequence is captured using the digital storage oscilloscope. The Discrete Fourier Transform of this signal is then divided by the Discrete Fourier Transform of one cycle of the input NRZ PRBS sequence. The result is the spectrum of the impulse response of the recording channel and performing the inverse DFT yields the time-domain impulse response. Because of the unique shift and add property of the PRBS, any non-linearities in the recording and playback process show up in the impulse response as echoes of the primary response. The position and amplitudes of these echoes indicate the cause and magnitude of the various non-linearities. The theory behind this method and the analysis for a number of common non-linearities is shown in appendix E. This method is used to determine the non-linear peak shift caused by adjacent recorded transitions in the media. For the 511 sequence length PRBS chosen, the adjacent transition shift echo appears at a position -225.5 bits away from the main impulse. The magnitude of transition shift is then given by twice the ratio of the echo amplitude to the main impulse

response amplitude (figure 4.6). By repeating the experiment over a range of recording densities, the non-linear transition shift as a function of normalised recording density may be obtained (figure 4.7).

The results in figure 4.7 show that the transition shift starts to become significant at normalised recording densities of around 1 and rises exponentially with increasing density. Therefore, when measuring the channel pulse response as a function of recording density, a correction must be applied to the analysis which takes into account the effect of the transition shift. This is done by assuming that if two transitions are recorded at a normalised density of 2, the second will be shifted towards the first by 12%. Therefore, the measured pulse response will in fact correspond to two transitions spaced at a normalised density of 2.24. This correction characteristic was used in the collection of the results for figure 4.2.

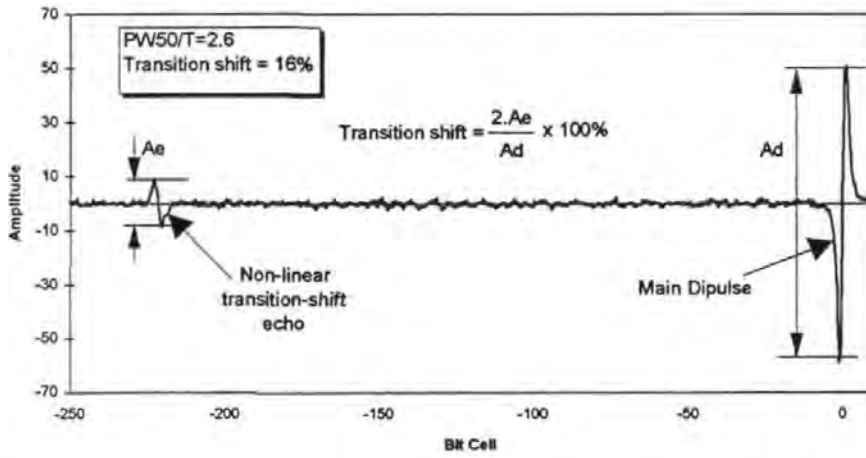


Figure 4.6 - Impulse response of recording channel derived using PRBS sequence. The echo at bit position - 225 is due to non-linear transition shift.

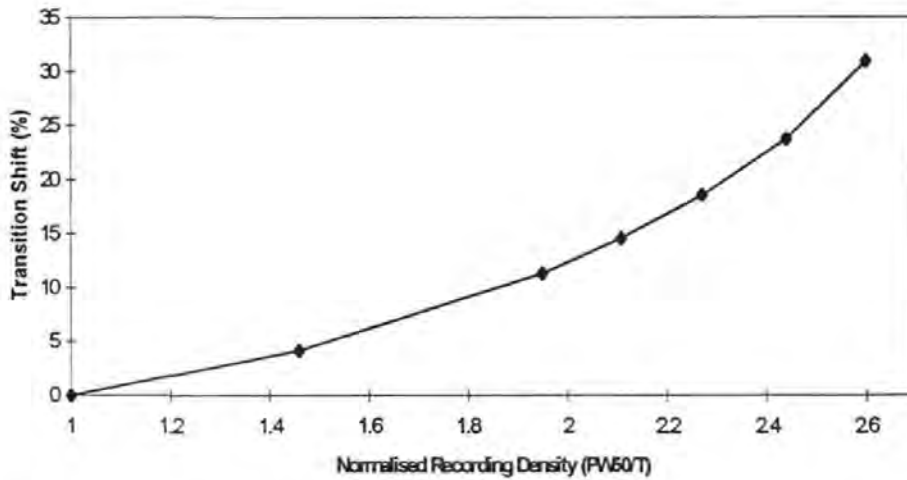


Figure 4.7 - Non-linear transition shift (% of bit period) as a function of recording density.

4.1.2 Signal and Noise Loss Through the Equaliser

When the equaliser functions in figure 4.4 are applied to the channel signal, the signal to noise ratio at the output of the equaliser will be modified from that at its input. To investigate this the channel model shown in Figure 4.8 is used to characterise the channel response and compare it to the target PR4 and EPR4 responses over a range of recording densities. The bandwidth requirements for the signal at each signalling rate are different and so in order to provide a realistic comparison in the presence of noise, the equaliser is preceded by a brick wall filter cutting off all signal and noise energy above the signalling rate. The SNR loss through the equaliser is determined by considering the relative effect of the equaliser on the signal and noise energy.

The signal and noise are characterised by their single-sided voltage spectral density functions, the total energy contained in which is given by Parseval's theorem,

$$E = \int_0^{1/2T} |V(f)|^2 df \quad (4.3)$$

The signal to noise loss through the equaliser is determined by the ratio of the output SNR to the input SNR,

$$SNR_{gain} = 10 \log \left(\frac{SNR_{out}}{SNR_{in}} \right) \quad dB \quad (4.4)$$

The input SNR is given by,

$$SNR_{in} = \frac{\int_0^{1/2T} |V_f(f)|^2 df}{\eta/2T} \quad (4.5)$$

where η is the input noise single-sided power spectral density (which is assumed to be additive Gaussian, white noise), and $V_f(f)$ is the voltage spectral density of the signal into the equaliser.

The output SNR is given by,

$$SNR_{out} = \frac{\int_0^{1/2T} |V_f(f) \cdot H_e(f)|^2 df}{\eta \int_0^{1/2T} |H_e(f)|^2 df} \quad (4.6)$$

Hence, the SNR gain through the equaliser is,

$$SNR_{gain} = 10 \log \left(\frac{\frac{1}{2T} \int_0^{1/2T} |V_f(f) \cdot H_e(f)|^2 df}{\int_0^{1/2T} |V_f(f)|^2 df \cdot \int_0^{1/2T} |H_e(f)|^2 df} \right) dB \quad (4.7)$$

The pulse response of the magnetic recording channel is measured at a specific normalised density which has been correctly identified in the presence of non-linear transition shift. The equaliser transfer functions for PR4 and EPR4 are then derived using (4.2) and the SNR gain through the equaliser is computed from (4.7) using numeric integration. This is repeated over a range of normalised densities. The results are shown in figure 4.9 as the dashed lines.

One can see from this figure that the SNR loss characteristic is curved; exhibiting a maximum loss at the extremes of recording density and a minimum at around 1.25 for PR4 and 1.75 for EPR4. This may be explained by noting that at low densities, the required equaliser function attenuates signal energy relatively more so than the available noise power

(figure 4.10). At high recording densities, the required equaliser function tends to boost high-frequency noise relatively more so than the signal (figure 4.11). Also, the absolute gain through the equaliser between 0.7 and 1.75 for PR4 and 1.05 and 2.25 for EPR4 is positive indicating an overall improvement in SNR. This is explained by noting that as the signalling rate approaches its optimum value, the corresponding equaliser response approaches that of a matched filter; the maximum theoretical gain of which is 3dB. From this data it appears that EPR4 outperforms PR4 at normalised densities above about 1.4.

Sugawara et. al. have studied the effect of noise correlation on the Viterbi detector from spectral shaping of the noise due to equalisation [Sugawara et. al., 1993]. In order to obtain a more realistic comparison of the two classes of response it is found that a correction for noise correlation needs to be applied. This is shown in the solid lines of figure 4.9 where their correction has been applied to the previously obtained results. On the basis of the corrected characteristics, EPR4 performance exceeds that for PR4 at a normalised density of about 1.65.

Comparing this result with that obtained by [Thapar & Patel, 1987] using a Lorentzian simulation, it is seen that the density at which EPR4 performance exceeds PR4 performance agrees well with their value of 1.6. Also, below this value, the characteristics of the curves are in good agreement. However, at densities above 1.6, the roll off with density is much more severe here than in the results presented by Thapar & Patel. For example, at a normalised density of 3 they predict that SNR loss should have increased by only 5dB for PR4 and by only 1.5 dB for EPR4. Here we find that at a normalised density of 3, the SNR loss for PR4 and EPR4 has increased by some 19dB and 9dB respectively. To investigate the possible reasons for this, an investigation was carried out to compare the shape of the MR head pulse to the Lorentzian model.

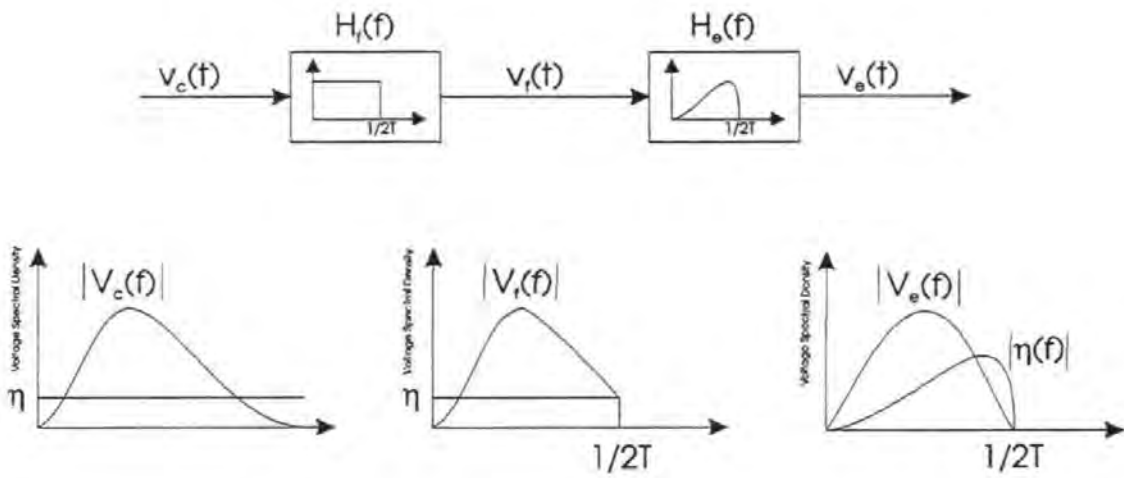


Figure 4.8 - Channel model for response analysis

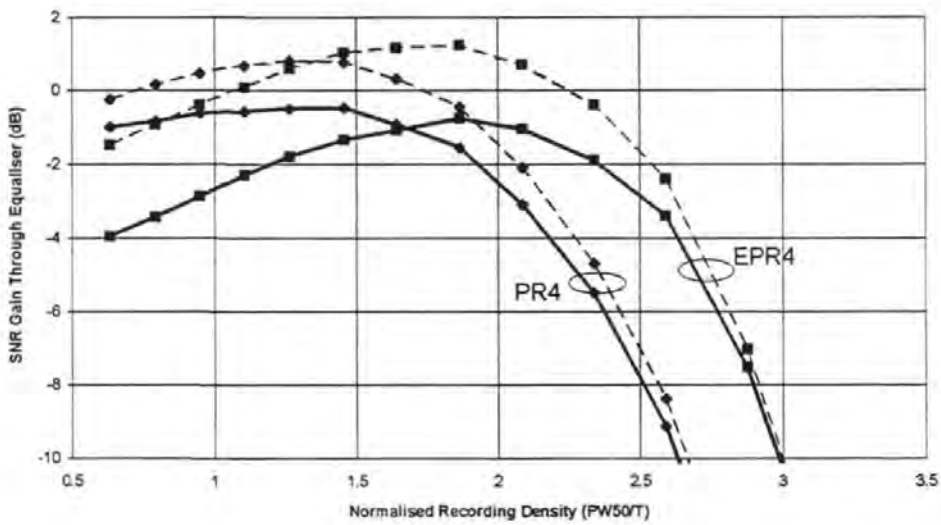


Figure 4.9 - SNR loss through PR4 and EPR4 equaliser before (dashed) and after (solid) taking account of the additional effective loss due to noise correlation.

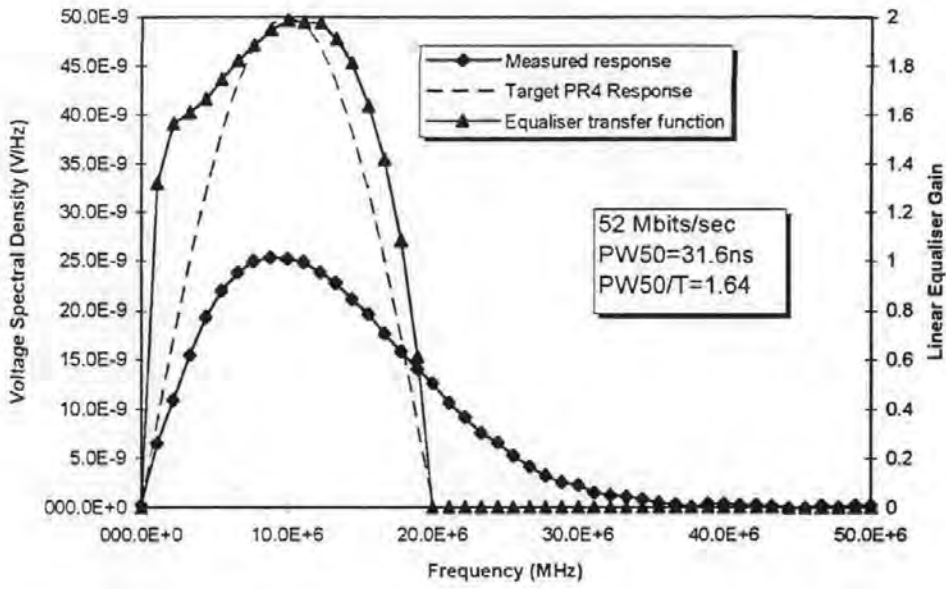


Figure 4.10 - Recording channel, target response and required equaliser transfer function at normalised recording density of 1.64.

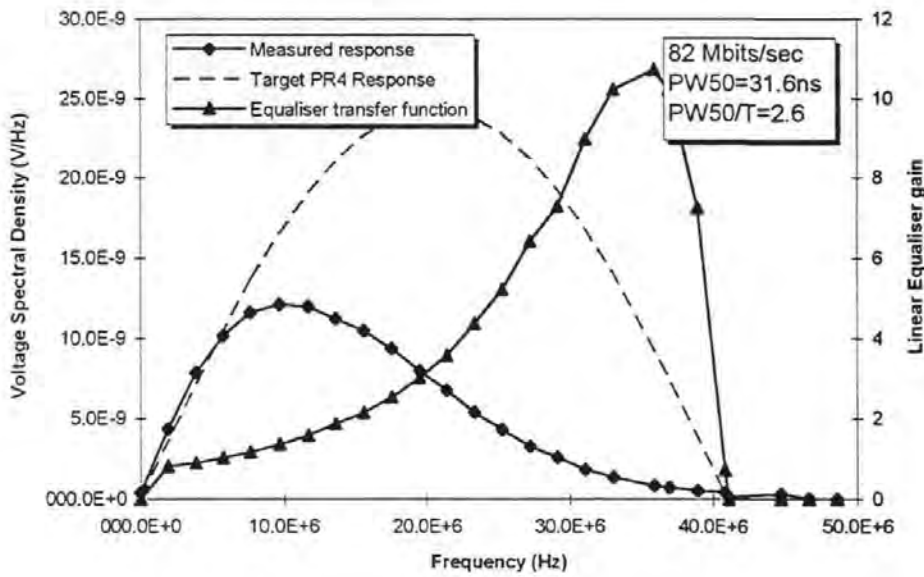


Figure 4.11 - Recording channel, target response and required equaliser transfer function at normalised recording density of 2.6.

The Lorentzian family of curves is given by,

$$e(t) = \frac{A}{1 + \left(\frac{2t}{PW50} \right)^x} \quad (4.8)$$

where A is the amplitude, PW50 is the pulse width, and x is the Lorentzian coefficient which is almost always assumed to be 2 (which yields the Lorentz shape) but where it has been noted that choosing $2 < x < 3$ can sometimes yield a more accurate model [Cioffi, 1990]. (Thapar & Patel use a value of $x=2$).

The step response pulse for the MR head is shown in figure 4.12 with the Lorentzian curves superimposed for various values of x. Computing the cross correlation coefficient between the measured pulse and the Lorentzian pulses yields the characteristic in figure 4.13. Here it can be seen that rather than it being the value of $x=2$ that is the best match to this recording pulse, it is in fact $x=2.6$. This higher value of x leads to the tails of the pulse decaying more rapidly than when $x=2$. In the frequency domain this corresponds to the frequency response of the measured pulse response rolling off much more rapidly at high frequencies than the Lorentzian model for $x=2$. The result of this is that the partial response equalisation required for the actual channel is much more severe at high densities than the Lorentzian model predicts. Therefore, significantly more high frequency boost is required corresponding to a larger increase in the loss of SNR through the equaliser.

It is concluded, therefore, that care must be taken when interpreting Lorentzian simulations since the assumption that the recording channel is approximated by the Lorentzian pulse may not actually be valid when specific heads / media are characterised. This is particularly so in the type of analysis here, where the desired equaliser function at high densities is very

sensitive to the relative amplitudes between the measured and target responses in the high frequency parts of the spectrum. It may be that this is a common feature of MR heads, or, it could be an anomaly for this particular design. It is concluded that further research would be required to answer this particular question.

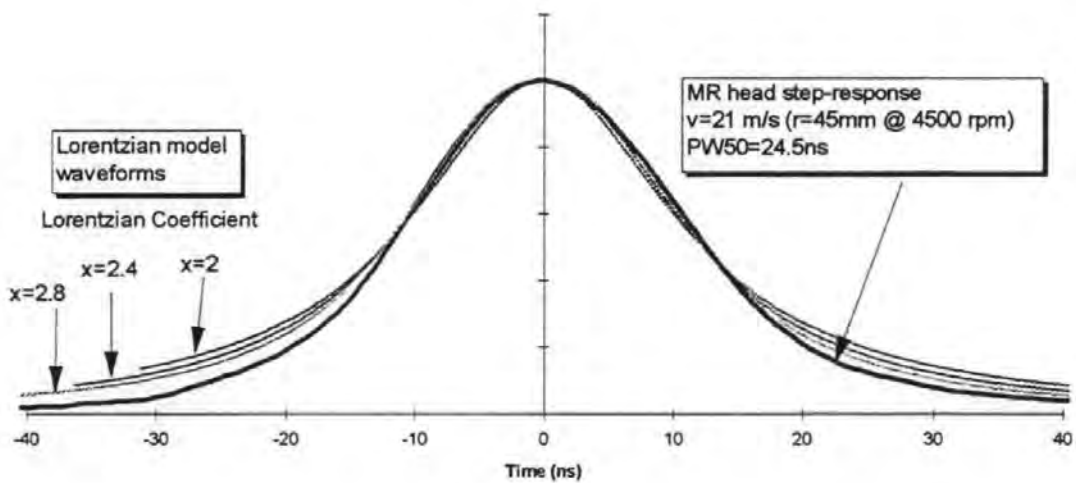


Figure 4.12 - The MR head step response and Lorentzian model

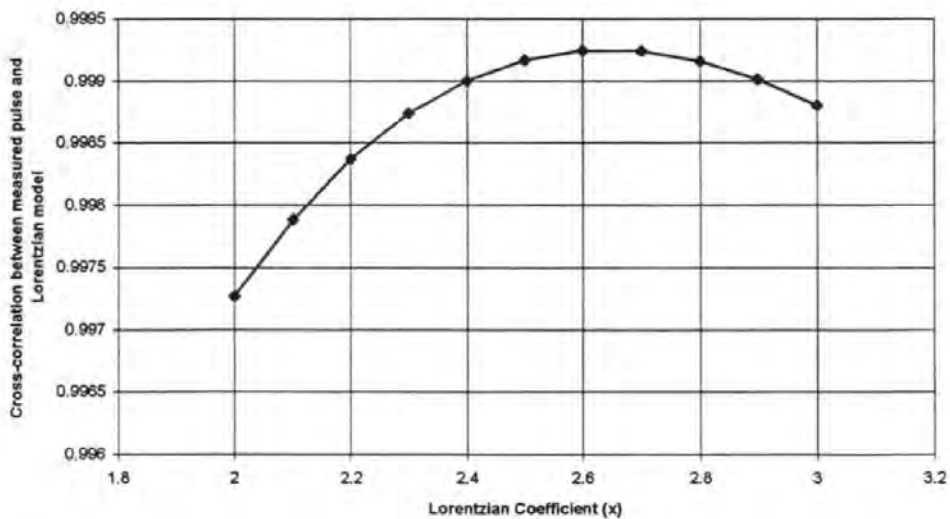


Figure 4.13 - Cross-correlation between Lorentzian model and MR head step response

4.1.3 Bit Error Rate

For the Viterbi detector, the probability of error for high signal to noise ratio is well approximated by [Forney, 1972],

$$P_e = K \cdot Q\left(\frac{d_{\min}}{2\sigma}\right) \quad (4.9)$$

where K is a small constant which relates to the number of bits per error event, σ is the signal to noise ratio into the detector, d_{\min} is the minimum Euclidean distance between two distinct input sequences which give rise to the same output sequence and $Q(\cdot)$ is the cumulative Gaussian error function given by,

$$Q(z) = \frac{1}{\sqrt{2\pi}} \int_z^{\infty} e^{-y^2/2} dy \quad (4.10)$$

For the same average input signal power, the signal to noise ratio for EPR4 is half that for PR4 since the number of levels is increased from 3 to 5. On the other hand, the Viterbi detector for EPR4 has twice the minimum distance, d_{\min} , that the equivalent detector for PR4 has. Therefore, there is no overall gain or loss in error rate in going from PR4 to EPR4 signalling with the same input signal to noise ratio into the detector [Thapar & Patel, 1987]. Consequently, the error rate curves as a function of input SNR are the same for both PR4 and EPR4.

The probability of bit error for PR4 detection is given by [Sugawara et. al., 1993],

$$P_e = 4 \cdot Q\left(\frac{\sqrt{2}}{2\sigma}\right) \quad (4.11)$$

where $1/\sigma$ is the signal to noise ratio defined as the zero-peak signal amplitude divided by the r.m.s. noise. The Bit Error Rate characteristic given by (4.11) is shown plotted in figure 4.14.

The results in figures 4.9 and 4.14 may be combined to yield the probability of error for the two classes of response as a function of signal to noise ratio into the equaliser and data density. Therefore, for a given recording channel SNR and a desired error rate, the maximum recorded density for each class that will meet the error rate criteria can be determined. This is shown in figure 4.15 where lines of constant error rate have been plotted as a function of normalised recording density and signal to noise ratio.

The results in figure 4.15 show that for normalised densities above 1.7, the EPR4 class of response can tolerate a higher recording density than PR4 for the same recording channel signal to noise ratio and the same target error rate. For example, if the measured recording channel signal to noise ratio were 24dB and the required error rate were 1 in 10^{10} bits, then the maximum density for PR4 would be 2.25 and EPR4 would be 2.7. Therefore at this SNR and error rate, by choosing EPR4, the density would be increased by 20%. The density increase of EPR4 over PR4 increases with signal to noise ratio for the corresponding densities above 1.7. For densities below this value, however, the achievable density is greater for PR4 than EPR4 for the same signal to noise ratio and required error rate.

It can be seen from figure 4.15 how the proposed adaptive channel is able to tune the data rate in order to meet a target error rate. Specifically, if the channel is given the ability to measure the signal to noise ratio and pulse width at a particular recording location, then, by

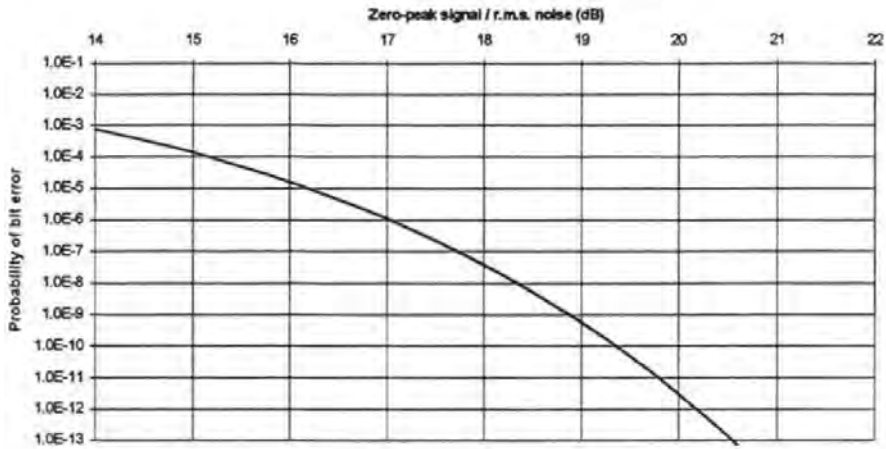


Figure 4.14 - Error rate vs signal to noise ratio at input to Viterbi detector for PR4 and EPR4

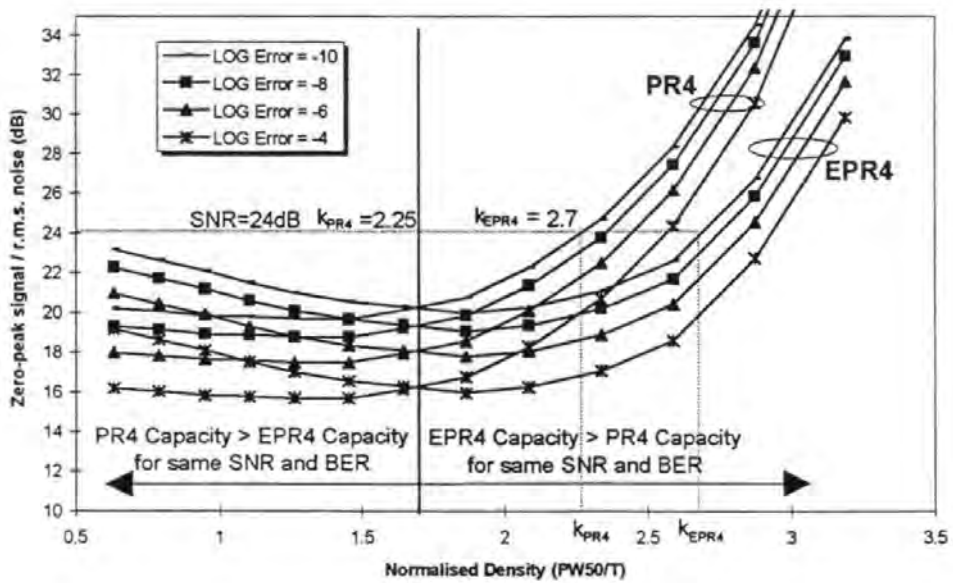


Figure 4.15 - Lines of constant error rate for actual signal to noise ratio vs normalised density. At normalised densities above approximately 1.7 EPR4 achieves higher capacity for the same signal to noise ratio and error rate.

reference to figure 4.15, the maximum normalised recording density corresponding to the measured signal to noise ratio and target error rate may be found. Then, the data rate is determined from,

$$R_D = \frac{k}{PW50} \quad (4.12)$$

where k is the maximum normalised density and $PW50$ is the measured pulse width.

4.2 Determination of the Recording Performance

The methods that the proposed channel would employ to measure the signal to noise ratio and pulse width will now be described. The key requirement is that they should be implementable using similar, if not the same components already found in the hard disk partial response signal processing system.

4.2.1 Measurement of Pulse Width (PW50)

The proposed method that the channel uses to measure PW50 is illustrated in figures 4.16 and 4.17. A constant frequency pattern of transitions is recorded at a low frequency over the sample space such that the replay pulses do not overlap. Such a frequency typically corresponds to a normalised density ($PW50/T$) of 0.25. It is assumed that the channel has some prior knowledge of the maximum expected pulse width and is therefore able to meet this criteria. For example, in the heads / media used in this investigation it is known that the pulse width is, on average, 47ns at the inside recording radius. Therefore, if it assumed that the maximum pulse width was 50ns a data rate of 5 MHz would be chosen (200 ns^{-1}).

The replay signal is fed through the Automatic Gain Control (AGC) amplifier which forces the peak-peak amplitude of the signal to a preset value (in this example 1.27 V_{p-p}). A voltage equal to half the zero-peak amplitude of the rectified signal is fed into one side of a comparator. The other side of the comparator is fed with the signal itself. The output from the comparator is fed into a charge pump which drives a capacitor with a fixed charging current. The voltage across the capacitor is then proportional to the input pulse width. The voltage across the capacitor is sampled by the analogue to digital converter and the value is stored by the microprocessor.

It was found that the variance of the measurements with respect to the mean value is approximately equal to the signal to noise ratio of the signal (figure 4.18) Therefore, to obtain an accurate measurement of PW50, the measurements are averaged. The variance of the averaged measurement is reduced as the square root of the number of measurements in the average. The number of averages taken is typically 100 which reduces the variance by ten times. One hundred transitions spaced 200ns apart corresponds to a measurement time of 20 μ s, or approximately 200 μ m of track length at the inside radius (assuming a linear velocity of 10 m./s). Hence it is concluded that the technique may be used accurately down to relatively fine resolutions, of the order of the amplitude modulation / spike noise feature lengths investigated in chapter 3.

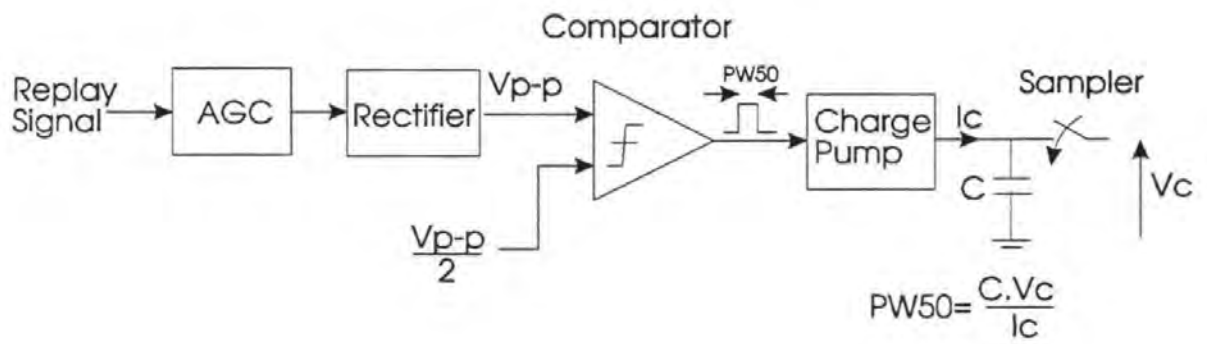


Figure 4.16 - PW50 measurement circuit.

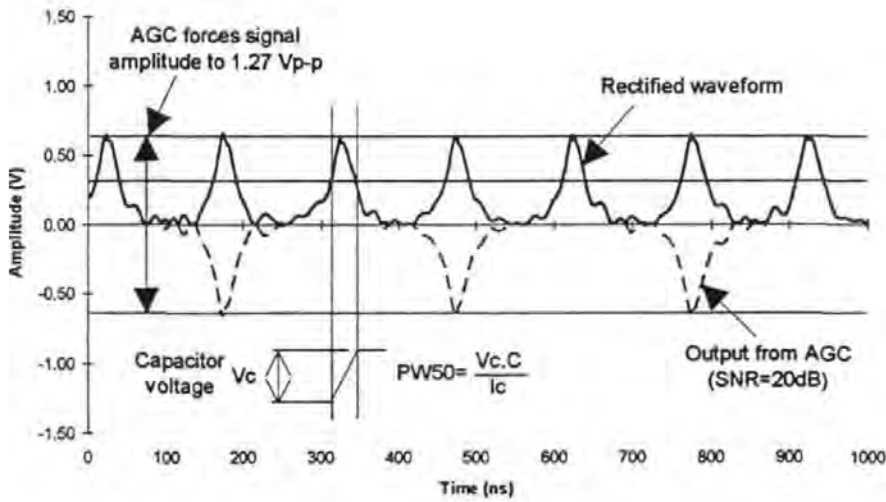


Figure 4.17 - Principle of PW50 measurement. The rectified signal is fed into the comparator which is set to switch at half the zero-peak signal amplitude. The comparator enables a charge pump which charges the capacitor. The voltage across the capacitor is sampled by the ADC and the PW50 is calculated from the known capacitance and charge current.

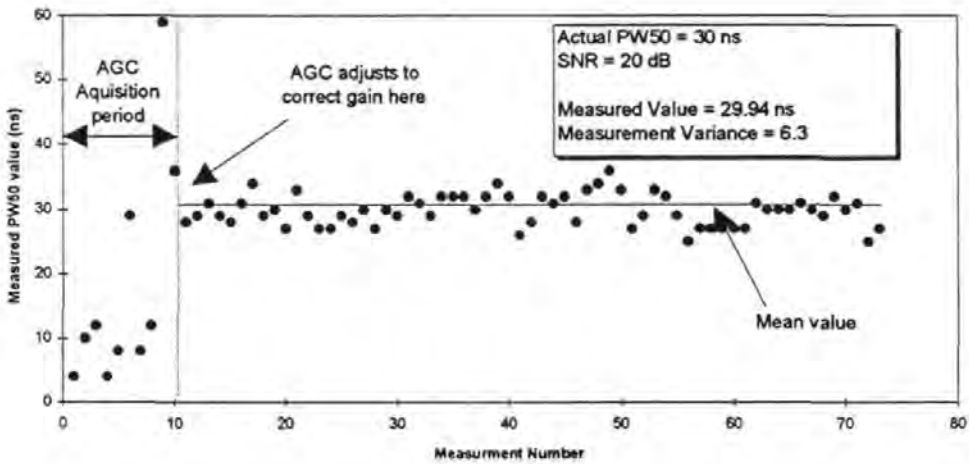


Figure 4.18 - Samples from the PW50 measurement circuit. The variance of the measurements about the mean is equal to the signal to noise ratio. Measurements are averaged to increase the accuracy.

4.2.2 Measurement of Signal to Noise Ratio

The proposed method that the channel uses to measure signal to noise ratio is illustrated in figure 4.19 A square wave recording current pattern is written to the disk over the sample space. The frequency of the written square wave is set equal to $1/PW50$ (which is determined from the previous technique). At this density the replay waveform is approximately a sinusoid. During the read phase, the phase locked loop locks onto the constant frequency pattern and the same decision directed timing algorithm that is used for data recovery adjusts the phase and frequency such that the samples yield the values. $+1,+1,-1,-1,+1,+1,\dots$. The variance of the samples and the signal amplitude over the sample space is then computed by the microprocessor which receives the samples from the ADC into a buffer. The ratio of the zero-peak signal amplitude to the square root of the variance of the samples (the standard deviation) is then computed which yields the signal to noise ratio over the sample space (figure 4.20).

At the same time a boundary searching algorithm can be used to identify large scale changes in sample values over the sample space. Such boundaries indicate performance degradation due to amplitude modulation or underlayer noise, or perhaps an asperity. If such a boundary is identified, its magnitude and position is noted. The channel may then avoid recording in regions of media where there is no recording performance (such as in the case of an asperity), or, could adapt its recording strategy to cope with the nominal change in signal and noise properties.

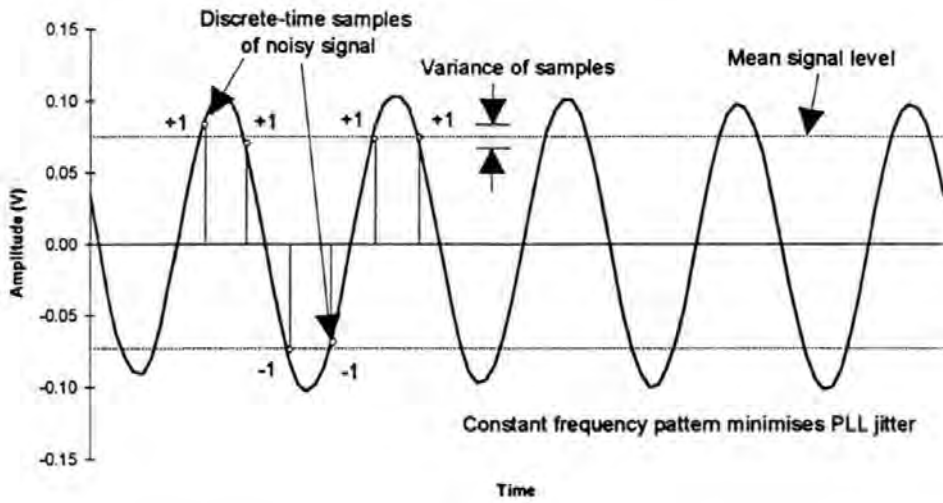


Figure 4.19 - SNR measurement technique principle. The Phase Locked Loop (PLL) is used to capture noisy samples of a constant frequency pattern.

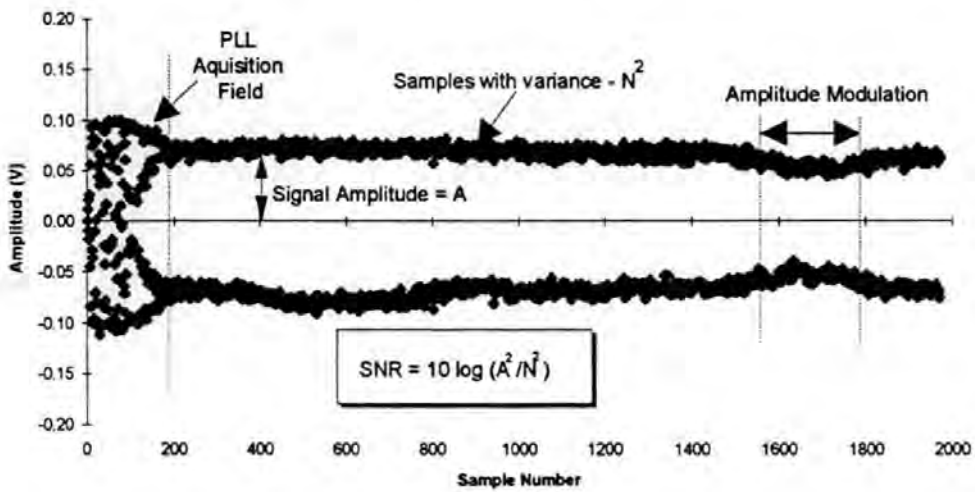


Figure 4.20 - SNR measurement technique applied over 2mm length of track. A boundary search algorithm is used to identify dropouts caused by asperities or amplitude modulation.

4.3 Performance Comparisons of the Adaptive Channel

In section 4.1 it was shown how the error rate varies as a function of normalised density (bits/PW50) and as a function of response class for a given recording performance. In section 4.2 it was shown how the proposed adaptive channel could measure the performance of the recording components over short sections of track length. The performance was characterised by measuring the signal to noise ratio and the isolated, step-response pulse width. In this section it is shown how the performance of the disk drive may be increased over a non-adaptive design by allowing the adaptive channel to compensate for the variations in recording performance identified in chapter 3.

The merits of PR4 and EPR4 signalling for the magnetic recording channel have been well reported elsewhere [Cioffi & Melas 1986; Wood & Petersen, 1986; Coker et. al., 1991a Moon & Carley, 1988; Kerwin et. al., 1993; Shafiee et. al., 1993]. It is therefore assumed that for a given signal to noise ratio into the Viterbi detector for either class of response, the detection channel is well behaved and will yield the error rate performance predicted by the response curves in figure 4.15. Therefore, in this section, recording performance is evaluated with respect to the measured signal to noise ratio and pulse width. Performance of the adaptive channel is compared against that for a fixed, non-adaptive channel design.

The performance of the adaptive channel is illustrated on recording components recording characteristics based on those used to characterise the channel response variation in chapter 3. The disk diameter is 95mm, rotating at a speed of 4500rpm. The head accesses tracks radially from 20mm to 45mm. The track width is 3 microns and the pitch is 5 microns (200 tracks/mm). The head is a thin-film dual mode inductive write / MR read. The head is assumed to have a constant flying height characteristic (in-contact) and the nominal signal

to noise ratio is therefore assumed to be constant over the recording surface and equal to 24dB (peak signal to r.m.s. noise). The nominal pulse width at any given radius is assumed to be directly inversely proportional to radius with a base value of 50ns at the inside radius at 4500 rpm (figure 4.21). The target error rate is assumed to be 1 in 10^{10} bits transferred.

4.3.1 Performance Variation with Radius

The first consideration of the adaptive channel is to cope with the change in pulse width over radius. Conventionally, the disk drive designer will make the channel a fixed data rate over all radii or band the data rate in a manner known as Zone-Bit-Recording (ZBR)¹. For a fixed data rate approach, the rate must be chosen such that the density it yields at the inner radius of the zone (which may also be the whole disk) yields the minimum required error rate performance. Then, at all radii between this and the start of the next zone (if there is one) the error rate will exceed the required minimum and useful capacity is effectively wasted.

The storage capacity of a zone is given by,

$$C_z = 2\pi r_{zi} D_{bi} \cdot (r_{zo} - r_{zi}) D_t \quad (4.13)$$

where r_{zo} and r_{zi} are the outside and inside radii of the zone respectively, D_t is the track density and D_{bi} is the linear bit density at the inside radius of the zone.

¹Zoned-Bit-Recording recovers lost capacity due to the increasing linear velocity between the inside and outside radius. If the data rate is held constant over radius, the transitions are placed further apart as the radius increases. In ZBR, the data surface is split into zones. At the inside radius of each zone the data rate is increased such that the linear bit density is the same at the inside radius of all zones.

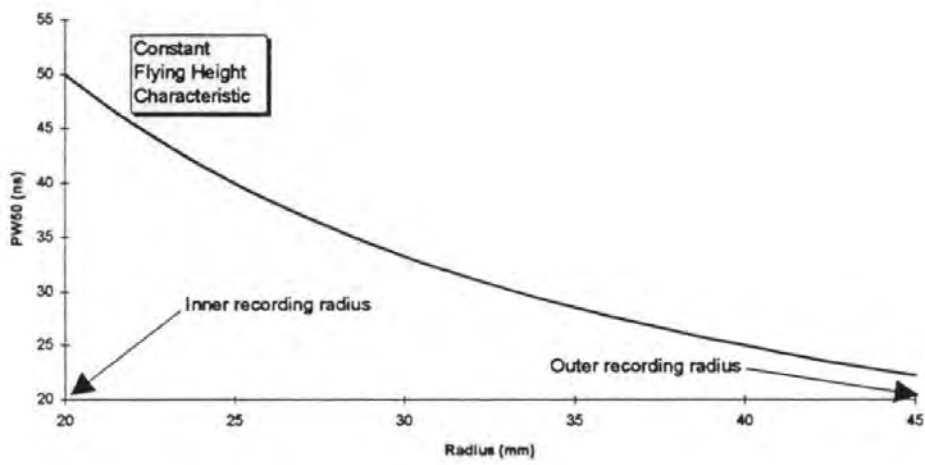


Figure 4.21 - Assumed nominal pulse width variation characteristic over radius.

For a disk with outer and inner recording radii of r_o and r_i respectively and divided into N_z equally spaced zones the capacity is given by,

$$C = 2\pi r_i D_{bi} (r_o - r_i) D_t \left[1 + \frac{(N_z - 1)(r_o - r_i)}{2r_i N_z} \right] \quad (4.14)$$

where D_{bi} is the linear bit density at the inside radii of each zone (which is the same for all zones). Hence, the increase in capacity achieved by going to N_z zones over a non-zoned design is given by,

$$C_{N_z} = \left[1 + \frac{(N_z - 1)(r_o - r_i)}{2r_i N_z} \right] C \quad (4.15)$$

Increasing the number of zones from 1 to 5 for a disk with inside and outside radii of 20mm and 45mm respectively yields an increase of 50% in recording capacity over the unzoned case and increasing the number of zones to 10 yields an increase of 56% in storage capacity over the unzoned case. Increasing the number of zones still further brings smaller and smaller reward for the added complexity in conventional disk drive design, and, depending on the variance of other variables (e.g. differences between different head/disk combinations) brings no benefit whatsoever if these approach the same spread of pulse widths nominally found across the zone.

The adaptive channel does not suffer from this limitation because it will also take account of variations from the nominal value at any particular radius on the disk. Therefore, the number of zones in the adaptive channel is equal to the number of tracks and nominally the full advantage of zoning is realised. Furthermore, the channel will also use the EPR4 class

wherever possible to further extend capacity over that which would be achieved with a class PR4 only implementation. Of course, it would be desirable for the channel to use EPR4 over all radii, but, in the presence of the finite processing speed constraint this is not always possible.

The channel operation is illustrated in figure 4.22 for the head / disk parameters detailed above. The two dotted lines extending from bottom left towards the upper right of the graph show the maximum channel data rate as a function of radius which achieves the desired error rate for both classes of response. The lines are obtained from figure 4.15 by extending a line corresponding to a signal to noise ratio of 24dB across to intersect the $1 \text{ in } 10^{10}$ error rate curve for both classes of response. The corresponding normalised density, k , to achieve this constraint is then read off the bottom axis. The channel data rate, R_D , is then obtained from (4.12).

Referring to figure 4.22 it can be seen that at radii below approximately 30mm, the data rate required to meet the error rate performance is greater for EPR4 than PR4. Hence, EPR4 is selected by the channel in order to maximise capacity / data rate. At 30mm, the maximum data rate of 80 Mbits/sec for EPR4 is reached. Between this radius and about 35.5 mm EPR4 still gives better performance than PR4 with a fixed data rate. Over this zone, the error rate improves over the required minimum. At 35.5mm, the performance of PR4 in terms of capacity / data rate for the minimum required error rate starts to exceed that of EPR4 at 80 Mbits/sec and so the channel switches to PR4 and returns to constant density recording.

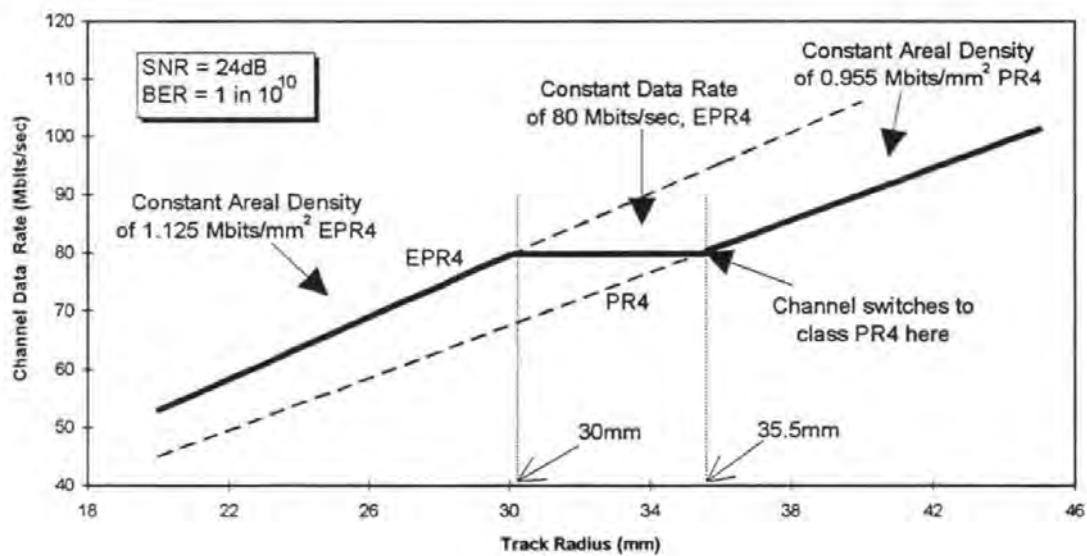


Figure 4.22 - Operation of the adaptive channel to maximise capacity in the presence of radial changes in pulse width

The overall capacity of the adaptive channel for this situation is compared to that for a conventional data channel design. Firstly, the simplest case of a fixed data rate PR4 implementation is considered. The data rate is determined by that which yields the minimum error rate performance at the inside radius for PR4. This corresponds to a data rate of 45 Mbits/sec and a linear bit density, D_b , of 4777 bits/mm. From (4.13) the capacity of this implementation would be 3 Gbits. If a zoned PR4 system were implemented with, for example, 5 zones, the capacity would, rise to 4.5 Gbits. On the other hand an EPR4 system with the same complexity could be implemented which had 4 zones from 20mm to 30mm and 1 zone from 30mm to 45mm (running at the maximum data rate.) The data rate and linear bit density at the inside radius for EPR4 from figure 4.15 are 52 Mbits/sec and 5520 bits/mm respectively. The capacity of this implementation would be $1.65 + 3.12 = 4.77$ Gbits.

The capacity of the adaptive channel in the regions where there is constant recording density may be found from,

$$C_{C.D.} = \text{Recording Area} \times \text{Areal Density}$$

$$\text{where, Areal Density} = D_b \cdot D_t \text{ (bits / mm}^2\text{)}$$

The capacity of the adaptive channel implementation is given by the sum of the achieved capacities over the three regions,

$$C_{20-30\text{mm}} = \pi(30^2 - 20^2) \cdot 200 \cdot 5520 = 1.73 \text{ Gbits}$$

$$C_{30-35.5\text{mm}} = 2\pi \cdot 30 \cdot 5520 \cdot (35.5 - 30) \cdot 200 = 1.14 \text{ Gbits}$$

$$C_{35.5-45\text{mm}} = \pi(45^2 - 35.5^2) \cdot 200 \cdot 4777 = 2.3 \text{ Gbits}$$

$$\text{TOTAL} \quad \quad \quad 5.17 \text{ Gbits}$$

Therefore, the adaptive channel is able to increase capacity by 72 % over the non-zoned PR4 implementation, 15% over the zoned PR4 implementation and 8% over the zoned EPR4 implementation. This is a significant increase in capacity over the fixed channel approach when applied to the components used here. Clearly, the actual increase in capacity will depend on the performance of the head / medium and the associated practical constraints. However, if this increase is possible for a particular implementation, it is obtained 'free of charge' - the channel is adaptive for other reasons than simply coping with deterministic variations in pulse width over radius.

4.3.2 Performance Variation along the Track Length

It was shown in chapter 3 that the recording performance of the medium can change significantly along the recorded track. For dual-layer perpendicular media, a noise attributed to domain walls in the underlayer can cause 'spikes' in the replay signal and which are fixed in positions over the disk surface. The well known phenomena commonly known as amplitude modulation which is due to sputtering inhomogenities during manufacturing was also illustrated. The effect of both these noise sources is to modulate the signal to noise ratio along the track length. Conventionally, the fixed channel has to be designed to yield the minimum required error performance in the presence of this type of variation. That is, the worst case signal to noise must be assumed along the track length. In all

regions where the signal to noise ratio is better than the worst case, channel capacity is wasted.

To investigate the significance of this loss and demonstrate the ability of the adaptive channel to recover it, the simple track-length signal to noise model illustrated in figure 4.23 is employed. Here, the nominal signal to noise ratio is assumed to be 24dB. However, over lengths of track which in total comprise 10% of the recorded track length, the signal to noise ratio drops by 2dB to 22dB. It is assumed that this model broadly reflects the effects of spike noise, and / or amplitude modulation presented in chapter 3.

The fixed channel design must assume the worst case signal to noise ratio along the length of the recorded track. Therefore, referring to figure 4.15 the normalised density which yields an error rate of 1 in 10^{10} for PR4 drops from 2.25 for a signal to noise ratio of 24dB to 2.03 for a signal to noise ratio 22dB. Similarly, the normalised density for EPR4 drops from 2.7 to 2.43. In both cases, the reduction in density to cope for the 2dB loss in signal to noise ratio is about 10%. Therefore, the overall capacity for a fixed implementation will also drop by the same proportion.

The adaptive channel will detect the performance of the track along its length and adjust the density accordingly. For 90% of the track length, the signal to noise ratio is 24dB and the channel chooses normalised densities of 2.25 and 2.7 for PR4 and EPR4 respectively and implements whichever gives the greater capacity. For 10% of the track length, the channel chooses normalised densities of 2.03 and 2.43 and, once again, implements whichever gives the greater capacity. Therefore, the channel capacity is reduced by 10% only in the 10% of the track length that is corrupted by the noise source. Overall, the track capacity is reduced

by only 1% as compared to 10% for the fixed design case. Therefore, the adaptive channel recovers 9% in capacity over the fixed design case.

Extending this analysis over a range of percentages that the track is corrupted by the noise, and, over a range of noise amplitudes yields the results in figure 4.24. One can see from this that as the percentage of track corrupted by the noise increases, the percentage of recovered capacity that the adaptive channel achieves over the fixed approach, reduces. On the other hand, as the significance of this noise increases (in terms of signal to noise loss), so too does the percentage of recovered capacity. One can see from this figure that the channel is particularly effective at recovering capacity when the noisy lengths of track are a small proportion of the total track length and relatively large in amplitude. For a disk with amplitude modulation of 30%, this corresponds to variations in 3dB in signal to noise along the track. If this covered 50% of the disk surface, then the loss recovered by the adaptive channel is about 10%. On the other hand, if this only covered 10% of the disk surface the recovered capacity is approximately 18%.

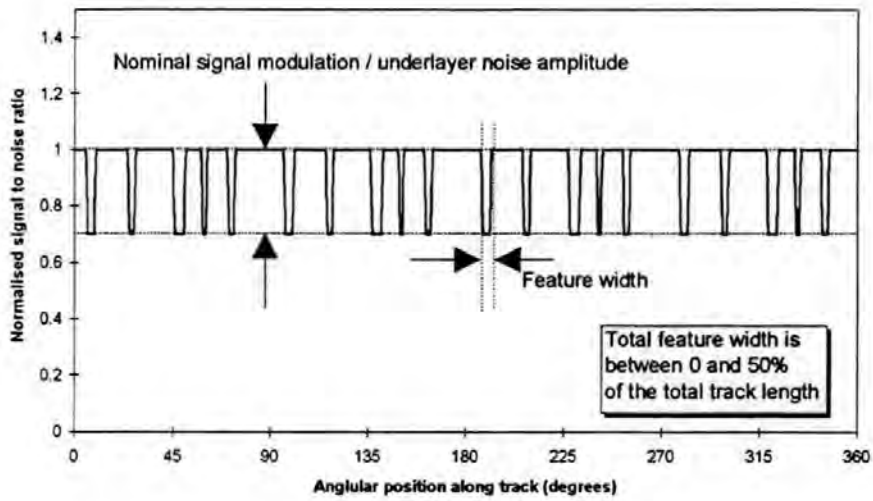


Figure 4.23 - Model of signal to noise variation along the track length

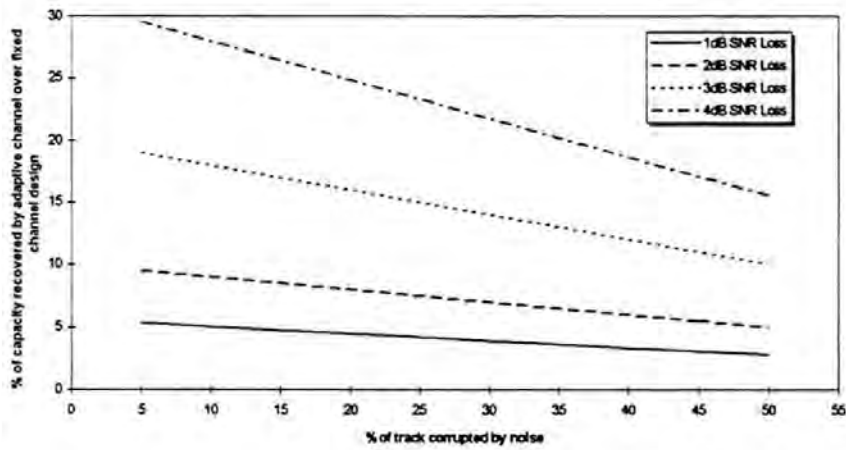


Figure 4.24 - Capacity that adaptive channel recovers over a fixed-design approach as a percentage of track corrupted over various degrees of corruption.

4.3.3 Channel Variations over Head /Media Population

In conventional fixed disk drive design a procedure known as matrix testing is employed to statistically find the spread of recording performance over a sample of components to be used in a particular disk drive product. Each head in the sample is tested against each disk in the sample. The result is a matrix of performance measurements which have a (assumed) Gaussian distribution about the nominal performance. The data channel is then designed to cope with all variations in channel performance which fall within a multiple of the standard deviation of the distribution about the mean (e.g. plus or minus three standard deviations). In practice this means that the data channel would be designed to yield the minimum error rate performance for the worst case head and disk which just falls inside the specified deviation from the mean. Therefore, for all head and disk combinations that perform better than this worst case situation, information capacity is wasted in the fixed channel design.

Figure 4.25 illustrates the fixed design approach which has to cope with variations in recording performance between different head / media combinations. The probability density function is assumed Gaussian and the random variable is some generalised measure of recording component performance (for example, signal to noise ratio, pulse width etc.).

For the purposes of the illustration we assume that a plus or minus 3-sigma deviation in pulse width between head / media combinations corresponds to a minimum and maximum of plus or minus 10% about the mean, i.e. at the middle radius of the disk, where the nominal pulse width across all heads and disks is 31ns, the channel is expected to cope with actual pulse widths between 27.9ns and 34.1ns. This corresponds to a standard deviation of 1.03ns at this radius. Assuming a nominal signal to noise ratio of 24dB we see from figure 4.15 that for an error rate of 1 in 10^{10} the maximum normalised densities for PR4 and

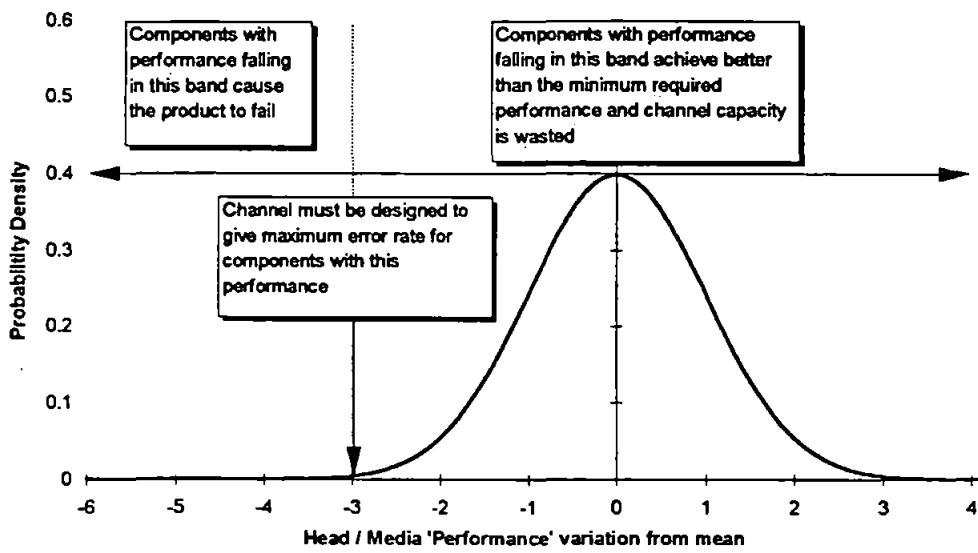


Figure 4.25 - Illustration of the distribution of recording component performance

EPR4 are, as before, 2.25 and 2.7 respectively. If the channel were designed with the nominal pulse width of 31ns, the required signalling rate would be 72.6 Mbits/sec for PR4 and 87.1 Mbits/sec for EPR4 to achieve the minimum error rate performance. However, if this were done, whenever the actual pulse width were greater than the nominal case, the normalised density would rise and the error rate performance would fall below the minimum requirement; the drive would fail. Therefore, the fixed channel must be designed for the widest pulse width such that all actual pulse widths in the specified distribution are narrower and therefore the density is lower. In this example this corresponds to signalling rates of 66 Mbits/sec and 79 Mbits/sec respectively. It is clear, therefore, that capacity is reduced from the nominal point by 10% - the width of the specified distribution.

By adjusting the signalling rate according to the head / media performance the adaptive channel is able to recover this loss in capacity. This is because it is not required to operate at the worst case point for all heads and disks but only those that require it. Furthermore, it is also able to exploit the conditions when the recording performance is better than the nominal case. Using the above example, a head / media combination at the other extreme of performance would yield an increase of 20% in capacity over the non-adaptive channel.

In chapter 3 it was shown that not only did pulse width vary considerably between head / media combinations (due primarily to differences in head-media spacing) but so too did the signal amplitude. Over the small sample tested, the signal amplitude varied by about 10% between the worst and best combination. This corresponds to a spread of 2dB in signal to noise ratio for a non-media noise limited channel. At moderate densities ($PW_{50}/T=2$ to 3) a drop in 1dB of signal to noise ratio from 24dB to 22dB corresponds to a drop in capacity of about 5%. Therefore, the fixed channel must, once again, be designed to yield the minimum error performance for the worst case situation and assume a signal to noise operating point

of 23 dB over all head / disk combinations. Then, whenever the actual performance is better, the potential increase in capacity is wasted. The adaptive channel, as before, regains this lost capacity.

If signal amplitude and pulse width are completely correlated, the nominal gain in capacity by moving from the fixed channel to the adaptive channel is equal to the sum of the widths of the deviations for the two distributions. That is, if the pulse width and signal amplitude are completely correlated, the widest pulse width in the distribution also corresponds to the lowest signal amplitude. This might be expected to occur if the variations between head / media pairs were due primarily to changes in head-media spacing rather than differences in recording medium performance. In such a situation a high flying head would be expected to give a wider pulse width with lower amplitude. Using the above example this means that the fixed channel must be designed to give the minimum error performance at a worst case signal to noise ratio of 23 dB with a worst case pulse width of 34.1ns. This corresponds to a signalling rate of 63Mbits/sec and a drop of 15% from the nominal case of 72.6 Mbits/sec for a SNR of 24dB and PW50 of 31 ns.

The result of the adaptive channel recovering lost capacity due to head / media performance variations is that the capacity of the average disk surface increases by, for example 15% over a fixed data channel design. Some disk surfaces will increase in capacity by as much as 30%. Indeed, the result will be that the capacity per surface will take on a probability distribution function the same form as that for the variation in head / media performance itself. If the capacity probability distribution function of each disk surface is Gaussian with mean μ_s and variance σ_s^2 then the probability density function of drive capacity (assuming independently distributed capacities per surface) is the linear sum of the individual surface

capacity distribution functions. If the drive contains N data surfaces, the mean drive capacity is;

$$\mu_d = N\mu_s ;$$

with standard deviation,

$$\sigma_d = \sigma_s \sqrt{N} .$$

From section 4.3.1. a fixed PR4 5-zoned implementation yielded a surface capacity of 4.5 Gbits before taking into account variations due to head / medium tolerances. If it is assumed that these tolerances are as the above discussion the capacity per surface of this fixed PR4 design must be dropped by 15% to account for the worst case head/media combination. This yields a fixed capacity of 3.91 Gbits/surface and for a 4 surface disk drive a total of 15.64 Gbits (1.96 GBytes). The adaptive channel would nominally regain the loss due to head / media population with a mean of 4.5 Gbits/surface and assuming that the 15% gain corresponds to 3-sigma standard deviation, a standard deviation of 197 Mbits/surface. Therefore, the adaptive channel would produce a 4-surface disk drive product with an average of 18 Gbits (2.25 GBytes) of capacity with a standard deviation of 788 Mbits (98.5 MBytes).

4.3.4 The User-Specified Self-Optimising Disk Drive

It has been shown that considerable increase in capacity can be achieved when the channel is made adaptive and allowed to alter its recording strategy according to the performance of the recording components. In the example taken, the objective was to maximise data rate and therefore storage capacity whilst maintaining a minimum error rate performance of 1 in 10^{10} bits. It would therefore be possible to also allow this requirement to be adaptive in the sense that the user (or manufacturer) could decide what the target error rate should be. This could prove advantageous if the disk drive were to be used (or marketed) in a variety of applications (markets).

For example, the requirements for storing digital video are somewhat different to those for computer data. Typically, a high data rate is required to ensure uninterrupted playback of the video caption. On the other hand, the error rate requirements are not so stringent. Therefore, by referring to figure 4.15 it can be seen that normalised density (and therefore data rate) can be increased at the expense of error rate requirement. For example, a digital video application may only require a raw error rate of 1 in 10^4 bits transferred. For a disk with the same nominal signal to noise performance as before, 24 dB, the corresponding normalised densities for PR4 and EPR4 are 2.6 and 3 respectively - an increase of 15% and 9% respectively over the normalised density to give an error rate of 1 in 10^{10} bits.

Furthermore, the adaptive channel could also be given the option of changing the disk rotation speed. Lowering the speed would allow the channel to use EPR4 over more of the disk surface (since in this example it is limited to 80 Mbits/sec at somewhere near the middle radius). EPR4 yields approximately 20% increase in density over PR4 at moderate densities ($PW50/T=2-3$) and high error rate performance. This might be useful for a user

who required maximum storage capacity and a high minimum error rate performance but was not too concerned about data rate. This is the classic requirement in archival storage where tape products currently dominate.

Therefore, not only may the adaptive channel recover wasted capacity over the fixed design approach but may also allow the user to tune its overall performance to more closely meet their needs.

4.4 Implementation Issues

The proposed adaptive data channel is shown in figure 4.26. The read and write process are as the conventional partial response maximum likelihood method [Dolivo, 1990] except that the precoder, adaptive equaliser and Viterbi detector may be switched between PR4 and EPR4 in operation. The data detection operation is illustrated in figures 4.27 - 4.29 for PR4..

A programmable filter is used to bandlimit the signal and attenuate the noise above the signalling bandwidth. Decision directed timing which compares the sample values from the AGC during a phase-lock acquisition field is used to derive a read clock (figure 4.27) (appendix D). The sample values are then fed through an adaptive equaliser which is trained with a preset sequence for either PR4 or EPR4 operation (figure 4.28). The adaptive algorithm uses the Least Mean Squares (L.M.S.) algorithm to derive the tap weights [Widrow & Stearns, 1985]. Investigation found that 10 taps was necessary to provide adequate equalisation of the incoming waveform; performance gradually improving from 3-taps to 10-taps with no detectable increase in performance thereafter. This was in agreement with recent results published elsewhere [Kerwin et. al., 1993]. The un-equalised and equalised outputs for the 10-tap equaliser for PR4 are shown in figure 4.29 (a) and (b) respectively. From the output of the adaptive equaliser the samples are fed into a Viterbi detector where the data is decoded. It is assumed that the interleaved 2-state decoder is implemented for PR4 operation and that the 8-state is implemented for EPR4 [Wood, 1986; Forney, 1973].

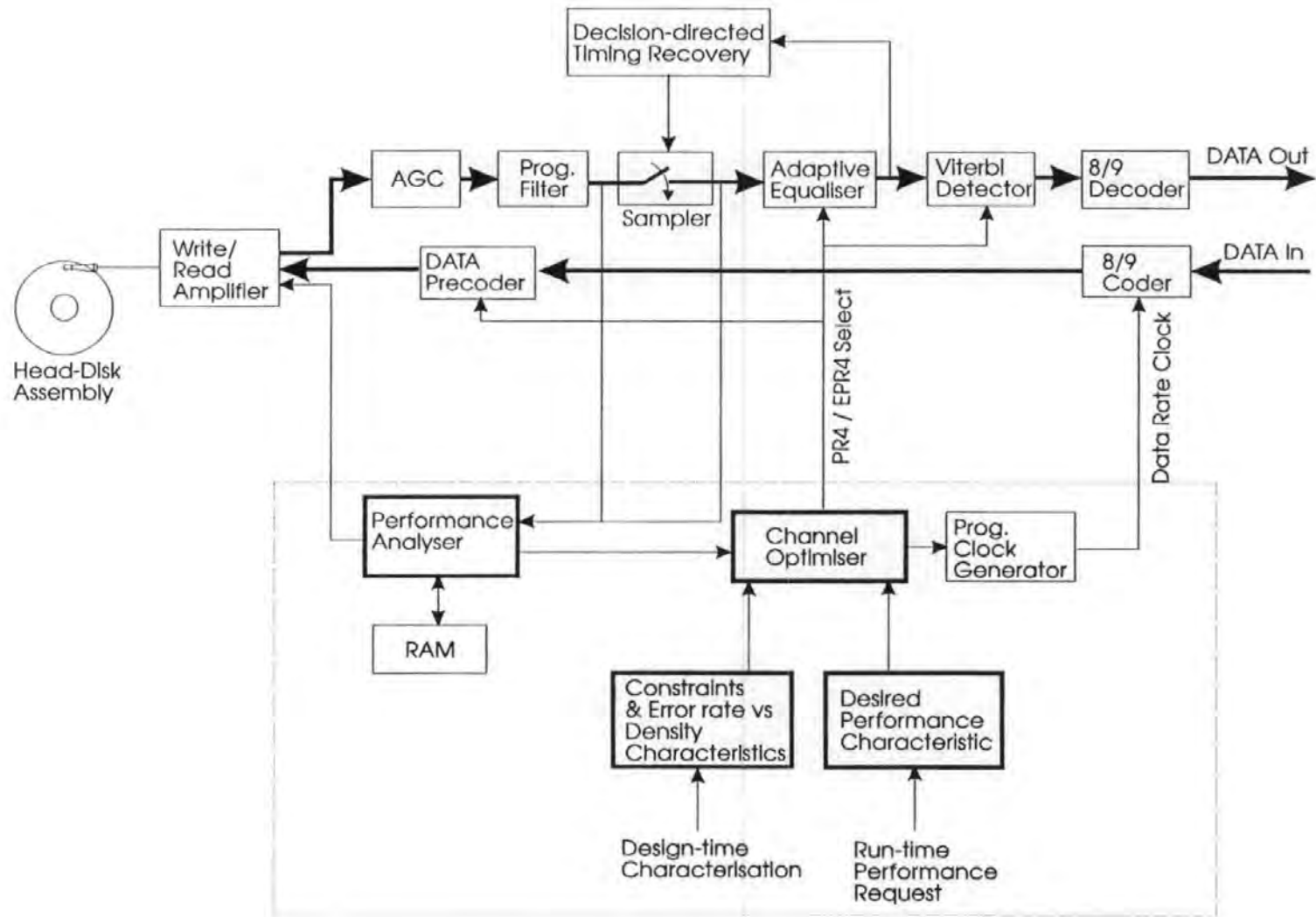


Figure 4.26 - The Adaptive Partial Response Data Channel

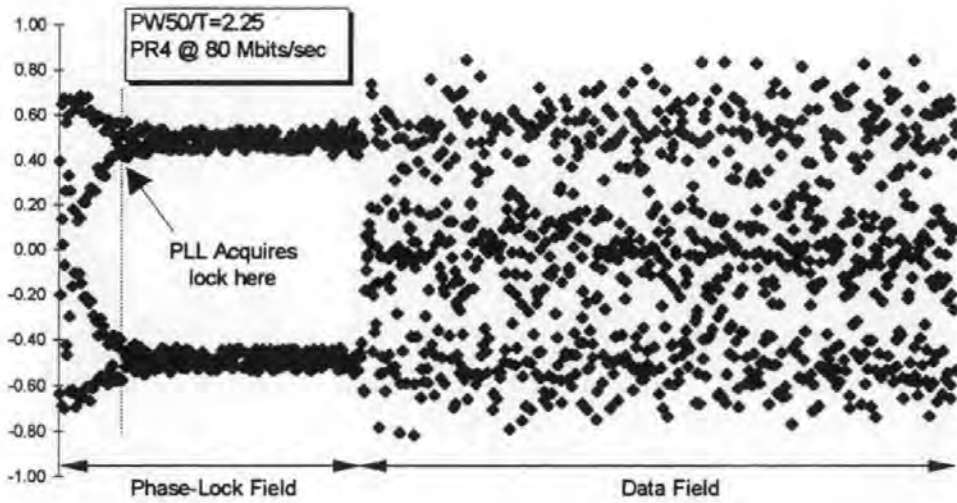


Figure 4.27 - Output from sampler showing PLL lock field and the non-equalised data samples.

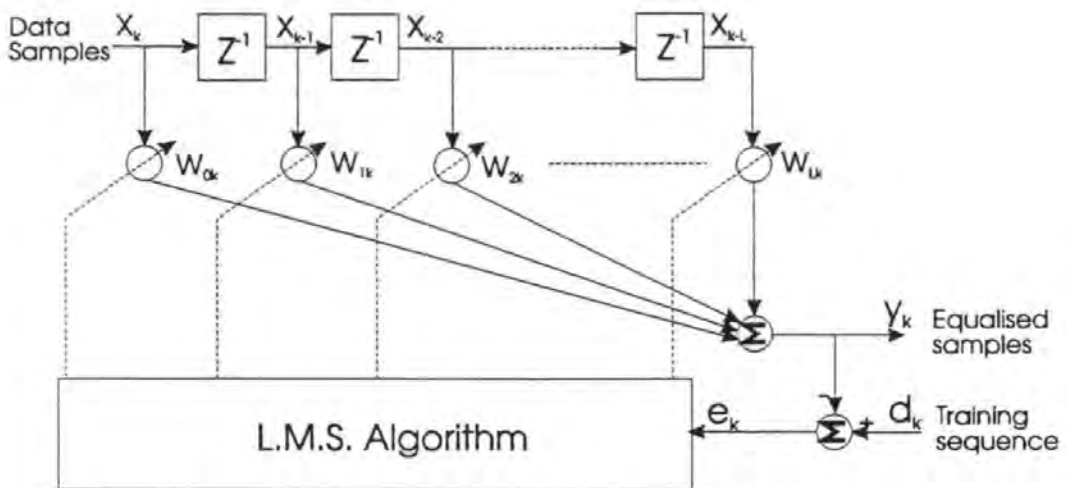
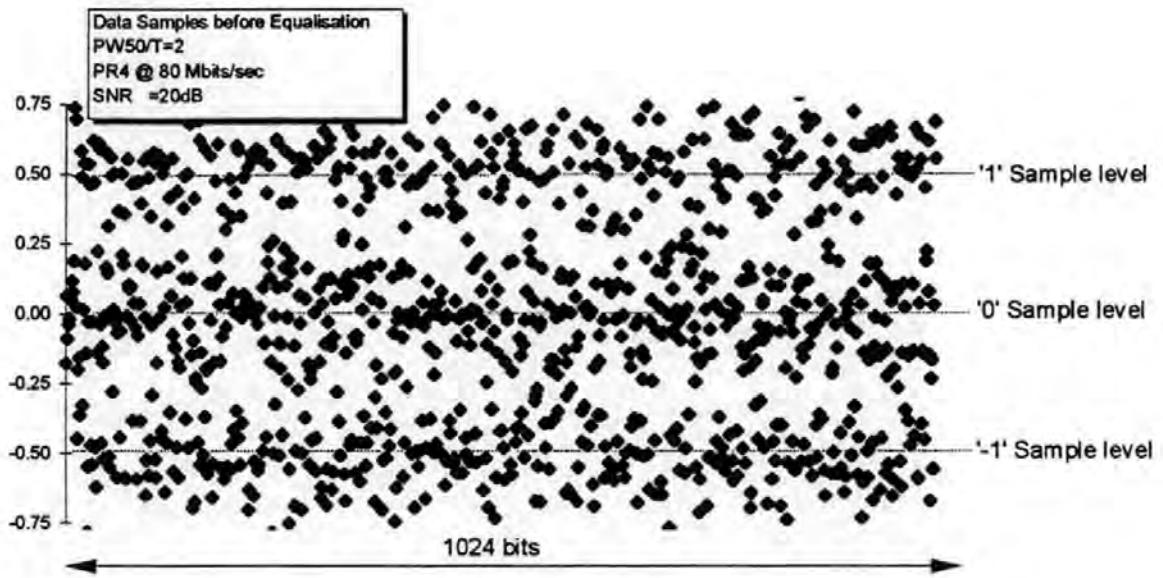
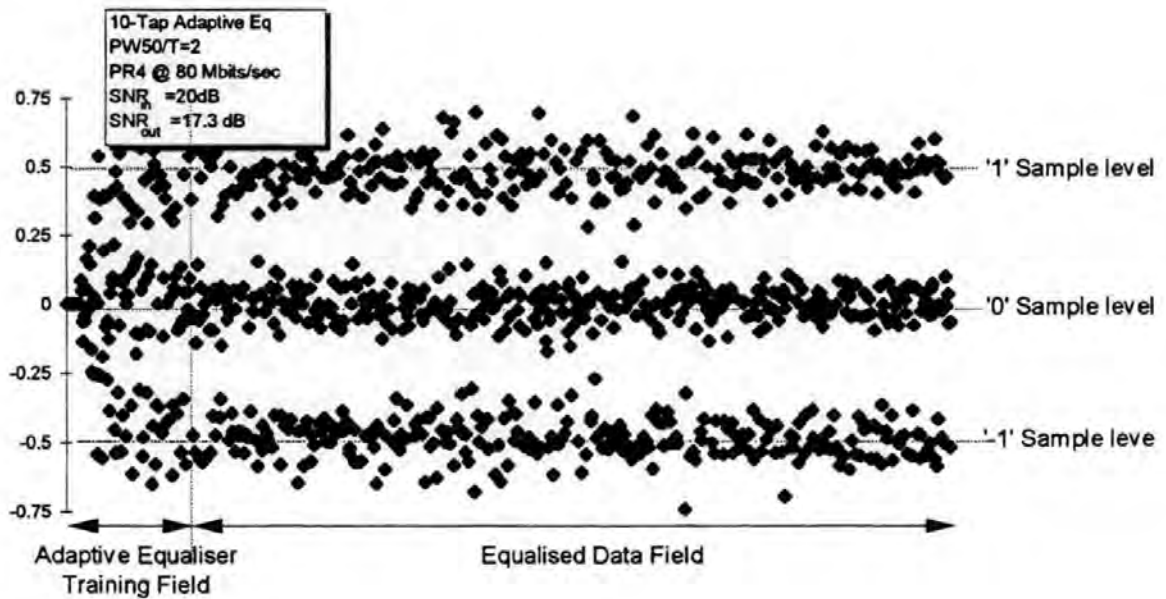


Figure 4.28 - Schematic diagram of adaptive equaliser.



(a)



(b)

Figure 4.29 - Operation of the adaptive equaliser. (a) Un-equalised and (b) equalised data samples. The output signal to noise ratio of the equaliser (17dB) is 2.7dB less than the input (20dB). This is in agreement with the SNR loss characteristic in figure 4.15 at this density.

In addition to the standard channel functions, the performance analyser and channel optimiser are added. The performance analyser, at some convenient time, takes control of the disk drives' electronics and performs the pulse width measurement and signal to noise measurements detailed previously. It is assumed that the channel will measure the surface performance and divide up each track into sectors; the start positions of which correspond to the locations of step variations in recording performance identified by the measurement techniques. In a less optimal design the sector positions and lengths could be fixed along the track length.

The time it takes to characterise the components in the disk drive will depend on the resolution of the required adaption with respect to the sector length. For example, assuming a product has 4 surfaces and 5000 tracks per surface, the total number of tracks to characterise is 20,000. If the number of sectors per track is 30, the total number of characterisations is 600,000. For a disk spinning at 4500 rpm with period of 13.33 ms, the head is over each sector for a period of 444 μ s. If it is assumed that each characterisation takes less time than this to perform (it was assumed earlier that the time for pulse width measurement was 20 μ s) then the system will be ready for the next characterisation well in advance of the next sector appearing under the head. The time it takes the head to see all sectors in all tracks is 20,000 tracks \times 13.33ms = 266 secs. If the head is not able to characterise the sectors one after another (because the processing time exceeds the sector length), it can be seen that the computation time could be increased very significantly due to the extra disk rotations that are involved. This may be a practical reason for fixing the sector lengths.

Having determined the performance of each sector, the channel must store the decision it has made about how to record there in some way. The problem is two-fold, the channel

must know in advance of recording in this sector what class of response will be used, and, what signalling rate to use. Furthermore, when it later comes to read the information, the phase-locked-loop must be able to lock on to the data frequency and the channel must know what class of response to decode. Two approaches could be taken.

The first is to store this information in programmable, non-volatile memory. If it is assumed that this information could be stored in 8 bits (1 bit for response class, 7 bits for signalling rate), the total required capacity, for the previous example, would be 600 kBytes - this is not an unrealistic size. 7-bit accuracy for the data rate should be sufficient when it is noticed that the data rate will be somewhat deterministic and so only the difference from the nominal value needs to be stored.

On the other hand, perhaps a more natural place to put this information is at the start of each sector; a part which is written to the disk when the drive is formatted (this information is not erased until the drive is formatted). Here, the phase-locked-loop lock field could be written at the previously determined signalling rate and a simple pattern following shortly afterwards could indicate the class of response that follows. This pattern would be decoded by a simple thresholding circuit and could use the same elements that are used in the PW50 measurement circuit. In write mode and read mode the channel clock would lock onto the frequency of this field before entering the data field. Therefore, the length of this field will need to be longer than in a fixed channel design where the phase-locked-loop is already running at a frequency very close to that recorded and where generally the time it takes to lock is determined only by the phase error. It is estimated that a phase-locked-loop field twice the length of that normally implemented would be required. It is estimated that this, along with the response class information would add approximately a 5% overhead to the sector.

Therefore, if the channel is made adaptive down to the sector level, it is assumed that the capacity gains discussed in section 4.3.2 would be reduced by 5%. It is estimated that the cost of implementing the adaptive channel in terms of extra circuitry required is minimal since many of the electronic functions it requires are already present in the partial response maximum likelihood method. However, some of these parts may need upgrading to a higher specification, in particular the microprocessor, which is required to perform the enhanced analysis.

Chapter 5.

Conclusions & Future Work

5.1 Conclusions

1. Variations in the nominal performance of the magnetic recording channel were investigated for longitudinal and perpendicular thin-film media in terms of their effect on signal amplitude and step response pulse width. The primary variation in pulse width is deterministic and due to the proportional change in linear velocity between the head and medium as the head moves from inside to the outside recording radius of the disk. This variation is countered somewhat for flying heads by the increased flying height at the outside radius. It was concluded that as the trend for flying height continues towards an in-contact environment, and, as form factors reduce, the variation in pulse width over radius will increase.
2. Signal amplitude exhibited a nominal change of about 10% between the inside and outside radius for the MR head and longitudinal thin-film media. It was concluded that this was due to radial changes in flying height. For a channel which was media noise limited it was concluded that since media noise scaled proportionally with signal amplitude, signal to noise ratio remained constant. Conversely, if the channel were electronic noise limited then the signal to noise ratio would increase towards the inner radius. It was observed that in the in-contact environment signal amplitude would not

change with radius and that if the channel were either media noise or electronic noise limited, the signal to noise ratio would also, therefore, not change as a function of radius.

3. Aspects of noise and distortion properties of perpendicular and longitudinal media were investigated in terms of their effects on the replay signal along the recorded track. It was discovered that dual-layer perpendicular media exhibited an additional low-frequency noise source which, through the application of a new observation technique, was attributed to domain wall formation in the underlayer of the media. It was noted that the position of these domain walls remained stable unless influenced by a dimensionally large magnetic field. The effect of these domain walls, which has been noted elsewhere, can lead to partial erasure of the data in the recording layer and therefore modulate the signal to noise ratio along the recorded track. An effect commonly known as amplitude modulation was illustrated with the MR head and longitudinal thin-film media. It was concluded that this significant phenomena also modulates the signal to noise ratio along the recorded track.

4. A limited study of recording performance over a sample of heads and media of the same type showed that there were significant changes between different combinations of the same components. It was found that there was a 15% difference in measured pulse width between the worst and best head and disk combination. Signal amplitude varied by 10% over the same components. It was concluded that the variation in pulse width between different head/media pairs was due to variance in head-media separation and not the recording performance of the media.

5. Error rate as a function of normalised recording density and signal to noise ratio was determined for the longitudinal MR head and media for the PR4 and EPR4 classes of partial response. It was discovered that the roll-off at higher densities did not agree with the results produced previously by other authors using a Lorentzian model. Investigation into this concluded that the step response for the MR head used in this investigation was not well approximated by the Lorentzian model with Lorentzian coefficient of 2 (a coefficient of 2.6 provided a closer fit).
6. Simple methods enabling the proposed adaptive channel to measure the signal to noise ratio and pulse width were presented. Analysis showed that such measurements could be made down to relatively small lengths of track (< 1mm) and gain the accuracy required.
7. Analysis of the adaptive channel's ability to recover capacity over a non-adaptive design was presented. The analysis showed that the adaptive channel fully realises the capacity gains associated with zoning since it adjusts the data rate accordingly at every track. In an example using recording components similar to those used in the variation characterisation, the capacity improvement of the adaptive channel over a 5-zoned PR4 implementation was 15%. The improvement over a 5-zoned EPR4 implementation was 8%.
8. The capacity gains to be realised by adjusting to recording performance variations along the recorded track were shown to be approximately 9% over the non-adaptive channel when the variations accounted for a 2dB (20% modulation) drop in signal to noise ratio from the nominal value and, in total, corrupted 10% of the track length. It was concluded that the adaptive channel would be particularly effective in recovering capacity when the total corruption length was short and its magnitude was large.

9. In responding to variations in recording performance between different head / media pairs it was found that the nominal capacity gain over a non-adaptive design was equal to the difference in performance between the worst expected and nominal head / disk pair in the manufacturing distribution. Assuming a value of 15%, the result of allowing the channel to recover this capacity was to produce a disk drive with an average capacity 15% higher than the non-adaptive design but with a distribution of capacities about the increased nominal value. It is suggested that the manufacturer could band the product into fixed capacity bands with the advantage that both the yield and average capacity would be increased significantly over the non-adaptive case.

10. Therefore it is concluded that the advantages of the adaptive channel over a non-adaptive design are that increased capacity for the same physical recording components over a non-adaptive design is achieved; higher manufacturing yields are obtained because the channel is able to identify and correct for poor performing components; and, flexibility in allowing the user to determine the disk drive performance according to their specific needs. It is believed that these advantages are achieved with a modest increase in complexity.

5.2 Future Work

The adaptive channel concept has been shown here to provide gains over the fixed design approach over three types of variation. The overall increase in capacity will depend on the interrelation between these variables. This is not well understood. In particular, it has been assumed that variations between different head / media pairs was attributable to differences in the flying height of the head and not due to differences in media performance. In practice this may not be the case. Also, the variations along the track length may be related to flying height and general media performance in a more complicated way than has been assumed here (zero correlation). Therefore, future work is required to better understand these variables and the interrelationship between them, in order to predict what the overall capacity gains of the adaptive channel would be.

This investigation has focused only on the signalling aspects of the information storage and Channel Coding and Error Control Coding issues have not been considered. The adaptive channel concept should naturally enclose these functions as well as the underlying signalling methods. Therefore, adaptive error control and channel coding methods need to be investigated in the context of the magnetic recording channel. It may be that some of the channel variations are better dealt with by variable coding and / or error rate control, rather than changing the underlying signalling method.

Bibliography

Aoi H., Saitoh M., Nishiyama M., Tsuchiya R., Tamura T., "Noise characteristics in longitudinal thin-film media", *IEEE Trans. Magn.*, MAG-22, No.5, pp.895-897 (Sept. 1986)

Arai R., Kato T., Takanami S., "Readback equalisation in digital magnetic recording", *IEEE Trans. Magn.*, MAG-20, No.5, (Sept. 1984)

Arnoldussen T.C., Tong H.C., "Zigzag transition profiles, noise and correlation statistics in highly oriented longitudinal film media", *IEEE Trans. Magn.*, MAG-22, No.5, pp.889, (Sept. 1986)

Barbosa L.C., "Minimum noise pulse slimmer", *IEEE Trans. Magn.*, MAG-17, No.6, pp.3340, (Nov. 1981)

Baugh R.A., Murdock E.S., Natarajan B.R., "Measurement of noise in magnetic media", *IEEE Trans. Magn.*, MAG-19, pp1722-1724, (1983)

Belk N.R., George P.K., Mowry G.S., "Noise in high performance thin-film longitudinal magnetic recording media", *IEEE Trans. Magn.*, Vol. 21, pp.1350-1355, (Sept. 1985)

Berghof W., Gatzen H.H., "Sputter deposited thin-film multilayer head", *IEEE Trans. Magn.*, MAG-16, pp.782, (1980)

Bertram H.N., Hallamasek K., Madrid M., "DC modulation noise in thin metallic media and its application for head efficiency measurements", *IEEE Trans. Magn.*, Mag-22, No.4., pp. 247-252, (July 1986)

Che Xiaodong, Bhattacharya M.K., Bertram H.N., "Studies of non-linear bit shift and partial erasure using pseudo-random sequence", *IEEE Trans. Magn.*, MAG-29, No.6, pp.3972, (Nov. 1993)

Cioffi J.M., Melas C.M., "Evaluating the performance of maximum likelihood sequence detection in a magnetic recording channel", *Proceedings of the Globecom '86 conference*, Houston, Texas, pp.1066, (Dec. 1986)

Cioffi J.M., Abbott W.L., Thapar H.K., Melas C.M., Fisher K.D., "Adaptive equalisation in magnetic-disk storage channels", *IEEE Comms. Magazine*, pp.14, (Feb. 1990)

Clark A.P., *Adaptive detectors for Digital Modems*, Chapter 2 - Maximum Likelihood Detection, Pentech Press, 1989

Cohn M., Jacoby G.V., Bates C.A., "Data encoding method and system employing two-thirds code rate with full word look-ahead", U.S. Patent 4,337,458, (29th June 1982)

Coker J.C., Galbraith R.L., Kerwin G.J., Rae J.W., Ziperovich P.A., "Integrating a partial response maximum likelihood data channel into the IBM 0681 disk-drive", *Proceedings of the 24th Asilomar Conf. (Monterey)*, pp.674, (Feb 1990)

Coker J.C. Galbraith R.L., Kerwin G.J., Rae J.W., Ziperovich P.A., "Implementation of PRML in a rigid disk drive", *IEEE Trans. Magn.*, MAG-27, No.6, pp.4538, (Nov. 1991a)

Coker J.C., Galbraith R.L., Kerwin G.J., "Magnetic characterisation using elements of a PRML channel", *IEEE Trans. Magn.*, MAG-27, No.6, (Nov.1991b)

Comstock R.L. *Magnetic Recording Handbook*, ed. C.D. Mee, E.D. Daniel, Part 2, Chapter 2, "Data storage on rigid disks", McGraw-Hill, 1989

Darragh N.R., Mapps D.J., Donnelly T., Wade J.G., Hoinville J.R., "Observation of underlayer domain noise in perpendicular recording disks", *IEEE Trans Magn.*, MAG-29, No.6., pp3472-3474, (Nov. 1993)

Dolivo, F. "The PRML recording channel", *IBM Research Magazine*, pp.11-13, (Summer 1990)

Druyvesteyn W.F., Van Ooyen J.A.C., Raemaekers E.L.M., Postuma L., Ruigrok J.J.M., de Wilde J., "Magnetoresistive heads", *IEEE Trans. Magn.*, MAG-17, pp.2884, (1981)

Forney G.D., "Maximum likelihood sequence estimation of digital sequences in the presence of intersymbol interference", *IEEE. Trans. on Information Theory*, VOL-18, No.3, pp.363, (May, 1972)

Forney G.D., "The Viterbi algorithm", *Proceedings of the IEEE*, Vol.61, No.3, pp.268, (March 1973)

Franaszek P.A., "Sequence state methods for run-length-limited coding", *IBM Journ. Res. & Dev.*, pp376, (July 1970)

Gorter F.W., Poggiesser J.S.L., Tjaden D.L.A., "Magnetoresistive reading of information", *IEEE Trans. Magn.*, MAG-10, pp.809, (1974)

Grochowski E.G., Hoyt R.F., "Magnetic hard disk form factor evolution", *IEEE Trans. Magn.*, MAG-29, No.6, pp.4065, (Nov. 1993)

Hansen N.H., "Magnetic recording techniques for buried servos", *IEEE Trans. Magn.*, MAG-17, pp.2735, (Nov. 1981)

Hoinville J.R., "Spatial media noise studies of longitudinal magnetic recording media", D.Sc. Thesis, Washington University, (Dec. 1991)

Hunt R., "A magnetoresistive readout transducer", IEEE Trans. Magn., MAG-7, pp.150, (1971)

Indeck R.S., Johnson M.N., Guo Mian, Hoinville J.R., Muller M.W., "Noise characterisation of perpendicular media", Journ. Mag. Soc. Japan, Vol.15, Supplement S2, pp.173-178, 1991

Iwasaki S., "An analysis for the magnetisation mode for high density magnetic recording", IEEE Trans. Magn., MAG-13, pp.1272, (1977)

Jones R.E., "Analysis of the efficiency and inductance of multiturn thin-film magnetic recording heads", IEEE Trans. Magn., MAG-14, pp.509, (1978)

Jones R.E., Mee C.D., *Magnetic Recording Handbook*, Part 1, Chapter 4, "Recording Heads", 2nd Ed., McGraw-Hill (1986)

Kabal P., Pasupathy S., "Partial-response signalling", IEEE Trans. Comms., COM-23, No.9, pp.921, (Sept. 1975)

Takehi A., Oshiki M., Aikawa T., Sasaki M., Kozai T., "A thin-film head for high density recording", IEEE Trans. Magn., MAG-18, pp.1131 (1982)

Kerwin G., Galbraith R., Coker J., "Performance evaluation of the disk drive industry's second-generation PRML data channel", IEEE Trans. Magn., MAG-29, No.6, pp.4005, (Nov. 1993)

Kobayashi H., Tang D.T., "Application of partial-response channel coding to magnetic recording systems", IBM Journ. Res. & Dev., (July 1970)

Kobayashi H., "Application of probabilistic decoding to digital magnetic recording", IBM Journ. Res. & Dev., Vol.-15, pp.64, (Jan. 1971)

Koshino N., Ogawa S., "Optical method of the head positioning in magnetic disk systems", IEEE Trans. Magn., MAG-16, pp.631, (Sept. 1980)

Koster E., Arnoldussen T.C., *Magnetic Recording Handbook*, ed. C.D. Mee, E.D. Daniel, Part 1, Chapter 3 "Recording Media", McGraw-Hill, 1989

Kretzmer E.R., "Generalisation of a technique for binary data communication", *IEEE Trans. Comms.*, COM-14, pp.67, (Feb. 1966)

Kryder M.H., "Proceedings of the symposium on magnetic materials, processes and devices", *Proceedings of the IEEE*, Vol.-90, No.8, pp.25, (1990)

Lender A., "Correlative digital communications techniques", *IEEE Trans. Comms.*, COM-12, pp.128, (1964)

Mackintosh N.D., Jorgensen F., "An analysis of multi-level encoding", *IEEE Trans. Magn.*, MAG-17, No.6, pp.3329-3331, (Nov. 1981)

Madrid M., Wood R., "Transition noise in thin-film media", *IEEE Trans. Magn.*, MAG-22, No.5, pp.892-894, (Sept. 1986)

Mapps D.J. et. al., "Magnetic recording technology in Japan", *Report on Overseas Scientific and Technical Experts Mission*, pp.28, (May.1988)

Mapps D.J., Pan G., "New materials for perpendicular magnetic disk recording", *Proceedings of the international conference on materials*, Ikebukuru, Tokyo, Japan, (Sept. 1993)

Melas M., Arnett P., "Noise in thin metallic medium : The connection with non-linear behaviour", *IEEE Trans. Magn.*, MAG-24, No.6, (Nov. 1988)

Middleton B.K., *Magnetic Recording Handbook*, ed. C.D. Mee, E.D. Daniel, Part 1, Chapter 2, "The recording and reproducing processes", McGraw-Hill, 1989

Mitsuya Y., Kogure K., Oguchi S., "Mechanisms for 3.2 GByte multi-device disk storage", *Rev. Elect. Comm. Labs.*, Vol.-20, pp.46, (1982)

Miura Y., Takahashi Y., Kume F., Toda J., Tsutsumi S., Kawakami S., "Fabrication of multi-turn thin-film head", IEEE Trans. Magn., MAG-14, pp.512, (1978)

Moon J.J., Carley R., "Partial response signaling in a magnetic recording channel", IEEE Trans. Magn., MAG-24, No.6, (Nov. 1988)

Moon J.J., "Signal to noise ratio degradation with channel mismatch", IEEE Trans. Magn., MAG-27, No.6, pp. 4837, (Nov. 1991)

Moon J.J., "Timing sensitivity in discrete-time equalisation", IEEE Trans. Magn., MAG-29, No.6, pp.4027, (Nov. 1993)

Mowry G.S., George P.K., Loeffler K.M., Belk N.R., "Thin-film magnetoresistive heads for narrow-track winchester applications", IEEE Trans. Magn., MAG-22, pp.671 (1986)

Newby P., Wood R., "The effects of nonlinear distortion on class IV partial response", IEEE Trans. Magn., MAG-22, No.5, pp. 1203, (Sept. 1986)

Newby P., "Sensitivity of partial response detection in the magnetic channel", Asilomar Conf.. Circuits, System & Computers, Vol.1, pp.456, (1989)

Nishiyama T.K., Noguchi K., Mouri K., Iwata H., Shinohara T., "Recording characteristics of metal-in-gap mini composite head", IEEE Trans. Magn., MAG-23, pp.2931, (1987)

Nyquist H., "Certain topics on telegraph transmission theory", Trans. of the AIEE, Vol.-47, pp.617, (April 1928)

Okabe A., Yamamoto T., "Structure and recording characteristics for CoPtB(O) rigid disk media", paper BB-13 presented at the 37th MMM conference, Houston, Texas, December 1992

Palmer D., Ziperovich P., "Identification of nonlinear write effects using pseudorandom sequences", IEEE Trans. Magn., MAG-23, No.5. (Sept. 1987)

Price, R., Craig J.W., Melbye H.E., Perahia A., "An experimental multilevel, high density disk recording system", *IEEE Trans. Magn.*, MAG-14, No.5, pp.315-317, (Sept. 1978)

Proakis J.G., *Digital Communications*, McGraw-Hill, 1989

Sato K., Wakamatsu H., Shinohara M., "Noise characteristics of CoCrTa / NiFe perpendicular recording media", *IEEE Trans. Magn.*, MAG-29, No.6, pp.3730, (Nov. 1993)

Schmerbeck T., Richetta R., Smith L., "A 27MHz mixed analog/digital magnetic recording channel DSP using partial response signalling with maximum likelihood detection", *ISSCC91, Digest of the Technical Papers*, Vol.34, pp.136, (Feb. 1991)

Schneider, R.C., "An improved pulse slimming method for magnetic recording", *IEEE Trans. Magn.*, MAG-11, No.5, pp.1240, (Sept. 1975)

Schneider R.C., "Write equalisation in high-linear-density magnetic recording", *IBM Journ. Res. & Dev.*, Vol.-29, No.6, pp.563, (Nov. 1985)

Seagle D.J., Buelieu T.J., Lambert S.E., Spectro C.J., "Underlayer noise in rigid-disk perpendicular recording", *Journ. Mag. Soc. Japan*, Vol.-13, Sup. No. S1, pp.633, PMRC (1989)

Shafiee H., Moon J.J., "Low-complexity Viterbi detection for a family of partial response systems", *IEEE Trans. Magn.*, MAG-28, No.5, (Sept. 1992)

Shafiee H., Melas M., Sutardja P., "Performance comparison of EPRML and peak detection in high density digital magnetic recording", *IEEE Trans. Magn.*, MAG-29, No.6, pp.4015, (Nov. 1993)

Shelledy,F.B., Brock G.W., "A linear self-biased magnetoresistive head", *IEEE Trans. Magn.*, MAG-11, No.5, pp.29, (Sept. 1975)

Sugawara T., Yamagishi M., Mutoh H., Shimoda K., Mizoshita Y., "Viterbi detector including PRML and EPRML", *IEEE Trans. Magn.*, MAG-29, No.6, pp.4021, (Nov. 1993)

Tang, Y.S., "Noise autocorrelation in magnetic recording systems", IEEE Trans. Magn., MAG-21, No.5, pp.1389, (Sept. 1985)

Tang, Y.S., "Noise autocorrelation in high density recording on metal film disks", IEEE Trans. Magn., MAG-22, No.5, pp.883, (Sept. 1986)

Thapar H.K., Patel A.M., "A class of partial response systems for increasing storage density in magnetic recording", IEEE Trans. Magn., MAG-23, No.5, pp.3666, (Sept. 1987)

Thornley R.F.M., "Compensation of peak shift with write timing", IEEE Trans. Magn., MAG-17, No.6, pp.3332, (Nov. 1981)

Tong H.C., Ferrier R., Chang P., Tzeng J., Parker K.L., "The micromagnetics of thin-film disk recording tracks", IEEE Trans. Magn., MAG-20, No.5, pp.1831-1833 (Sept. 1984)

Uesaka Y., Koizumi M., Tsumita N., "Noise from the underlayer of perpendicular magnetic recording medium", Journ. Appl. Phys., Vol. 57, pp.3925, (April 1985)

Viterbi A., "Error bounds for convolutional codes and an asymptotically optimum decoding algorithm", IEEE Trans. Comms., Vol.-13, No.2, (April 1967)

Warner M.W., "Flying magnetic transducer having three rails", U.S. Patent 3,823,416, (1974)

Widrow B., Stearns S., *Adaptive Signal Processing*, Prentice-Hall, 1985

Wolf J.K., Siegel P.H., "Modulation and coding for information storage", IEEE Comms. Magazine, pp.68, (Dec. 1991)

Wood R., Petersen D.A., "Viterbi detection of class IV partial response on a magnetic recording channel", IEEE Trans. Comms., COM-34, pp.454, (May, 1986)

Wood R., "Turbo-PRML : A compromise EPRML detector", IEEE Trans. Magn., MAG-29, No.6, pp.4018, (Nov. 1993)

Yamamoto S., Nakamura Y., Iwasaki S., "Extremely high bit density recording with single pole perpendicular head", IEEE Trans. Magn., MAG-23, No.5, pp.2070, (1987)

Yarmchuk E.J., "Spatial structure of media noise in film disks", IEEE Trans. Magn. MAG-22, pp.877, (Sept. 1986)

Yogi T., Tsang C., Ngugen T.A., Ju K., Gorman G.L., Castillo G., "Longitudinal media for 1 Gb/in² areal density", IEEE Trans. Magn., MAG-26, No.5, pp.2271 (Sept 1990)

Zeng W., Moon J.J., "Modified Viterbi algorithm for a jitter-dominant 1-D² channel", IEEE Trans. Magn., MAG-28, No.5, pp.2895, (Sept. 1992)

Zhu J.G., Bertram H.N., "Reversal mechanisms and domain structures in thin-film recording media", Journ. Appl. Phys., Vol. 69(8), pp.6084-6089, (April 1991)

Appendix A

Published Paper

Observation of Underlayer Domain Noise in Perpendicular Recording Disks

N.R. Darragh, D.J. Mapps, T. Donnelly, J.G. Wade, J.R. Hoinville

The Centre for Research in Information Storage Technology, University of Plymouth,
Drake Circus, Plymouth, Devon, United Kingdom PL4 8AA

Abstract - We have employed our disk test system to extract samples of media noise from dual layer perpendicular recording disks. The samples of the media noise show it to have a distinct high and low frequency structure. The high frequency structure is the noise arising from the micromagnetics of the CoCr recording layer. The low frequency structure does not arise from the recording layer but from the NiFe underlayer. Using an imaging technique, the underlayer noise is characterised by lines that span inwards from the outside diameter of the disk. The appearance and behaviour of these lines shows them to be attributable to domain walls in the underlayer of the disk.

I. INTRODUCTION

The importance of media noise increases as flying heights reduce and improvements are made in the noise properties of the electronics used in the magnetic recording data channel. In the future, media noise may well become the dominant noise component in the channel. Media noise in longitudinal recording has been shown to increase with increasing transition density; arising from its close association with the irregularity of the recorded transition [1]. In perpendicular recording it has been modelled [2] and shown experimentally [3] that the media noise reduces with increasing transition density. This is because it is believed to be associated with the recorded bit cell area *between* transitions rather than any irregularity in the transitions themselves.

In this paper we show that there is an additional and significant noise component in dual layer perpendicular recording media which arises from the inclusion of the low permeability underlayer.

II. EXPERIMENTAL

Figure 1 illustrates our method used to study media noise. The method is similar to that used in [4]. In addition we use a laser beam reflecting off a front silvered mirror on the disk spindle to generate an index signal. This index signal is used to trigger the digital storage oscilloscope which can take repeated time domain samples of the head signal from the same angular position on the disk and then

Manuscript received February 15, 1993.

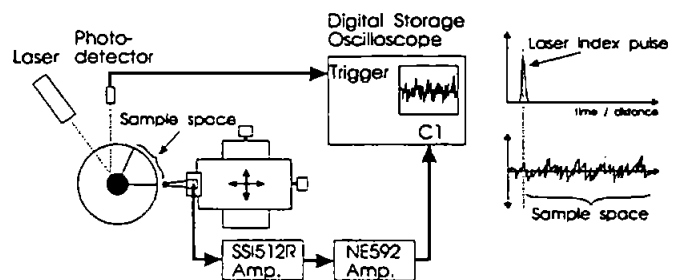


Figure 1 - Experimental set-up used to study media noise.

average them to reduce the random head and electronics noise. We typically average 1000 such samples which consequently reduces this unwanted noise component by 30dB. The signal remaining after applying this technique is the deterministic media noise. The use of the laser index allows freedom of movement of the head over the surface of the disk while maintaining an accurate angular reference. The experimental details of this study are as follows:

Head: Single pole perpendicular, 25 turns, 12 μm track width, 0.3 μm pole depth, resistance 50 Ω .

Disk: Dual layer perpendicular, Al substrate. Underlayer - 10 μm 80:20 Ni:Fe (wt%) $\mu_r=500$. Recording layer - 160 nm 79:21 Co:Cr (at%), $H_c=800$ Oe, $M_s=225$ emu/cc.

Amp.: SSI521 read/write device - 40dB gain $NF=0.9\text{nv}/\sqrt{\text{Hz}}$
NE592 video amplifier - 20 dB gain

Isolated transition pulse amplitude was measured to be 150mV @ 4000 rpm, 60mm radius. The digital storage oscilloscope used in this study is a Lecroy 9310 with 10000 sample memory, 100 MS/s maximum sampling frequency (single shot) and on-board waveform processing functions.

III. RESULTS AND DISCUSSION

Figure 2(a) shows a typical 12.5 mm sample of the perpendicular noise signal taken using the multiple waveform averaging technique described in section II. The relative head/media velocity was 25 m/s. The media is dc-erased in a band spanning the sample space prior to taking

the sample. The fine detail of the noise signal is not visually resolved in this figure but the readers attention is drawn to its dual frequency nature; a high frequency signal superimposed with lower frequency perturbations. Figure 2(b) (upper trace) is an expanded 125 μm section of the 12.5mm sample and shows the high frequency signal in closer detail and its spectrum (lower trace). We have analysed this high frequency noise component and produce results that agree well with [5]. We conclude that the high frequency noise is attributable to the recording layer; and is the 'expected' media noise process for perpendicular recording.

A. Low Frequency Noise Signal Analysis.

Initial observations of the low frequency component would suggest that it originates from a different source to the high frequency noise by nature of its magnitude, low spatial frequency and large feature width. To investigate its properties it is desirable to filter out the high frequency noise from the original sample. Figure 3(a) shows the result of applying a 300kHz low-pass linear phase Finite Impulse Response (FIR) filter to the sample shown in figure 2(a). The perturbations range from widths of 100-500 μm . This is further concurred by the spectral analysis shown in figure 3(b) where we see that the low frequency noise is characterised by a peak at a spatial frequency of 1 cycle/mm. The rms amplitude of this low frequency noise is 1.47 mV rms and is of the same order of magnitude as the recording

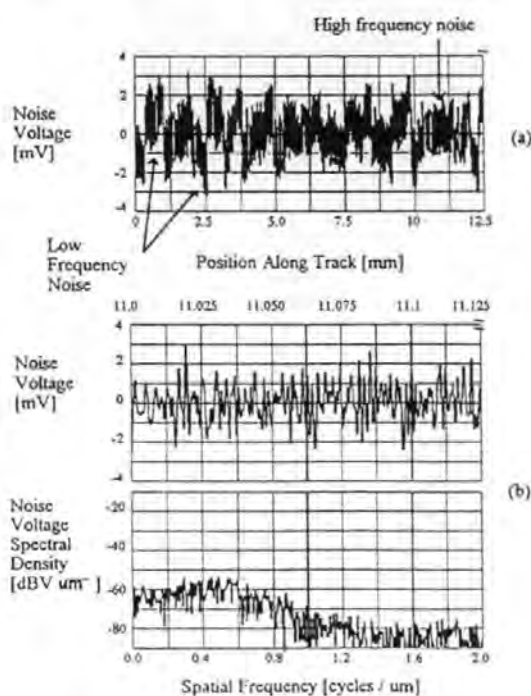


Figure 2 - (a) Perpendicular media noise sample 12.5mm long. (b) Section of sample in (a) showing the high frequency media noise. The lower trace is its spectral density.

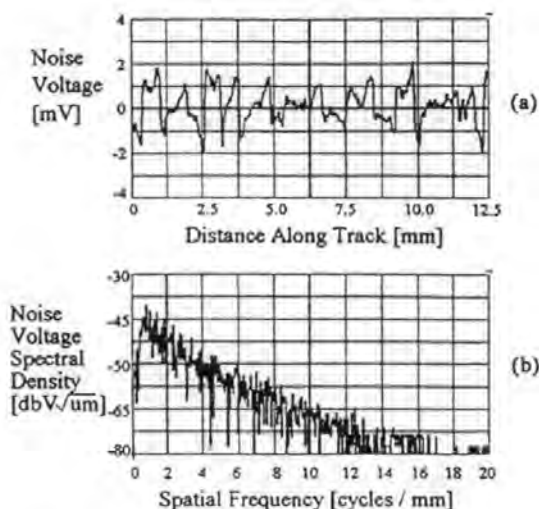


Figure 3 - (a) Low frequency noise after the high frequency media noise has been removed by a filter. (b) Spectral density of (a).

layer media noise (1 mV rms) and the unattenuated electronics noise (5 mV rms). Because of its large feature width, the low frequency noise will affect the amplitude of many hundreds of adjacent transitions (which for this media have a PW50 of 1 μm).

To determine whether the low frequency noise is affected by fields from the recording head, we write over the sample space using different recording conditions and analyse the effect on its structure by means of the cross correlation coefficient. In one such experiment a sample of the noise is taken before and after reverse erasure of the sample space by the head. Despite the fact that the recording layer for the two samples is in opposite directions, the cross correlation coefficient for the two samples is always very close to unity (0.97 or greater). This important result tells us that the low frequency noise cannot originate from the recording layer, since if it did, the second sample in this experiment would be the mirror image of the first; yielding a cross correlation coefficient of minus unity. For the same reason it also tells us that the low frequency noise cannot be due to physical irregularities in the CoCr recording layer or repeatable variations in the flying height perhaps due to asperities in the recording surface. We therefore conclude from these investigations that the source of the low frequency noise is arising from some other magnetic source in the disk; most likely, the low permeability NiFe underlayer.

B. Underlayer Domain Noise Images

In an attempt to show that the low frequency noise is arising from the underlayer we conduct an experiment to determine whether it exhibits any overall pattern over the surface of the disk. This is done by extracting samples of the low frequency noise in steps from radii between 60mm and 30mm, each starting at exactly the same angular reference.

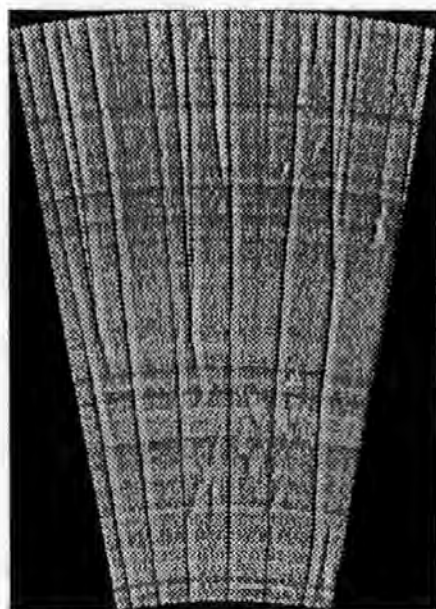


Figure 4 - Picture of low frequency noise over a section of disk surface. Noise amplitude is represented by pixel brightness. The picture is to scale and 2.5 times actual size.

Using pixel brightness to represent noise voltage amplitude, each sample of each waveform is plotted in its correct radial position to build up a grey scale picture of the low frequency noise over that section of disk. The result of such an experiment is shown in figure 4. From the figure it is clear that this low frequency noise has a structure over the disk surface characterised by lines that span inwards radially from the outside diameter.

The lines may be re-set using a suitable magnetic field. Figure 5 shows the result after bringing a large magnet near the sample space imaged in figure 4. One observes that the pattern of the lines has changed completely. These results strongly suggest that the low frequency noise is attributable to domain wall formation in the NiFe underlayer.

We have conducted a number of experiments to determine what parameters affect the characteristics of the domain walls in the underlayer. This work will be continued and reported in a future paper.

IV. CONCLUSION

We have shown that the media noise signal from a dual layer perpendicular recording disk has a distinct high and low frequency nature. We have analysed the high frequency noise component and conclude that it is attributable to the CoCr recording layer; the expected media noise process. We have analysed the low frequency noise and show it to have large feature widths (100-500 μ m compared to transition pulse width, PW50, of 1 μ m). We find that the amplitude of the low frequency noise is of the same order of magnitude as the CoCr media noise and the system electronics noise.

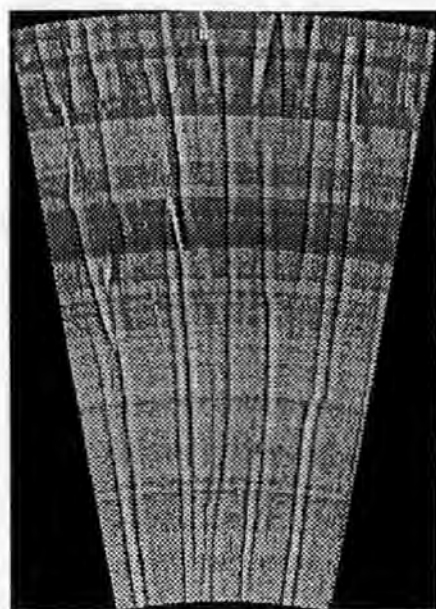


Figure 5 - A picture of the noise from the same section of disk as figure 4 after it has been subjected to a magnetic field. The noise lines have been re-set into new positions.

Importantly, we have shown that this noise component *is not* arising from the recording layer. Using our experimental technique we have produced images of the noise over a section of the disk from radii of between 60mm and 30mm. These images show the pattern of this noise to be characterised by lines that span inwards from the outside diameter of the disk. We conclude from the appearance and behaviour of these lines that they coincide with domain walls in the underlayer of the media which may be re-set when placed under the influence of a dimensionally large magnetic field.

ACKNOWLEDGEMENT

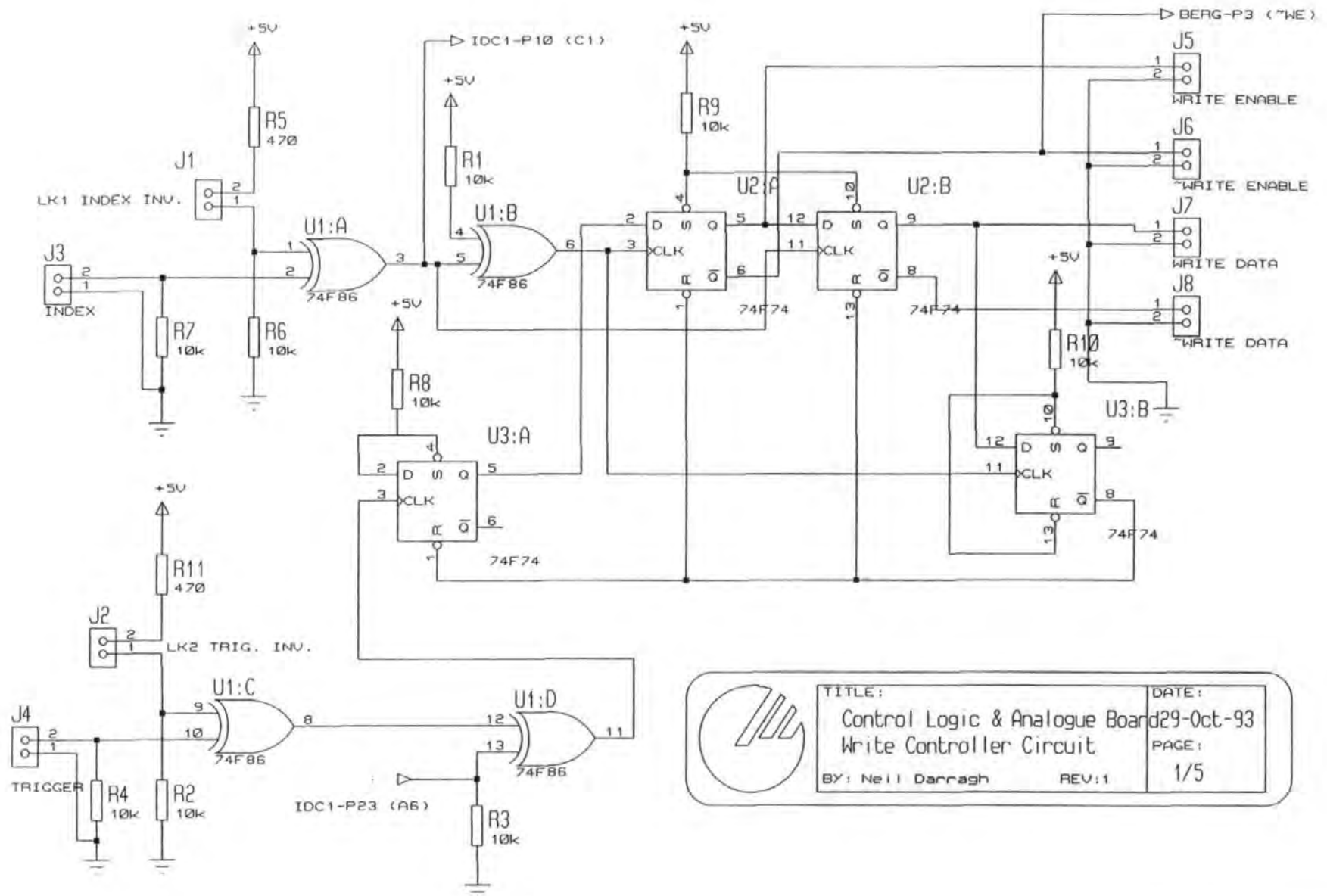
The S.E.R.C. and Pilkington plc are acknowledged for their financial support of this work.

REFERENCES

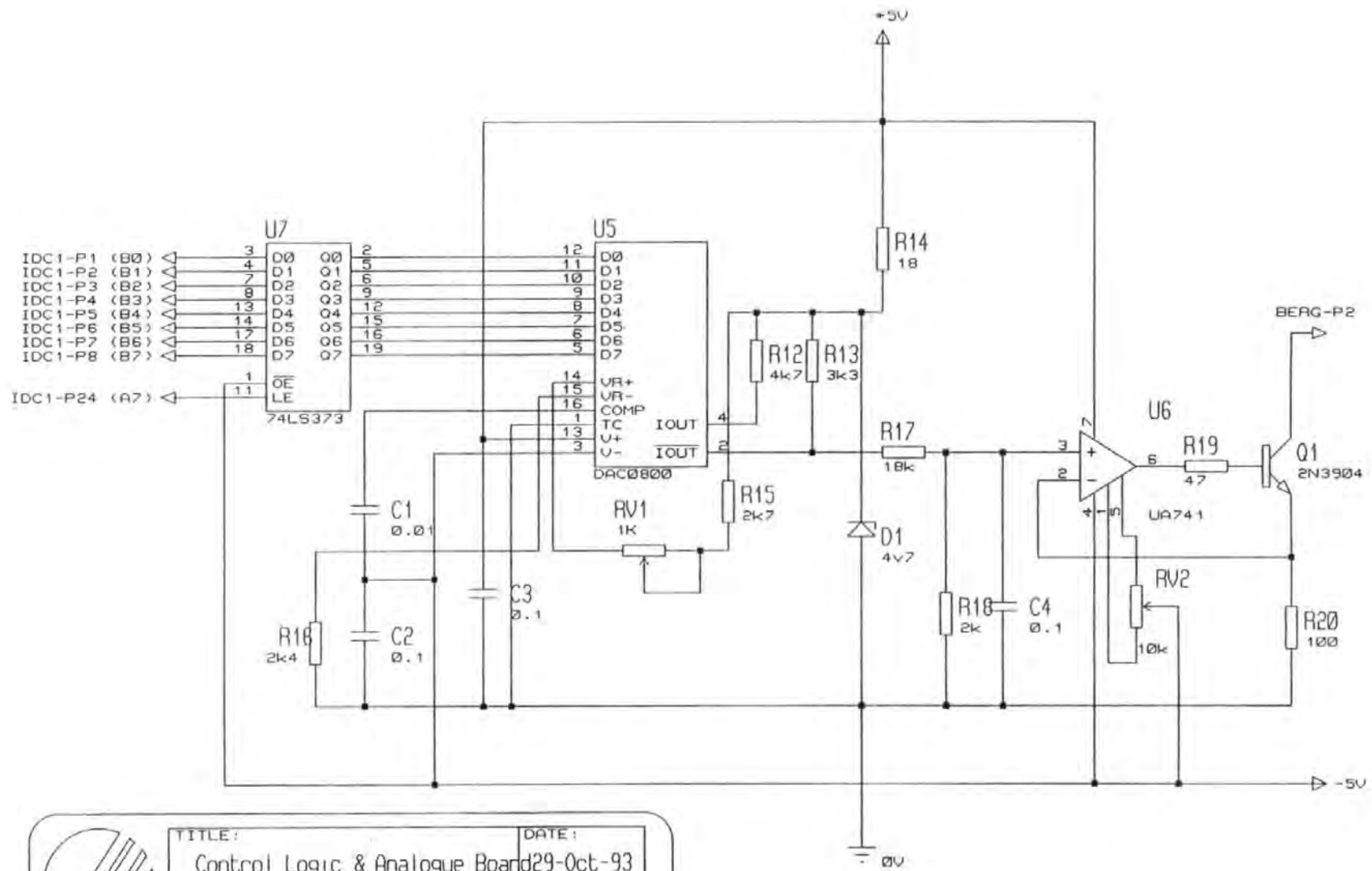
- [1] N.R. Belk, P.K. George, G.S. Mowry, "Noise in high performance thin-film longitudinal magnetic recording media," *IEEE Trans. Magn.*, vol. 21, pp. 1350-1355, Sept. 1985.
- [2] J.G. Zhu, H.N. Bertram, "Reversal mechanisms and domain structures in thin-film recording media," *Journ. Appl. Phys.* vol. 69(8), pp.6084-6089, April 1991.
- [3] A. Okabe, T. Yamamoto, "Structure and recording characteristics for CoPtB(O) rigid disk media," paper BB-13 presented at the 37th MMM conference, Houston, Texas, December 1992.
- [4] E.J. Yarmchuk, "Spatial structure of media noise in film disks," *IEEE Trans. Magn.*, vol. 22, pp. 877-882, Sept. 1986.
- [5] R.S. Indeck, M.N. Johnson, Guo Mian, J.R. Hoinville, M.W. Muller, "Noise characterisation of perpendicular media," *Journ. Mag. Soc. Japan*, vol. 15, Supplement S2 pp. 173-178, 1991.

Appendix B

Experimental Test-station Circuit Diagrams



	TITLE:	DATE:
	Control Logic & Analogue Board	29-Oct-93
	Write Controller Circuit	PAGE:
	BY: Neil Darragh	REV:1



	TITLE:	DATE:
	Control Logic & Analogue Board	29-Oct-93
	Write Current Generator	PAGE:
	BY: Neil Darragh	REV:1

Appendix C

**Method for determining the head gap/pole radius and
absolute coordinates with respect
to the centre of the disk.**

**ACCURATE DETERMINATION OF HEAD GAP/POLE RADIUS
AND ABSOLUTE CO-ORDINATES USING IN-SITU
RECORDING MEASUREMENTS ON HARD DISCS.**

NEIL DARRAGH

Centre for Research in Information Storage Technology (C.R.I.S.T.)
University of Plymouth
Drake Circus
Plymouth
Devon
United Kingdom
PL4 8AA

ABSTRACT

A simple method of accurately determining the radius and absolute co-ordinates of a magnetic disc recording head with respect to the disc centre is presented. Conventional methods require the production of 'standard' discs or may require complex calibration procedures to be followed. This method requires only those pieces of apparatus that are normally employed on disc test stations and does not require the removal or replacement of the head or disc under test. Error analysis of the technique shows that radius and co-ordinate determination to an accuracy of the same order of magnitude as the head gap/pole width is possible.

INTRODUCTION

A problem often encountered by researchers is the calibration of head positioning equipment used in experimental disc stands; that is, knowing the exact radius and absolute co-ordinates of a recording head with respect to the centre of the disc. This may or may not be important depending on the nature of the work being undertaken. Sometimes, however, it is extremely useful to know these parameters, for example, in the preparation of media samples for TEM or Lorentz imaging analysis of pre-recorded signals or ensuring that head addressing is performed precisely radially.

A typical experimental disc stand comprises a disc mounting spindle & clamp mechanism and an x-y table (micro-positioner) upon which the recording head is mounted. Although the table is typically capable of sub-micron step positioning, the precise radius or the absolute co-ordinates of the head with respect to the disc centre is often unknown to any degree of accuracy. Classical solutions to this problem are to calibrate the position of the head under test with some form of standard disc with tracks pre-recorded at known radii. The standard disc is then removed and the disc under test is placed onto the spindle. Problems with this method are however that standard discs must firstly be created themselves, and further, maintained to keep up with developments in head technology. Also, each time the head gap/pole position with respect to the table changes, the calibration process must be repeated, or, if the relative movement is known then a correction to the previous calibration must be made. These methods are time consuming and may lead to inaccuracies over time.

Presented here is a method by which head radius and absolute co-ordinates may be accurately determined using the same equipment that is typically used in recording experiments without the need for standard discs, heads or calibration equipment. The entire measurement is made using magnetically recorded signals and simple, widely employed measurement equipment.

EXPERIMENTAL SET-UP

Figure 1 shows the set-up of our experimental disc stand. A stable index signal is derived from a laser focused on a reflective spot on the spindle mechanism. Each time the disc rotates, the laser beam is reflected into a fast photo-diode which then generates an index pulse. This pulse may be squared-up using a fast comparator. In an alternative system, another head could be mounted and a single transition used to generate an index signal. The important factor is that the index signal must relate precisely to the same radial position on the disc each time it rotates. Any jitter of this pulse must be small compared the width of recorded pulses, and consequently, we have found that conventional LED's and Photo-detectors are of little use for this method since they have slow response times and large time jitter.

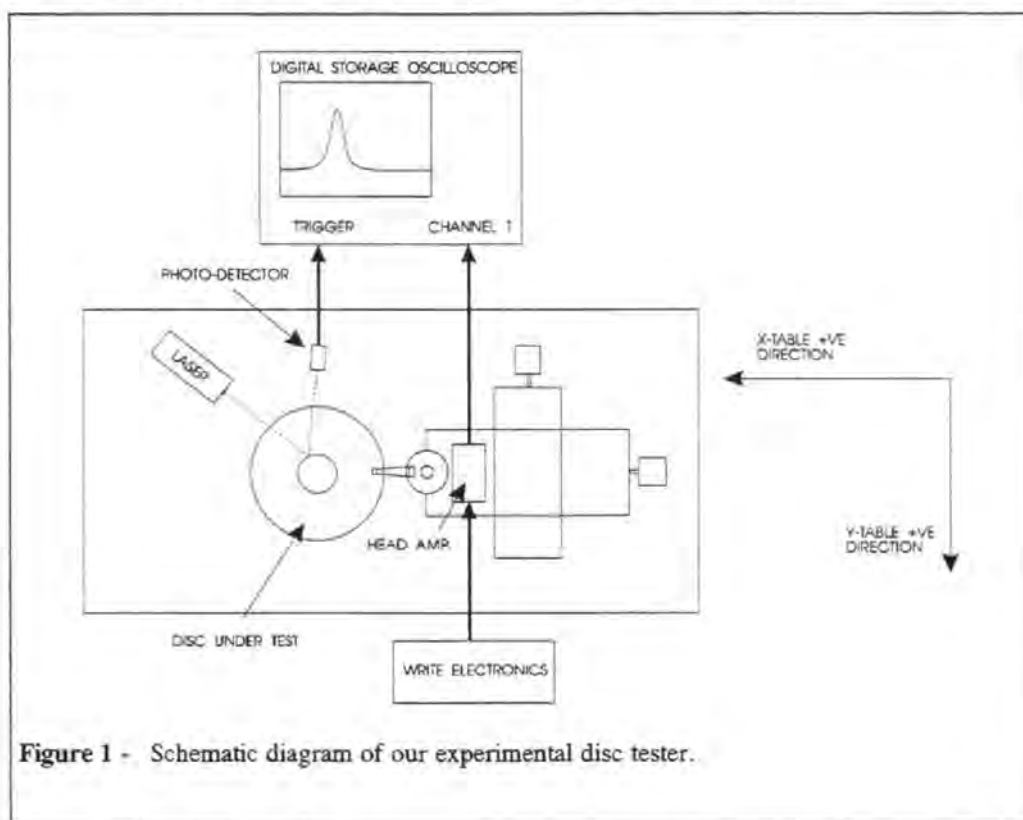


Figure 1 - Schematic diagram of our experimental disc tester.

An oscilloscope is required to measure accurately the time delay between the stable index signal and recorded (test) signals on the disc. Cursor capability is ideal for this application. In our system we use a fast digital storage oscilloscope which is used to capture (and later compare) the recorded waveforms in the time domain. In either case the important point is that some method of time delay measurement between two separate events (in arbitrary time) can be made either relative to each other or to the fixed index signal.

METHOD

The radius and co-ordinate measurement method is described as follows.

- (i) The disc must be initially completely erased in the region around where the radius is to be measured. For a typical $10\mu\text{m}$ track width, an erase band of 5mm is found to be suitable.
- (ii) A single pulse, dibit or short recognisable burst of data is recorded onto the disc a short distance from the position of the index pulse.
- (iii) The oscilloscope should be set-up to measure the time delay between the stable index signal and a chosen point on the recorded test signal (e.g. the peak of the first pulse - figure 2). A note of the signal amplitude is also made. Alternatively, if using a digital storage oscilloscope, the waveform may be captured using the stable index pulse as the trigger and using an appropriate trigger delay.
- (iv) The y-table is moved along the track direction by a fixed amount - e.g. 10mm . The x-table is now moved (positive or negative) until the head is once again directly over the recorded track (figure 2). This can be determined by a maxima in signal amplitude as the head is stepped across the track centre. With a typical $10\mu\text{m}$ track width, the head should be able to be centralised back on track to within plus or minus $1\mu\text{m}$ in the x-direction.
- (v) A new measurement of the time between the index pulse and the same point on the recorded test signal is made. If using a digital storage oscilloscope a new sample of the waveform is taken using the same trigger delay as before.

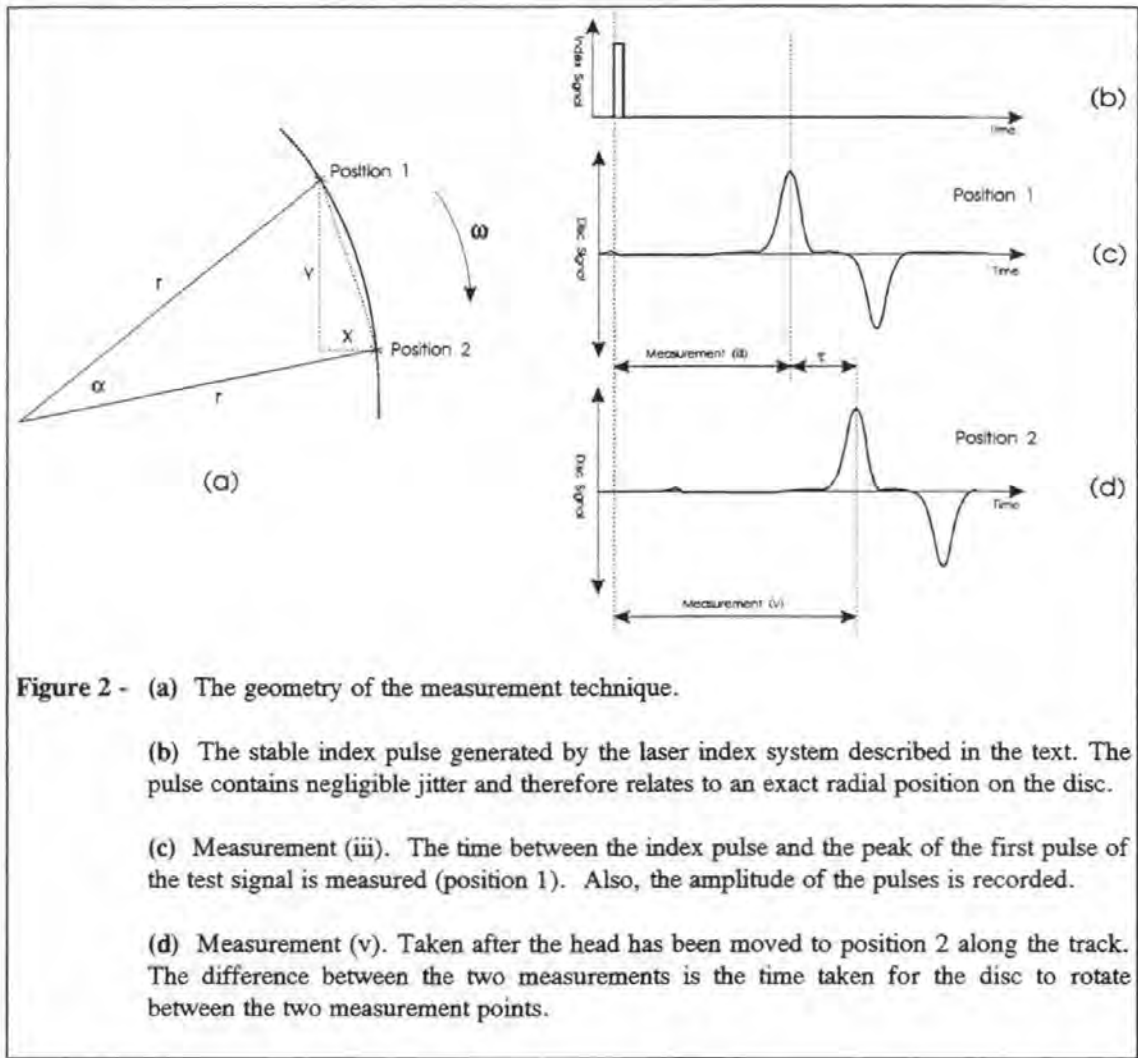


Figure 2 - (a) The geometry of the measurement technique.

(b) The stable index pulse generated by the laser index system described in the text. The pulse contains negligible jitter and therefore relates to an exact radial position on the disc.

(c) Measurement (iii). The time between the index pulse and the peak of the first pulse of the test signal is measured (position 1). Also, the amplitude of the pulses is recorded.

(d) Measurement (v). Taken after the head has been moved to position 2 along the track. The difference between the two measurements is the time taken for the disc to rotate between the two measurement points.

Referring to figure 2. We know from the measurements made in (iii) and (v) the time, τ , the disc takes to travel from measurement position 1 to measurement position 2 at an angular velocity of ω rads/sec. Hence the angle of rotation is given by:

$$\alpha = \omega\tau \text{ rads} \quad (1)$$

Similarly, we also know the orthogonal co-ordinates that have moved the head from position 1 to position 2. So we can directly write the following:

$$\sin\alpha = \frac{\sqrt{x^2 + y^2}}{2r} \quad (2)$$

Hence, combining (1) and (2) we obtain an expression for the radius, r , in terms of known quantities:

$$r = \frac{\sqrt{x^2 + y^2}}{2 \sin\left(\frac{\omega\tau}{2}\right)} \quad (3)$$

The absolute co-ordinates of the head with respect to the disc centre can be determined from observing (figure 3) that the angle, θ , between the normal to the cord formed between measurement position 1 and 2 and the horizontal is given by:

$$\theta = \tan^{-1}\left(\frac{x}{y}\right) \text{ rads}$$

from which the absolute co-ordinates of the head at position P1 with respect to the disc centre may be calculated using:

$$P1_x = r \cos\left(\theta + \frac{\alpha}{2}\right) \quad P1_y = r \sin\left(\theta + \frac{\alpha}{2}\right)$$

where: $\alpha = \omega\tau$ (the angle of rotation between P1 and P2)

and, similarly, for measurement position 2:

$$P2_x = r \cos\left(\theta - \frac{\alpha}{2}\right) \quad P2_y = r \sin\left(\theta - \frac{\alpha}{2}\right)$$

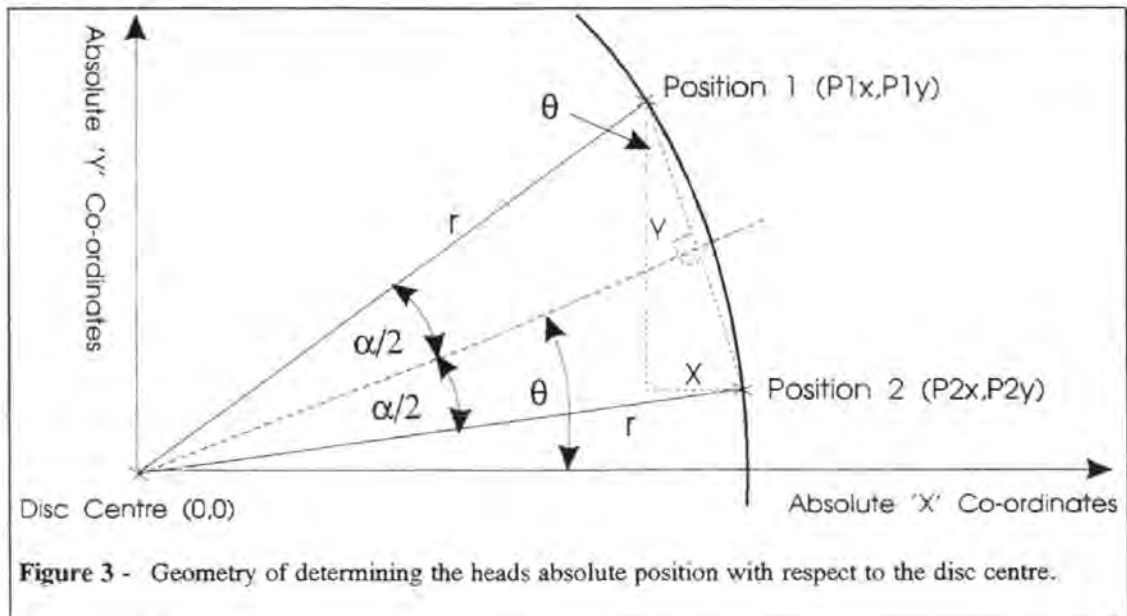


Figure 3 - Geometry of determining the heads absolute position with respect to the disc centre.

Having determined the absolute co-ordinates of the head gap/pole with respect to the disc centre it is then possible to accurately position the head at a desired point using appropriate offsets from the table co-ordinates at position 1 or 2.

ERROR ANALYSIS

In this section the measurement errors that can occur in this method are analysed and their effect on the accuracy of the radius measurement is quantified. Firstly, the effect of errors in the determination of the x and y co-ordinates is examined.

It is possible to centralise the head at position 2 to within plus or minus 10% of the track width. A 10% error in head placement either side of the track centre leads to a signal reduction of approximately 10% and such a reduction in signal amplitude is easily observed on the oscilloscope. So, for example, a $10\mu\text{m}$ wide head can be centralised on a $10\mu\text{m}$ wide track to within plus or minus $1\mu\text{m}$.

The x-y tables are typically accurate to an absolute position error of $0.5\mu\text{m}$. Hence, we can conclude that the maximum error in the determination of x and y is plus or minus $1.5\mu\text{m}$ and $0.5\mu\text{m}$ respectively. This error is fixed and not proportional to the distance travelled and so can be reduced by making the distance traversed in both directions large by comparison. A relationship of these errors to the errors introduced in the calculation for the radius (3) is given by:

$$Er(\%) = \frac{\sqrt{(x+e_x)^2 + (y+e_y)^2} - \sqrt{x^2 + y^2}}{\sqrt{x^2 + y^2}} \times 100\% \quad (4)$$

where: $Er(\%)$ is the percentage error in the radius calculation.

e_x & e_y are the absolute maximum errors in the values for x and y respectively.

For example, at a radius of approximately 50mm, a shift of 10mm in the y-direction will require a shift of approximately 2mm in the x-direction to bring the head back onto the track centre. The absolute errors, e_x & e_y , for the lengths x and y are $1.5\mu\text{m}$ & $0.5\mu\text{m}$ respectively. Evaluating (4) for this example we find that the percentage error in the radius calculation (3) will be 0.008%. This corresponds to a distance, and hence error at this radius of plus or minus $4\mu\text{m}$.

Accurate determination of angular velocity of the disc stand is made relatively easily by counting revolutions in a long time period (i.e. 1 minute) or measuring accurately the period of 1 revolution. In our disc stand we measure the period to an accuracy of plus or minus $1\mu\text{s}$. This corresponds to an error of 0.012% at a 3600rpm rotation rate and an error in the radius calculation (3) at a radius of 50mm, for example, of plus or minus $6\mu\text{m}$.

The final area where errors can affect the value for the radius determination is the time delay measurement between position 1 and position 2. The accuracy of this measurement is dependent on the stability of the index pulse and the resolution and accuracy of the time delay measurement equipment itself. In our disc stand the index pulse is found to have a stability better than 1ns and this can be neglected when compared to typical delay measurements of 500 μsecs .

The accuracy and resolution of the time delay measurement equipment will vary greatly and depend on many factors, including how it is operated. In our disc stand we find that we can measure the 500 μs typical time delays between position 1 and position 2 at a radius of 50mm to a resolution of 10ns and an accuracy of plus or minus 100ns. This corresponds to an uncertainty in the time delay measurement for this example of plus or minus 0.02%. By examination of (3) we note that the determination of radius subject to a 0.02% error in this measurement will also be approximately in error by 0.02%. At this radius this corresponds to an error of plus or minus $10\mu\text{m}$.

The above analysis shows that the expected errors incurred in the measurements for this method would yield errors in the determination of radius of the following amounts:

X-Y position :	0.008%
angular velocity :	0.012%
time delay measurement :	0.02%

Combining these errors we would therefore expect to obtain an accuracy for the radius determination of typically plus or minus 0.04%. At a radius of 50mm this corresponds to an accuracy of plus or minus $20\mu\text{m}$.

This prediction was tested by making repeated measurements of a head placed at a radius of approximately 50mm and performing the method with different values of x and y displacement. The results are tabulated in table 1.

Measurement No.	$\sqrt{(x^2 + y^2)}$ (mm)	Time Delay (μ s)	Calculated Radius (mm)
1	7.050	385.25	48.586
2	8.068	441.09	48.575
3	9.089	469.90	48.594 (max)
4	10.115	553.45	48.568
5	11.145	610.08	48.567
6	12.180	667.10	48.563 (min)
7	13.221	724.34	48.570
8	14.268	782.04	48.573
Mean			48.575
max - mean			0.019
mean - min			0.012
S.D.			0.00979

Table 1 - Repeated measurements from the same radius show close correlation to within the accuracy predicted (plus or minus 20μ m)

CONCLUSION

It has been shown that using the equipment that is commonly found on hard disc test stands a very accurate measurement of the head gap/pole radius may be made at an accuracy of the same order of magnitude as the head gap/pole dimensions. Using this information it is then possible to determine the absolute co-ordinates of the head with respect to the disc centre.

Analysis of the errors that may occur during the method show that accuracy is primarily limited by the resolution and accuracy of the time delay measurement equipment.

Appendix D

Software Models

PRBS Generator

```

/*****
/* PRBS.C
/* AUTHOR : N.DARRAGH
/* DATE : 6th February 1993
/*****

/*****
Takes a polynomial as input and generates the PRBS.
*****/

#include <stdio.h>
#include <stdlib.h>
#include <math.h>

main(int argc, char *argv[])
{
int num_taps;

int c,d,value,e;
int r[20]={0};
int t[20]={0};
int tapsum;
int sequence_length,*output,*soutput,*soutput1;
int shift,result,firstresult;
FILE *fp;
int num_cycles;
char filename[16];

if (argc<2)
{
printf("\nUsage - PRBS <filename> <N> <X(n)> <X(n-1)> ... 1,\n");
printf("\t<filename>=output file name\n");
printf("\t<N>=number of cycles of sequence\n");
printf("\t<X(n)> etc are 0 or 1\n\n");
printf("e.g. 25 cycles into file 'fred' of polynomial X6+X4+X3+X1+1 is :-\n\n");
printf("PRBS fred 25 1 0 1 1 0 1 1\n");
printf("\n\nN.Darragh, January 1994\n");
exit(1);
}

if (!(fp=fopen(argv[1],"w")))
{
printf("ERROR : Could not open output file - %s\n",argv[1]);
exit(1);
}

fprintf(fp, "\n; PRBS SEQUENCE GENERATION AND DIBIT EXTRACTON.");
fprintf(fp, "\n; =====\n\n");

fprintf(fp, "; Neil Darragh\n");
fprintf(fp, "; The Centre for Research in Information Storage Technology (C.R.I.S.T.)\n\n");

```

```

num_taps=argc-3;
sequence_length=(int)(pow(2,num_taps-1)+0.5)-1;

fprintf(fp, " ; Filename : %s\n\n",argv[1]);
printf("PRBS polynomial is : ");
fprintf(fp, " ; PRBS polynomial is : ");

for (c=0;c<num_taps;c++)
{
    sscanf(argv[c+3],"%d",&value);
    t[num_taps-c-2]=value & 0x01;

    if (value && c<num_taps-1)
    {
        printf("x%d + ",num_taps-c-1);
        fprintf(fp,"x%d + ",num_taps-c-1);
    }
}
printf(" 1\n\n");
fprintf(fp," 1\n\n");

r[0]=1;

output=malloc(sizeof(int) * (int)(pow(2,num_taps-1)+0.5)-1);
soutput=malloc(sizeof(int) * (int)(pow(2,num_taps-1)+0.5)-1);
soutput1=malloc(sizeof(int) * (int)(pow(2,num_taps-1)+0.5)-1);

printf("This generates output sequence : \n");
fprintf(fp, " ; This generates output sequence :");

for (c=0;c<sequence_length;c++)
{
    if (!div(c,63).rem)
    {
        printf("\n");
        fprintf(fp," \n");
    }

    tapsum=0;
    for (d=num_taps-2;d>=0;d--)
    {
        if (t[d])
            tapsum^=r[d];
    }

    for (d=num_taps-2;d>0;d--)
        r[d]=r[d-1];

    r[0]=tapsum;
    output[c]=tapsum;
    printf("%d",tapsum);
    fprintf(fp,"%d",tapsum);
}
printf("\n\n");
fprintf(fp,"\n\n");

if (!result)

```

```

{
printf("This is not a maximal length PRBS sequence!\n");
fprintf(fp, "; This is not a maximal length PRBS sequence!\n");
exit(1);
}

printf("Dibit extraction properties :-\n\n");
fprintf(fp, "; Dibit extraction properties\n");
fprintf(fp, "===== \n\n");

shift_and_add(output,soutput,sequence_length,1);
firstresult=findshift(output,soutput,sequence_length);
fprintf(fp, "; Easy / hard pulse echo          : %2.1f bits early/late\n\n", (float)(firstresult-0.5));
printf("Easy / hard pulse echo : %2.1f bits early or late\n\n", (float)(firstresult-0.5));

shift_and_add(soutput,soutput1,sequence_length,-firstresult-1);
result=findshift(output,soutput1,sequence_length);
fprintf(fp, "; Previous transition part-percolation echo   : %2.1f bits early\n", (float)(result-0.5));
fprintf(fp, ";                               and   : 1.5 bits late\n\n");
printf("Previous transition part-percolation echo : %2.1f bits early\n", (float)(result-0.5));
printf("                               and : 1.5 bits late\n\n");

shift_and_add(soutput,soutput1,sequence_length,-firstresult-2);
result=findshift(output,soutput1,sequence_length);
fprintf(fp, "; 2nd previous transition part-percolation echo : %2.1f bits early\n", (float)(result-0.5));
fprintf(fp, ";                               and   : 2.5 bits late\n");
fprintf(fp, "; plus contributions at 'previous transition' echo locations\n\n\n");
printf("2nd previous transition part-percolation echo : %2.1f bits early\n", (float)(result-0.5));
printf("                               and : 2.5 bits late\n");
printf("plus contributions at 'previous transition' echo locations\n\n");

num_cycles=atoi(argv[2]);

fprintf(fp, "; %d cycles of this PRBS sequence in 3-digit (9-bit) hex :\n", num_cycles);

for (c=0;c<num_cycles * sequence_length;c+=9)
{
if (!div(c,16).rem)
    fprintf(fp, "\n");

value=0;
e=256;
for(d=0;d<9;d++)
{
if (output[div(c+d,sequence_length).rem])
    value+=e;
e/=2;
}
fprintf(fp, "%03x ", value);
}

fclose(fp);
}

shift_and_add(int *output,int *soutput,int sequence_length,int shift)
{
int c;
int shift_index;

```

```

for (c=0;c<sequence_length;c++)
{
    shift_index=div(c-shift,sequence_length).rem;
    if (shift_index<0)
        shift_index+=sequence_length;

    soutput[c]=output[c]^output[shift_index];
}
}

findshift(int *output,int *soutput,int sequence_length)
{
    int c;
    int searchshift=0;
    int match=0;
    int shift_index;

do {
    match=0;
    for (c=0;c<sequence_length;c++)
        {
            shift_index=div(c-searchshift,sequence_length).rem;
            if (shift_index<0)
                shift_index+=sequence_length;

            if (output[shift_index]==soutput[c])
                match++;
        }
    searchshift++;
    kbhit();
    } while (match<sequence_length && searchshift<=sequence_length);

if (searchshift>sequence_length)
    return(0);

searchshift=1;

if (searchshift > sequence_length/2)
    searchshift=sequence_length;

return(searchshift);
}

```

Lorentzian Waveform Generator

```
/* **** */
/* LORWAVE.C */
/* AUTHOR : N.DARRAGH */
/* DATE : 29th January 1993 */
/* **** */
```

```
*****
Takes coded and pre-coded 3 digit hex bytes and creates an
lorentzian waveform.
```

1st argument - filename of source coded NRZ data.
2nd argument - filename of destination (floating point) values.
3rd argument - number of destination samples (integer).
4th argument - period between each sample (seconds).
5th argument - symbol period (seconds).
6th argument - PW50 (seconds).
7th argument - Lorentzian coefficient (often 2).
8th argument - output full or amplitude only values

$$y=1/(1+(2x/PW50)^{coeff})$$

```
*****
```

```
typedef enum {FALSE,TRUE} boolean;
```

```
#include <stdio.h>
#include <math.h>
#include <stdlib.h>
#include <pgchart.h>
#include <graph.h>
#include <malloc.h>
```

```
float *samples;
double sample_period;
double symbol_period;
double PW50;
float coefficient;
float PI=3.1415927;
long num_samples;
```

```
main(int argc,char *argv[])
{
FILE *fp,*fpout;
int precodedword;
boolean cont=TRUE;
char hexnum[3];
int c,previous,bit;
double timepnt=0;
long symbol_count=0;
long lc;
if (argc!=9)
{
```

```

printf("\nUsage : <Src. file> <Dest. file> <No. smpls> <Smpl period> <Symbol Period>\n");
printf("    <PW50> <Lorentzian coefficient> <Graph? Y/N>\n\n");
printf("\t<Src. file> = input file of 3 digit (9-bit) coded words\n");
printf("\t<Dest. file> = output of floating point waveform values\n");
printf("\t<No. smpls> = Number of samples required\n");
printf("\t<Smpl period> = Sample period in seconds\n");
printf("\t<Symbol period> = Symbol period in seconds\n");
printf("\t<PW50> = Pulse width at 50 percent amplitude in seconds\n");
printf("\t<Lorentzian Coefficient> = normally set to 2\n");
printf("\t<Graph? Y/N> = Graph the output waveform\n");
exit(1);
}

```

```

printf("\nLorentzian Waveform Generator - ");
printf("Neil Darragh V2.0 (5/4/94)\n\n");

```

```

if (!(fp=fopen(argv[1],"r")))
{
printf("ERROR : Could not open source file : %s\n",argv[1]);
exit(1);
}

```

```

if (!(fpout=fopen(argv[2],"w")))
{
printf("ERROR : Could not open destination file : %s\n",argv[2]);
exit(1);
}

```

```

sscanf(argv[3], "%ld",&num_samples);
sscanf(argv[4], "%lf",&sample_period);
sscanf(argv[5], "%lf",&symbol_period);
sscanf(argv[6], "%lf",&PW50);
sscanf(argv[7], "%f",&coefficient);

```

```

if (!(samples = malloc(num_samples,sizeof(float)) ) )
{
printf("\nERROR: Not enough memory to generate waveform\n");
exit(1);
}

```

```

printf("No. symbols calculated : \n");
previous=0;
timepnt=symbol_period/2;
do {
cont=fscanf(fp,"%3s",hexnum);
if (hexnum[0]!=';' || hexnum[1]!=';')
{
do {
cont=fscanf(fp,"%c",hexnum);
} while (cont>=0 && hexnum[0]!=10);
}
else
{
if (cont>=0)
{
sscanf(hexnum, "%x",&precodedword);
}
}
}

```

```

    for (c=256;c>=1;c/=2)    /* Start with MSB, end with LSB */
    {
        if (precodedword & c)
            bit=1;
        else
            bit=0;

        pulse(timepnt,bit - previous);
        timepnt += symbol_period;
        symbol_count++;

        if (timepnt > num_samples*sample_period)
        {
            cont--1;
            c=1;
        }

        previous=bit;
        printf("\r%d",symbol_count);
    }
}
} while (cont>=0);

printf("\n\n");
if (timepnt<= num_samples * sample_period)
{
    num_samples=(long)((timepnt/sample_period)+(10*symbol_period));
    printf("There were not enough input bits to create desired no of samples\n");
    printf("There are only %ld samples in this file\n",num_samples);
}
else
{
    printf("There were not enough samples to generate the requested waveform\n");
    printf("There are %ld symbols in this file\n",symbol_count);
}

for (lc=0;lc<=num_samples;lc++)
    fprintf(fpout,"%5.5e\n",samples[lc]);

fclose(fp);
fclose(fpout);

strupr(argv[8]);
if (!strcmp(argv[8],"Y"))
    graph(samples,num_samples);

printf("\n* DONE *\n");
}

pulse(double timepnt,int pulse_polarity)
{
    double phaseoffset,sample_time;
    long centreindex;
    float value;
    long c;
    int width;

```

```

long start,stop;

if (!pulse_polarity)
    return(FALSE);

centreindex=(int)(timepnt/sample_period);
phaseoffset=timepnt-(centreindex * sample_period);

width=(int)((float)10*symbol_period/sample_period);

start=centreindex-width;
stop=centreindex+width;

start=(start < 0)? 0 : start;
stop=(stop>num_samples)? num_samples : stop;

for (c=start;c<stop;c++)
    {
    sample_time=((c-centreindex)*sample_period)-phaseoffset;
    sample_time=(sample_time<0) ? sample_time*-1 : sample_time;

    value=pulse_polarity/(1+pow(2*(sample_time)/PW50,coefficient));
    samples[c]+=value;
    }
}

graph(float *yvals,int numvals)
{
chartenv env;
int c;
palettetype palette_struct;
char far *labels[40];
float *xval;

if (!(xval=malloc(sizeof(float) * numvals)))
    {
    printf("\nERROR: Not enough memory to generate graph\n");
    exit(1);
    }

for (c=0;c<numvals;c++)
    xval[c]=c;

_setvideomode(_VRES16COLOR);

_pg_initchart();
_pg_defaultchart(&env,_PG_SCATTERCHART,_PG_POINTANDLINE);

_pg_getpalette(palette_struct);

palette_struct[1].plotchar=' ';
palette_struct[2].plotchar=' ';
palette_struct[1].color=15;
palette_struct[2].color=2;

_pg_setpalette(palette_struct);

```

```
env.legend.legend=FALSE;

_pg_chartscafterms(&env,xval,yvals,1,numvals,numvals,labels);
getch();
_setvideomode(_TEXTC80);
}
```

Automatic Gain Control (AGC)

```
/*
 * NAME : AGC.C
 * AUTHOR : N.DARRAGH
 * DATE : 6th April 1994
 */

#include <stdio.h>
#include <math.h>
#include <stdlib.h>
#include <float.h>
#include <graph.h>
#include <pgchart.h>

main(int argc, char *argv[])
{
FILE *fpin,*fpout;
int c,count,num_samples,d;
char asciirvalue[80];
int cont;
float speriod;
float gain,charge,current;
float decay_current,attack_current;
float rectval;
float value,yval;

if (argc!=6)
{
printf("Usage - AGC <inp file> <out file> <I Attack> <I Decay> <Sample period> \n\n");

printf("e.g. AGC fred.sam fred.agc 20 10 ");
printf("Attack current = 20 uA, Decay=10 uA.\n\n");
printf("Attack current is increased by 7 times if signal level exceeds 125% of \n");
printf("nominal signal level\n");
printf("AGC attempts to derive an output signal with amplitude 1.27Vppd\n\n");
exit(1);
}

if (!(fpin=fopen(argv[1],"r")))
{
printf("Error : Could not open source file - %s\n",argv[1]);
exit(1);
}

if (!(fpout=fopen(argv[2],"w")))
{
printf("Error : Could not open destination file - %s\n",argv[2]);
exit(1);
}

sscanf(argv[3],"%f",&attack_current);
sscanf(argv[4],"%f",&decay_current);
sscanf(argv[5],"%f",&speriod);

printf("Counting samples in source file.");
```

```

count=0;
do {
    cont=fscanf(fpin,"%s",asciivalue);

    if (asciivalue[0]!=';')
        {
            do {
                /* strip out comments */
                cont=fscanf(fpin,"%c",asciivalue);
            } while (cont>=0 && asciivalue[0]!=10);
        }
    else
        {
            if (cont>=0)
                count++;

            if (!div(count,1000).rem)
                printf(".");
        }
    } while (cont>=0);

fclose(fpin);

printf("\nNo. of source file samples : %d\n",count);

num_samples=count;

fpin=fopen(argv[1],"r");

printf("Reading source file values.");

count=0;
charge=4e-10;
gain=80*charge/1e-9;

do {
    cont=fscanf(fpin,"%s",asciivalue);

    if (!div(count,1000).rem)
        printf(".");

    if (asciivalue[0]!=';')
        {
            do {
                /* strip out comments */
                cont=fscanf(fpin,"%c",asciivalue);
                fprintf(fpout,"%c",asciivalue);
            } while (cont>=0 && asciivalue[0]!=10);
        }
    else
        {
            if (cont>=0)
                {
                    sscanf(asciivalue,"%f",&value);

                    yval=value*gain;
                    rectval=sqrt(pow(yval,2));

                    if (rectval>0.635)

```

```

        {
            if (rectval>0.794)
                current=attack_current*7;
            else
                current=attack_current;
        }
    else
        current=-decay_current;

    charge-=(current*speriod);

    gain=80*charge/1e-9;

    if (gain>64)
        gain=64;

    fprintf(fpout,"%e\n",yval);
    count++;
}
} while (cont>=0 && count<num_samples);

fclose(fpin);
fclose(fpout);

}

```

Decision Directed Timing Recovery

```
/******  
* NAME : PLL.C *  
* AUTHOR : N.DARRAGH *  
* DATE : 6th April 1994 * *  
******/  
  
#include <stdio.h>  
#include <math.h>  
#include <stdlib.h>  
#include <float.h>  
#include <graph.h>  
#include <pgchart.h>  
#include <malloc.h>  
  
float interpolate(float *,float,double);  
  
main(int argc, char *argv[])  
{  
FILE *fpin,*fpout,*fpout1;  
float *wave;  
long c,count,num_samples;  
char asciivalue[80];  
int cont;  
float value;  
float bperiod;  
float speriod;  
float loopgain;  
double stime;  
float phaseerror;  
float previous_diff;  
float ztime,previous_ztime,m,cval;  
float clock_error;  
int sfc;  
float averageval;  
int printout=0;  
float yval0,yval1;  
  
if (argc!=8)  
{  
printf("Usage - PLL <inp file> <out file> <out file 2> <bit period> <sample period>\n");  
printf(" <Loop gain> <Synch field count>\n\n");  
exit(1);  
}  
  
if (!(fpin=fopen(argv[1],"r")))  
{  
printf("Error : Could not open source file - %s\n",argv[1]);  
exit(1);  
}  
  
if (!(fpout=fopen(argv[2],"w")))  
{  
printf("Error : Could not open destination file - %s\n",argv[2]);
```

```

    exit(1);
}

if (!(fpout1=fopen(argv[3],"w")))
{
    printf("Error : Could not open destination file - %s\n",argv[2]);
    exit(1);
}

sscanf(argv[4],"%f",&bperiod);
sscanf(argv[5],"%f",&speriod);
sscanf(argv[6],"%f",&loopgain);
sscanf(argv[7],"%d",&sfc);

printf("Counting samples in source file.");

count=0;
do {
    cont=fscanf(fpin,"%s",asciivalue);

    if (asciivalue[0]!=';')
        {
            do {
                /* strip out comments */
                cont=fscanf(fpin,"%c",asciivalue);
            } while (cont>=0 && asciivalue[0]!=10);
        }
    else
        {
            if (cont>=0)
                count++;

            if (!div(count,1000).rem)
                printf(".");
        }
    } while (cont>=0);

fclose(fpin);

printf("\nNo. of source file samples : %ld\n",count);

num_samples=count;

if (!(wave = malloc(num_samples,sizeof(float)) ) )
{
    printf("\nERROR: Not enough memory to generate waveform\n");
    exit(1);
}

fpin=fopen(argv[1],"r");

printf("Reading source file values.");

count=0;

do {
    cont=fscanf(fpin,"%s",asciivalue);

```

```

if (!ldiv(count,1000).rem)
    printf(".");

if (asciivalue[0]!=';')
    {
    do {
        /* strip out comments */
        cont=fscanf(fpin,"%c",asciivalue);
        fprintf(fpout,"%c",asciivalue);
        } while (cont>=0 && asciivalue[0]!=10);
    }
else
    {
    if (cont>=0)
        {
        sscanf(asciivalue,"%d",&value);
        wave[count]=value;
        count++;
        }
    }
} while (cont>=0 && count<num_samples);

fclose(fpin);

printf("\n\n");

previous_ztime=0;
phaseerror=0;
clock_error=0;
yval0=interpolate(wave,speriod,0);
c=1;
for (stime=bperiod;stime<num_samples*speriod;stime+=bperiod)
    {
    yval1=interpolate(wave,speriod,stime);

    if (c<sfc)
        {

        if (yval0<0 && yval1 >0)
            {
            if (bperiod != 0)
                m=(yval1-yval0)/bperiod;
            cval=yval1-(m*stime);
            if (m != 0)
                ztime=-cval/m;
            clock_error=bperiod-((ztime-previous_ztime)/4);

            if (clock_error<bperiod/2)
                bperiod=(clock_error/10);

            previous_ztime=ztime;
            }

        if (yval0 < 0 && yval1 <0)
            {
            phaseerror=(yval1-yval0)*speriod*-loopgain;
            stime+=phaseerror;
            }
        }
    }

```

```

if (yval0 > 0 && yval1 > 0)
{
    phaseerror=(yval1-yval0)*speriod*loopgain;
    stime+=phaseerror;
}

    averageval=yval1;
    if (averageval<0)
        averageval*=-1;
}

if (c>sfc)
{
    if (yval1 < averageval/2 && yval1 > -averageval/2)
        printout=1;

    if (yval1<0)
        averageval=(averageval+(yval1*-1))/2;
    else
        averageval=(averageval+yval1)/2;
}

if (printout)
    fprintf(fpout,"%e\n",yval1);

    fprintf(fpout1,"%e\n",yval1);

/* printf("period=%e\n",bperiod); */

    c++;
    yval0=yval1;
}
}

float interpolate(float *wave,float speriod,double stime)
{
    long index1,index2;
    float m,c,y;

    index1=(int)(stime/speriod);
    index2=index1+1;

    m=(wave[index2]-wave[index1])/speriod;
    c=wave[index1]-(m*index1*speriod);

    y=(m*stime)+c;

/* printf("sample time=%e\n",stime);
printf("1st=%ld\tval=%e\t2nd=%ld\tval=%e\n",index1,wave[index1],index2,wave[index2]);
printf("m=%e\tc=%e\tnew value=%e\n",m,c,y);
getch(); */
return(y);
}

```

Adaptive Equaliser

```
/*
 * NAME : ADAPTEQ.C
 * AUTHOR : N.DARRAGH
 * DATE : 12th April 1994
 */

#include <stdio.h>
#include <math.h>
#include <stdlib.h>
#include <malloc.h>

main(int argc, char *argv[])
{
FILE *fpin1,*fpin2,*fpout;
int cont1,cont2;
int count=0;
char asciivalue[80];
char asciivalue1[80];
float *tapreg,*weights,sum,error;
int numtaps;
float mu;
int c;
float trainval,dataval;

if (argc!=6)
{
printf("Usage - ADAPTEQ <Training file> <Data file> <output file> <No Taps> <Mu>\n");
exit(1);
}

if (!(fpin1=fopen(argv[1],"r")))
{
printf("Error : Could not open training samples file - %s\n",argv[1]);
exit(1);
}

if (!(fpin2=fopen(argv[2],"r")))
{
printf("Error : Could not open data file - %s\n",argv[2]);
exit(1);
}

if (!(fpout=fopen(argv[3],"w")))
{
printf("Error : Could not open destination file - %s\n",argv[3]);
exit(1);
}

sscanf(argv[4],"%d",&numtaps);
sscanf(argv[5],"%f",&mu);

if (!(weights=malloc(sizeof(float) * numtaps))
{
```

```

printf("Not enough memory to generate taps\n");
exit(1);
}

if (!(tapreg=malloc(sizeof(float) * numtaps))
{
printf("Not enough memory to generate tapregs\n");
exit(1);
}

for (c=0;c<numtaps;c++)
{
tapreg[c]=0;
weights[c]=0;
}

printf("Symbol No:\n");

do {
if (count>=numtaps/2)
{
cont1=fscanf(fpin1,"%s",asciivalue);
sscanf(asciivalue,"%f",&trainval);
}
else
{
trainval=0;
cont1=0;
}

cont2=fscanf(fpin2,"%s",asciivalue1);
sscanf(asciivalue1,"%f",&dataval);

if (cont1>=0 && cont2>=0)
{
/* printf("%d\t%e\t%e\n",count,trainval,dataval); */
for (c=numtaps-1;c>0;c--)
tapreg[c]=tapreg[c-1];
tapreg[0]=dataval;

sum=0;
for (c=0;c<numtaps;c++)
{
/* printf("tap=%d\tvalue=%e\tweight=%e\n",c,tapreg[c],weights[c]); */
sum+=(tapreg[c] * weights[c]);
}

error=trainval-sum;

for (c=0;c<numtaps;c++)
weights[c]+=(2 * mu * error * tapreg[c]);

fprintf(fpout,"%e\n",sum);
/* printf("sample=%d\toutput=%e\terror=%e\n",count,sum,error); */
count++;
printf("\r%d",count);
}
}

```

```
    }  
    } while (cont1>=0 && cont2>=0);  
  
    printf("\n");  
    fclose(fpin1);  
    fclose(fpin2);  
    fclose(fpout);  
  
    printf("\n\n* DONE *\n");  
}
```

Viterbi Detector

```
/*
 * NAME : VITERBI.C
 * AUTHOR : N.DARRAGH
 * DATE : 6th April 1994
 */
```

```
#include <stdio.h>
#include <math.h>
#include <stdlib.h>
#include <float.h>
#include <graph.h>
#include <pgchart.h>
```

```
char Y3string[100],Y2string[100],Y1string[100],Y0string[100];
char Y3stringold[100],Y2stringold[100],Y1stringold[100],Y0stringold[100];
```

```
main(int argc, char *argv[])
{
FILE *fpin,*fpout;
float *wave;
int c,count,num_samples;
char asciivalue[80];
int cont;
float value;
float Y3,Y2,Y1,Y0,Y3old,Y2old,Y1old,Y0old;
float error0,error1,errorml;
int e,f;
int word,power;
int g=0;
```

```
if (argc!=3)
{
printf("Usage - VITERBI <inp file> <out file>\n");
exit(1);
}
```

```
if (!(fpin=fopen(argv[1],"r")))
{
printf("Error : Could not open source file - %s\n",argv[1]);
exit(1);
}
```

```
if (!(fpout=fopen(argv[2],"w")))
{
printf("Error : Could not open destination file - %s\n",argv[2]);
exit(1);
}
```

```
printf("Counting samples in source file.");
```

```
count=0;
do {
```

```

cont=fscanf(fpin, "%s", asciivalue);

if (asciivalue[0]!=';')
    {
    do {
        /* strip out comments */
        cont=fscanf(fpin, "%c", asciivalue);
        } while (cont>=0 && asciivalue[0]!=10);
    }
else
    {
    if (cont>=0)
        count++;

        if (!div(count,1000).rem)
            printf(". ");
        }
    } while (cont>=0);

fclose(fpin);

printf("\nNo. of source file samples : %d\n",count);

num_samples=count;

if (!(wave=malloc(sizeof(float) * (count+1))))
    {
    printf("\nERROR: Not enough memory to generate waveform\n");
    exit(1);
    }

fpin=fopen(argv[1], "r");

printf("Reading source file values.");

count=0;

do {
    cont=fscanf(fpin, "%s", asciivalue);

    if (!div(count,1000).rem)
        printf(". ");

    if (asciivalue[0]!=';')
        {
        do {
            /* strip out comments */
            cont=fscanf(fpin, "%c", asciivalue);
            fprintf(fpout, "%c", asciivalue[0]);
            } while (cont>=0 && asciivalue[0]!=10);
        }
    else
        {
        if (cont>=0)
            {
            sscanf(asciivalue, "%f", &value);
            wave[count]=value;
            count++;
            }
        }
}

```

```

    }
} while (cont>=0 && count<num_samples);

fclose(fpin);

printf("\n\n");

Y3old=Y2old=Y1old=Y0old=0;

e=0;
word=0;
power=256;
for (c=0;c<num_samples;c++)
{
    error0=pow(wave[c],2);
    error1=pow(1-wave[c],2);
    errorml=pow(-1-wave[c],2);

    Y3=(Y3old+error0 < Y1old+error1) ? Y3old+error0 : Y1old+error1;
    Y2=(Y3old+errorml < Y1old+error0) ? Y3old+errorml : Y1old+error0;
    Y1=(Y2old+error0 < Y0old+error1) ? Y2old+error0 : Y0old+error1;
    Y0=(Y2old+errorml < Y0old+error0) ? Y2old+errorml : Y0old+error0;

    if (Y3old+error0 < Y1old+error1)
    {
        memcpy(Y3string+1,Y3stringold,e);
        Y3string[0]=0;
    }
    else
    {
        memcpy(Y3string+1,Y1stringold,e);
        Y3string[0]=1;
    }

    if (Y3old+errorml < Y1old+error0)
    {
        memcpy(Y2string+1,Y3stringold,e);
        Y2string[0]=-1;
    }
    else
    {
        memcpy(Y2string+1,Y1stringold,e);
        Y2string[0]=0;
    }

    if (Y2old+error0 < Y0old+error1)
    {
        memcpy(Y1string+1,Y2stringold,e);
        Y1string[0]=0;
    }
    else
    {
        memcpy(Y1string+1,Y0stringold,e);
        Y1string[0]=1;
    }

    if (Y2old+errorml < Y0old+error0)

```

```

        {
        memcpy(Y0string+1,Y2stringold,e);
        Y0string[0]=-1;
        }
else
    {
    memcpy(Y0string+1,Y0stringold,e);
    Y0string[0]=0;
    }

if (e>99)
    exit(1);

while ((Y3string[e]==Y2string[e]) && (Y2string[e]==Y1string[e]) && (Y1string[e]==Y0string[e]) &&
e>=0)
    {
    if (Y3string[e])
        word+=power;
    power/=2;
    if (power<1)
        {
        fprintf(fpout,"%03x ",word);
        word=0;
        power=256;
        g++;
        if (!div(g,16).rem)
            fprintf(fpout,"\n");
        }
    e--;
    };
e++;
memcpy(Y3stringold,Y3string,e);
memcpy(Y2stringold,Y2string,e);
memcpy(Y1stringold,Y1string,e);
memcpy(Y0stringold,Y0string,e);

Y3old=Y3;
Y2old=Y2;
Y1old=Y1;
Y0old=Y0;
}
}

```

Appendix E

Background Theory

The Theory of Non-linear Dibit Response Extraction Using Pseudo-Random Binary Sequences

The linear time domain response of the magnetic recording channel is given by,

$$V(t) = \sum_k \frac{1}{2}(a_{k+1} - a_k)h(t - kT) \quad (1)$$

where $h(t)$ is the time domain response of the channel to an isolated transition centred at $t=0$, T is the length of the bit cell and a_k is the magnetisation level in the k th cell where $a_k \in \{-1, 1\}$.

Hence an isolated transition response is characterised by the input sequence,

$$a = \{\dots, -1, 1, \dots\},$$

and a dibit (NRZ 1) response is described by the input sequence,

$$a = \{\dots, -1, 1, -1, \dots\}.$$

Case (a) - Non-linear Overwrite bit-shift.

The first non-linear effect in the magnetic recording process is where the existing magnetisation of the media affects the writing field of the head causing transitions written against the sense magnetisation of the media to be shifted later and those in the same sense not to be.

This may be expressed as,

$$v(t) = \sum_k \frac{1}{2}(a_{k+1} - a_k)h(t - kT - \frac{1}{2}\epsilon_0 + \frac{1}{4}\epsilon_0(a_{k+1} - a_k)) \quad (2)$$

where the $h(\dots)$ term includes an additional time shift, ϵ_0 , which is present for transitions in the $\{1, -1\}$ sense and not for the $\{-1, 1\}$ sense.

h may be expanded as a Taylor series of the form,

$$f(x+c) = f(x) + cf'(x) + \frac{c^2}{2!}f''(x) + \dots + \frac{c^n}{n!}f^n(x)$$

such that $f(x) \equiv h(t - kT - \frac{1}{2}\epsilon_0)$ and $c \equiv \frac{1}{4}\epsilon_0(a_{k+1} - a_k)$ and limiting to only the first 2 coefficients,

$$h(\dots) = h(t - kT - \frac{1}{2}\epsilon_0) + \frac{1}{4}\epsilon_0(a_{k+1} - a_k)h'(t - kT - \frac{1}{2}\epsilon_0) \quad (3)$$

Then substituting back into (2),

$$v(t) = \sum_k \frac{1}{2} (a_{k+1} - a_k) [h(t - kT - \frac{1}{2} \epsilon_0) + \frac{1}{4} \epsilon_0 (a_{k+1} - a_k) h'(t - kT - \frac{1}{2} \epsilon_0)] \quad (4)$$

and noting that the first term in [...] of (4) multiplied by the summation term is $v(t - \frac{1}{2} \epsilon_0)$ then,

$$v(t) = v(t - \frac{1}{2} \epsilon_0) + \frac{1}{4} \epsilon_0 \sum_k \frac{1}{2} (a_{k+1} - a_k)^2 h'(t - kT - \frac{1}{2} \epsilon_0) \quad (5)$$

which yields.

$$v(t) = v(t - \frac{1}{2} \epsilon_0) + \frac{1}{8} \epsilon_0 \sum_k (a_{k+1}^2 - 2a_{k+1}a_k + a_k^2) h'(t - kT - \frac{1}{2} \epsilon_0) \quad (6)$$

The terms a_{k+1}^2 and a_k^2 are always equal to 1 and therefore introduce two terms of $h'(\dots)$ periodic at the clock frequency, the summation of each will be infinite. However, the finite difference approximation to h' yields,

$$\begin{aligned} \sum_k h'(t - kT - \frac{1}{2} \epsilon_0) &\approx \sum_k \frac{h(t - (k - \frac{1}{2})T - \frac{1}{2} \epsilon_0) - h(t - (k + \frac{1}{2})T - \frac{1}{2} \epsilon_0)}{T} \\ &= \frac{h(+\infty) - h(-\infty)}{T} = 0 \end{aligned}$$

Therefore,

$$v(t) = v(t - \frac{1}{2} \epsilon_0) - \frac{1}{4} \epsilon_0 \sum_k a_k a_{k+1} h'(t - kT - \frac{1}{2} \epsilon_0) \quad (7)$$

If the a_k 's form a pseudorandom sequence of length N , the 'shift-and-add' property states that,

$$a_k a_{k+p} = a_{k+M \bmod N}$$

i.e., a maximal length PRBS multiplied by a shifted version of itself (by p bits) produces the same sequence again shifted by M to the original sequence.

Let $a_k a_{k-1} = a_{k+M0}$, then,

$$v(t) = v(t - \epsilon_0) - \frac{1}{4} \epsilon_0 \sum_k a_{k+M0} h'(t - kT - \frac{1}{2} \epsilon_0) \quad (8)$$

Using a linear difference approximation to h' we have,

$$v(t) \approx v(t - \frac{1}{2} \epsilon_0) - \frac{1}{4} \epsilon_0 \sum_k a_{k+M0} \left(\frac{h(t - (k - \frac{1}{2})T - \frac{1}{2} \epsilon_0) - h(t - (k + \frac{1}{2})T - \frac{1}{2} \epsilon_0)}{T} \right) \quad (9)$$

and by noting that,

$$a_{k+m}h(t-kT) \equiv a_k h(t-kT-m)$$

we can re-write the summation indices to yield an expression for $v(t)$ in terms of time shifted versions of itself, via,

$$v(t) \approx v(t - \frac{1}{2}\epsilon_0) - \frac{\epsilon_0}{T} \sum_k \frac{1}{2}(a_{k+1} - a_k)h(t - (k - M_0 + \frac{1}{2})T - \frac{1}{2}\epsilon_0) \quad (10)$$

which reduces to,

$$v(t) \approx v(t - \frac{1}{2}\epsilon_0) - \frac{\epsilon_0}{T} v(t - \frac{1}{2}\epsilon_0 + (M_0 - \frac{1}{2})T) \quad (11)$$

Hence, the distorted output waveform comprises a net (late) shift of the original waveform, $v(t)$ by $\frac{1}{2}\epsilon_0$ and an echo of $v(t)$ at position $(M_0 - \frac{1}{2})$ bit periods early.

Therefore, the magnitude of the shift may be determined from,

$$\epsilon_0 = 2T \frac{V_{p-p \text{ echo}}}{V_{p-p \text{ main pulse}}} \quad (12)$$

The net (late) shift arises because half of the transitions will be written against the sense of the media magnetisation (causing the shift) and half will not be (which yields zero shift).

Case (b) - Adjacent Transition Non-linear Bit-shift

This is the non-linear bit shift caused by adjacently written transitions. The second transition is shifted towards the first by an amount ϵ_1 . The input sequence is $a = \{\dots -1, 1, -1, \dots\}$ and an analysis similar to the above method yields,

$$v(t) \approx v(t + \frac{1}{2}\epsilon_1) + \frac{\epsilon_1}{T} v(t + \frac{1}{2}\epsilon_1 - \frac{1}{2}T) - \frac{\epsilon_1}{T} v(t + \frac{1}{2}\epsilon_1 + (M_1 - \frac{1}{2})T) \quad (13)$$

There are two echoes produced, one with a time shift of 1.5 bits later than the main dipulse, the second term in (13), and one $(M_1 - \frac{1}{2})$ bits early, the third term in (13).

Once again, the ratio of either of the echo amplitudes to the main pulse yields the bit shift,

$$\epsilon_1 = 2T \frac{V_{p-p \text{ echo}}}{V_{p-p \text{ main pulse}}} \quad (14)$$

The echo 1.5 bits later than the main pulse will be distorted by the main pulse itself since it is generally wider than 1 bit. Therefore, for analysis purposes the $(M_1 - \frac{1}{2})$ echo is used. This time the net shift is early, since the second transition is pulled towards the first.

Case (c) - Adjacent transition-but-one non-linear bit shift.

This is a similar case to that of (b) except that the distance between the transitions is two bit periods. However, the direction of the bit shift depends on the directions of the two transitions under consideration; earlier for opposites (no intervening transitions between the two) and later for transitions in the same direction (where there is a transition recorded between the two).

Analysis similar to the previous two cases yields,

$$\begin{aligned}
 v(t) \approx & v(t) - \frac{1}{2} \frac{\epsilon_2}{T} v(t - \frac{3}{2} T) + \frac{1}{2} \frac{\epsilon_2}{T} v(t - \frac{1}{2} T) \\
 & + \frac{1}{2} \frac{\epsilon_2}{T} v(t + (M_1 - \frac{1}{2}) T) - \frac{1}{2} \frac{\epsilon_2}{T} v(t + (M_2 - \frac{1}{2}) T)
 \end{aligned}
 \tag{15}$$

Hence, there are echoes at 1.5 and 2.5 bits late and $(M_1 - \frac{1}{2})$ and $(M_2 - \frac{1}{2})$ bits early. The first and third are essentially as those produced by case (b). The second and third are additional echoes. There is no net shift in the main response since 1 quarter of the transitions are shifted early, one quarter late and one half unaffected.

Fourier Analysis and the Fourier Transform

Any real periodic waveform may be represented by an infinite summation of sinusoids scaled in both amplitude and phase and at frequencies which are integer multiples of the fundamental frequency of the function, viz,

$$v(t) = \sum_{k=0}^{\infty} a_k \cos\left(\frac{2\pi k}{T}t + \phi_k\right) \quad (1)$$

$$a_k = \frac{1}{T} \left[\left(\int_{-T/2}^{T/2} v(t) \cos\left(\frac{2\pi k}{T}t\right) dt \right)^2 + \left(\int_{-T/2}^{T/2} v(t) \sin\left(\frac{2\pi k}{T}t\right) dt \right)^2 \right]^{1/2}$$

where a_k is the amplitude of the k th frequency component and ϕ_k is its phase, and, T is the fundamental period of the waveform $v(t)$. This is the Fourier Series and the amplitudes of the Fourier series components (the a_k 's) describe the discrete voltage spectrum of the signal $v(t)$.

The Fourier series in this form is only useful for describing real, power signals. In order to represent complex functions, a more general periodic function, the complex exponential may be used where,

$$e^{j2\pi ft} = \cos 2\pi ft + j \sin 2\pi ft$$

$$e^{-j2\pi ft} = \cos 2\pi ft - j \sin 2\pi ft$$

and where therefore the exponential Fourier series is given by,

$$v(t) = \sum_{k=-\infty}^{k=\infty} a_k e^{j2\pi kt/T}$$

$$a_k = \frac{1}{T} \int_{-T/2}^{T/2} v(t) e^{-j2\pi kt/T} dt \quad (2)$$

By considering 1 cycle of the waveform and extending the fundamental period, T , to infinity we can deduce the series for a finite duration time function.

as $T \rightarrow \infty$, $1/T \rightarrow df$ and $k/T \rightarrow f$, therefore,

$$v(t) = \int_{-\infty}^{\infty} \left[\int_{-\infty}^{\infty} v(t) e^{-j\omega t} dt \right] e^{j\omega t} df \quad (3)$$

This is the Fourier Integral and the $[..]$ term is the Fourier Transform which yields the voltage spectral density, $V(f)$,

$$V(f) = \int_{-\infty}^{+\infty} v(t) e^{-j2\pi ft} dt \quad \text{Volts/Hz} \quad (4)$$

Parseval's theorem states that the energy, E , contained in the signal is given by,

$$E = \int_{-\infty}^{+\infty} |v(t)|^2 dt = \int_{-\infty}^{+\infty} |v(f)|^2 df \quad \text{joules} \quad (5)$$

Note that a finite duration signal contains finite energy and the voltage spectral density, $V(f)$ is continuous.

The Fourier Transform may only be extended to power signals (with infinite energy) by means of devious mathematics (in order to meet the Dirichlet conditions). It can be shown that by multiplying the power signal, $v(t)$, by a convergence factor, $g(t)$, where,

$$g(t) = \lim_{\alpha \rightarrow 0} e^{-\alpha|t|}$$

the Power Spectral Density, $S(f)$, is given by,

$$S(f) = \lim_{T \rightarrow \infty} \frac{|V(f)|^2 df}{T} \quad \text{watts/Hz} \quad (6)$$

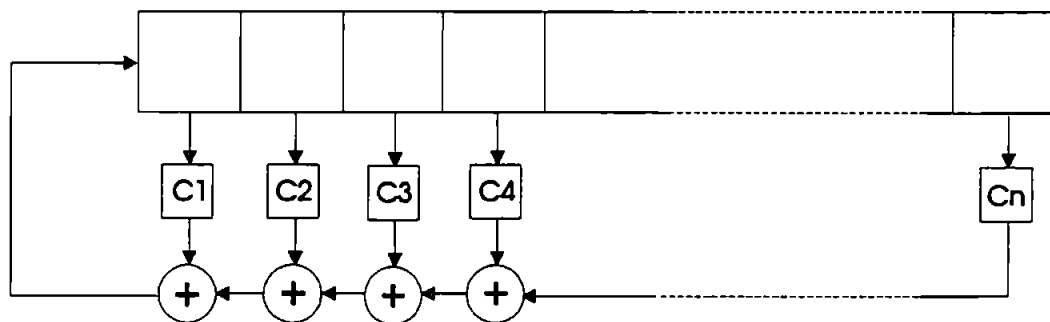
where $V(f)$ is the Fourier Transform of $v(t)$ for $-T/2 \leq t \leq T/2$. Then Parseval's theorem for power signals, of fundamental period T , is,

$$P = \lim_{T \rightarrow \infty} \frac{1}{T} \int_{-T/2}^{T/2} |v(t)|^2 dt = \int_{-\infty}^{+\infty} S(f) df \quad (7)$$

i.e. whereas the integral of the Energy Spectral Density of an energy signal yields the total signal energy, the integral of the Power Spectral Density of a power signal yields the total signal power.

Generation of Maximal Length Pseudorandom Binary Sequences Using Feedback Shift Registers

$$m(x) = C_n x^n + C_{n-1} x^{n-1} + \dots + C_1 x + 1$$



n	$C_n C_{n-1} \dots C_1 1$	n	$C_n C_{n-1} \dots C_1 1$	n	$C_n C_{n-1} \dots C_1 1$
5	100101 101001 101111 110111 111011 111101	7	11100101 11101111 11110001 11110111 11111101	9	1000110011 1001011001 1001011111 1001101001
6	1000011 1011011 1100001 1100111 1101101 1110011	8	100011101 100101011 100101101 101001101 101011111 101100011 101100101 101101001	10	10000001001 10000011011 10000100111 10000101101 10001100101 10001101111 10010000001 10010001011
7	10000011 10001001 10001111 10010001 10011101 10100111 10101011 10111001 10111111 11000001 11001011 11010011 11010101	9	101110001 110000111 110001101 110101001 111000011 111001111 111100111 111110101	11	100000000101
				12	1010000000111
				13	11000000000111
				14	101000000000111
				15	1000000000000111